# A STUDY OF THE ADSORPTION POTENTIAL OF $CO_2$ ON SOUTH AFRICAN ASH

Mookho Kholumo

A research report submitted to the Faculty of Engineering and the Built Environment of the University of the Witwatersrand, in partial fulfilment of the requirements for the degree of Master of Science in Engineering.

Johannesburg, 2011

# DECLARATION

I declare that this research report is my own unaided work. It is being submitted for the degree of Master of Science to the University of the Witwatersrand, Johannesburg. It has not been submitted before for any degree or examination in any other University.

---

(Signature of candidate)

_____day of _____ (year) _____

# ABSTRACT

As the global demand for energy increases, $CO_2$ discharge will also increase due to power stations and other coal-dependent industries. It therefore becomes necessary to develop processes that will enable the capture and storage of $CO_2$ from flue gas in combustion processes, in order to mitigate the undesirable consequences of $CO_2$ emission. It is for this reason that research on carbon capture and storage has received considerable attention recently. Adsorption of $CO_2$ onto coal ash is a potentially attractive alternative to capturing $CO_2$ from stationary sources in the context of carbon capture and storage technologies.

Four coal ash samples were used as $CO_2$ adsorbents in this study, obtained from three different industries, namely: 1) coal power station 2) a petrochemical industry and, 3) a metallurgical plant. Thermogravimetric analysis, X-ray diffraction spectroscopy, and BET isotherms were used to analyse the nature of the samples prior to the adsorption process. A volumetric adsorption system was used to facilitate the adsorption process.

The pulverized fuel ash sample had the highest $CO_2$ adsorption capacity, followed by the spreader stoker ash sample, the chain grate ash sample, and finally the gasification ash sample. The as received ash was found to have a potential to uptake $CO_2$ in a capacity range of 0.17 – 2.8 Mt $CO_2$, meaning that 1.28 % of the annual sequestrable $CO_2$ produced in South Africa could be captured using all of the ash produced in one year in South Africa. Coal ash is a suitable material for the adsorption of $CO_2$, however its adsorption capacity needs to be improved by treatment with acids and amines in order to introduce active functional groups.

# ACKNOWLEDGEMENTS

None of this work would have been possible without the constant guidance and patience my supervisor, Prof. Nicola Wagner, have given me during the course of my research. Thank you for not only steering my project, but for steering and guiding my career in such a manner that I leave with a solid career path to follow. I would also like to thank Prof. Johannes van Herdeen, Rets'ilisitsoe Taole and Bonny Nyangwa for providing me with the samples. My sincere gratitude goes to Dr. Frederic Doucet for helping me with the basics on mineral carbonation. My sincere gratitude also goes to Gregory Okolo, at Northwest University Potchefstroom campus, for conducting BET analysis on my samples. Many thanks also go to Bruce and Doctor for assistance with laboratory equipment. Throughout this work my friends and colleagues in the Coal and Carbon Research Group have provided tremendous moral support which does not go unappreciated. Most importantly, I wish to express their sincere gratitude and appreciation to the South African Centre of Carbon Capture and Storage for the financial support during the period of my study.

Many thanks to my wonderful husband Tebello Mathaba for his love and support throughout the undertaking of this research project, I cannot thank him enough for all the help he has shown toward me. Thanks to my wonderful dad and dearest siblings Matseleng Moledi, Lefatle Mofokeng and Tankiso Mofokeng for their love and support as a family and for always being there for me when I needed them. I would like to thank the Mathaba's family as well as my friends Mpeo, Maliile, Polo, Matsheliso, 'Mahalieo, Sithembile, Michelle, Lebo and Lineo for making my stay at varsity memorable. Thanks to David Kumi and Gail Gordon, who helped with the proof-reading of my research report. Last but not least, I extend my sincere gratitude to the most high God for making it possible for me to get this far. To God be the Glory!!!

# TABLE OF CONTENTS

**CONTENTS** **Page**

## LIST OF FIGURES

**Figure** **Page**

## LIST OF TABLES

**Table** **Page**



## LIST OF SYMBOLS

| | |
|---|---|
| ˚C | degree celcius |
| Bt | Billion tons |
| g | gram |
| min | minutes |
| Mt | Million tons |
| ppm | parts per million |
| $n_{intro}$ | Number of moles of $CO_2$ introduced to the sample |
| $n_{total}$ | Total number of moles of $CO_2$ adsorbed by the sample |
| $n_{(PBeq)}$ | Number of moles of $CO_2$ at an equilibrium pressure in the sample cell |
| $P_{Astart}$ | Initial pressure recorded in the reference cell |

| | |
|---|---|
| $P_{Aend}$ | Final pressure of the reference cell |
| T | Temperature |
| $V_A$ | Volume of chamber A or reference cell |
| $V_B$ | Volume of chamber B or sample cell |
| $V_D$ | Dead Volume |
| $V_s$ | Volume of the sample |

## LIST OF ABBREVIATIONS

| | |
|---|---|
| BET | Brauner, Emmett and Tellet |
| CCS | Carbon Capture and Storage |
| CCSEM | Computer-Controlled Scanning Electron Microscopy |
| CCTs | Clean Coal Technologies |
| CG | Chain grate |
| G | Gasification |
| GHG | Green House Gas |
| ICP-MS | Inductively Coupled Plasma Mass Spectroscopy |
| ICP-OES | Inductively Coupled Plasma Optical Emission Spectroscopy |
| $NO_x$ | Nitrogen Oxides |
| PEI | polyethyleneimine |
| PF | pulverised fuel |
| $SO_x$ | Sulphur Oxides |
| SACCCS | South African Centre for Carbon Capture and Storage |
| SEM | Scanning Electron Microscopy |
| SS | Spreader Stoker |
| TGA | Thermogravimetric Analysis |
| TPD | Temperature Programed Desorption |
| UCG | Underground Coal Gasification |
| VAS | Volumetric Adsorption System |

| | |
|---|---|
| XRD | X-Ray Diffraction spectroscopy |
| XRF | X-Ray Fluorescence spectroscopy |

# CHAPTER 1

# INTRODUCTION

## 1.1 BACKGROUND

Coal is a combustible carbonaceous rock that contains varying amounts of carbon, hydrogen, nitrogen, oxygen, sulphur and mineral matter (Speight, 2005). It is an important energy resource necessary to meet the future demand of electricity as its reserves are more abundant than those of other fossil fuels (University of California College Prep, 2009). South Africa is by far the largest producer of coal in Africa, and is a major global producer, after China, Australia, Canada, USA, and Indonesia (Mbendi Information Systems, 2011). South Africa is the 5$^{th}$ largest producer of coal in the world, 4$^{th}$ largest exporter of coal, largest supplier of coal to the European Union, and possesses 10% of the world's reserves (Mbendi Information Systems, 2011). Coal accounts for approximately 75% of primary energy production in South Africa (Surridge, 2009). Apart from energy production and steel making, coal also caters for about 35% of liquid fuel requirements in South Africa (Surridge, 2009). It is evident that the South African energy economy relies heavily on coal.

Although coal has played a significant role in the advancement of civilization in South Africa, the value of its utilisation is partly offset by the impact it has on the environment and human health. Coal combustion emits various gases that adversely affect the environment, one of which is carbon dioxide ($CO_2$). Carbon dioxide is a primary greenhouse gas (GHG), which initiates predicaments related to global warming, such as increased ambient temperatures, melting glaciers and rising sea levels. The largest anthropogenic source of $CO_2$ is the combustion of fossil fuels (mainly being coal) for power generation. Carbon dioxide concentrations in the atmosphere have increased from approximately 280 parts per million (ppm) in pre-

industrial times to 392 ppm in 2006 (Conway and Tans, 2011), and are projected to rise to 625 ppm by 2050 should $CO_2$ emissions continue to increase in a business-as-usual scenario (Hawksworth, 2006).

In the quest to minimize the effects of global climate change, research is being conducted to establish the methods of reducing $CO_2$ emissions. One measure for reducing $CO_2$ emissions is Carbon Capture and Storage (CCS). Carbon capture and storage involves separating $CO_2$ from gas streams or capturing $CO_2$ from power plants before emission, and injecting it at high pressures into deep geologic formations or oceans for permanent storage (ASME, 2009; Pires, 2011). The CCS technology have already been implemented in areas such as Sleipner in Norway, and Otway in Australia (Surridge, 2009). South Africa, being a developing country that has the highest dependence on coal for energy in the continent, could employ CCS technologies to reduce $CO_2$ emissions from its power plants, gasification plants, and metallurgical industries.

Led by the Department of Environmental Affairs and the South African National Energy Research Institute (SANERI), the South African Government has established the South African Carbon Capture and Storage Roadmap (SACCSR) with an ultimate aim to construct a commercial CCS plant by the year 2020 (Cloete, 2010).

## 1.2 PROBLEM STATEMENT

Recently, much research is being conducted with the aim of fabricating suitable adsorbents for $CO_2$ as a means of reducing its emission. Different materials have been tested for their ability to adsorb $CO_2$, and these include low-cost biomass residue (olive stones) (Plaza *et al*., 2009), carbon fibre composites (Thiruvenkatachari *et al*., 2009), and fly ash (Muriithi *et al.*, 2011). Coal ash is among the most widely used material in the synthesis of $CO_2$ adsorbents because;

- it has high porosity, which translates into increased surface area;
- it has a relatively high carbon content, which could be altered to upgrade the adsorption capacity of ash. The carbon atoms in coal ash may be activated through the introduction of active functional groups that have high affinity for $CO_2$. The active functional groups may be introduced by impregnating the coal ash with an acid, strong base, or a salt;
- it is highly abundant, which makes it cheap and readily available. Usage of coal ash also alleviates ash handling problems facing the world today.

Although a considerable amount of literature exists on the adsorption of $CO_2$ onto coal ash, little is known about the adsorption potential of South African coal ash in particular.

## 1.3 AIMS AND OBJECTIVES OF THE PROJECT

This research project aims to study the adsorption potential of $CO_2$ on coal ash and to determine which type of coal ash is the most suitable adsorbent for $CO_2$. A positive outcome of this investigation could be useful in the synthesis of cost-effective $CO_2$ adsorbents in the future.

The objectives of the project are:

- to determine the chemical and physical composition of ash samples to be used;
- to determine the relationship between the adsorptivity and composition of the ash samples;
- to establish the effect of pressure on the adsorption potential of $CO_2$ on ash samples;
- to determine whether metal oxides in ash have a direct effect on the adsorption potential of $CO_2$ on the ash, or not.

## 1.4 HYPOTHESIS

- South African coal ash is a suitable material to use as a $CO_2$ adsorbent.

## 1.5 RESEARCH QUESTIONS

1) What is the chemical composition of the ash samples?
2) Which external factors could affect the adsorptivity of $CO_2$ on coal ash?
3) Which variables may be manipulated to maximize the adsorption capacity of the samples?

## 1.6 OUTLINE OF CHAPTERS

This research report is divided into five chapters. The first chapter provides an overall introduction to the study. Chapter two is an overview of the nature of South African coals, coal and the environment and carbon capture and storage. Chapter three outlines the sample preparation and describes the adsorption experimental procedure. Chapter four discusses sample characterisation and the adsorption results. Chapter five covers the conclusions drawn from the study, and recommendations for continued research in this area.

# CHAPTER 2

# LITERATURE REVIEW

This chapter briefly describes the nature of the South African coals and the deposition of coal within the country. It also outlines the impact coal has on the environment and the mitigation strategies that have been implemented to curb the emissions due to coal utilisation. The last part of the chapter describes CCS and gives an overview of how coal ash may be used as a mitigation strategy.

## 2.1 SOUTH AFRICAN COALS

Laurasian coals, coals in the Northern hemisphere, were formed by giant water-loving sub-tropical equatorial types of lycopod horsetails and fleshy-barked trees, which could not be easily swept away by the floods (Falcon and Ham, 1988). These trees have been found to have an amazing feature of growing one on top of the other, which explains why Laurasian coal-seams are so thick, with low mineral content (Falcon and Ham, 1988).

Conversely South African coals, in common with coals from other Gondwana provinces (India, Australia, and South America), are generally mineral-rich and more difficult to beneficiate than those found in the Laurasian region. This is attributable to the conditions which reigned during the time when the coals were formed (Falcon and Ham, 1988). The Gondwana coal-bearing sediments amassed in stable continental depressions along the margins of glacial valleys, lakes and shallow inter-continental seas (Falcon and Ham, 1988). These water-bodies are very rich in mineral matter. When seasonal floods occurred, other forms of vegetation were washed from the mountainous areas into the water-bodies, hence leading to formation of mineral-rich coals, which are frequently difficult to beneficiate (Falcon and Ham, 1988). Utilisation of mineral-rich coal releases various obnoxious gases to the atmosphere,

and results in the formation of large volumes of ash. Companies such as Eskom (the South African power utility) and Sasol (the South African petrochemical company) convert coal with 30 – 40% ash, which implies that 30 – 40% of the coal being fed to be processed is recovered as coal ash. Ash management and stack emissions are, for this reason, a cause of concern in South Africa.

## 2.2 SOUTH AFRICAN COAL RESOURCES

Coal resources are abundant in Southern Africa, especially in South Africa, where recoverable reserves were estimated at 55.1 billion tons (Bt) in the 1990s (Energy Information Administration, 2000). South Africa is particularly well endowed with coal resources, this partly due to the existence of the Karoo basin within the country (Cairncross, 2001). However, the South African coal reserves have now decreased to about 30 Bt due to intense extraction triggered by an increasing energy demand (Prevost, 2004). In South Africa, coal is found in 19 different coalfields, located mainly in KwaZulu-Natal, Mpumalanga, Limpopo, and the Free State, with lesser amounts in Gauteng, the North West Province, and the Eastern Cape (Mbendi Information Systems, 2011).

South Africa is by far the largest producer of coal in Africa and is a major global producer, after China, Australia, Canada, USA and Indonesia (Mbendi Information Systems, 2011). South Africa is the $5^{th}$ largest producer of coal in the world, $4^{th}$ largest exporter of coal, largest supplier to the European Union and possesses 10% of the world's reserves (Prevec, 2006). Since 1997, South Africa and Zimbabwe have been the leading countries, as far as coal consumption is concerned (Energy Information Administration, 2000). The remaining sub Saharan countries mine and consume considerably less coal than these two countries.

## 2.3 COAL AND THE ENVIRONMENT

As South Africa does not have oil, it relies primarily on coal for energy production. Other sources of energy such as hydrothermal power, wind, and solar power are very limited in the country due to cost and availability, making it very difficult for coal to be replaced as the major energy source. Therefore, coal shall be used for many years to come. Coal accounts for approximately 75% of primary energy production (Surridge, 2009). Besides providing almost entirely for all the electrical energy required, coal also caters for about 35% of liquid fuel requirements (Surridge, 2009). However, the value of coal utilisation is partly offset by the impact it has on the environment and human health.

Coal combustion emits various gases that adversely affect the environment, particularly the ground-level air quality. The emitted gases include $CO_2$, nitrogen oxides ($NO_x$), sulphur oxides ($SO_x$), trace elements, and particulate matter. Although these emissions have an insignificant effect on the environment when emitted from natural processes due to nature's assimilative capacity, they present negative impacts on the environment due to large quantities which are being emitted from anthropogenic activities each year, when vast amounts of coal are utilized (Hu *et al*., 2000). Effects of some of these emissions are given below:

- $CO_2$ - the primary source of global warming, which in turn initiates predicaments such as rising sea level, melting glaciers, and increased ambient temperatures.
- $SO_2$ (sulphur dioxide) - a major contributor to acid rain, which increases the acidity of the water bodies and soil, killing the aquatic life and plants thereof. It also initiates respiratory diseases.
- $NO_x$ - play an important role in the formation of photochemical smog and acid rain. Photochemical smog causes eye and respiratory tract irritation.

Due to the strain posed by the environmental regulations against emissions of harmful pollutants, South Africa is currently facing environmental pressures both locally and globally. Recently, consumers around the world (especially in Europe and North America) are increasingly buying coal on the basis of the impact the coal on the environment (Bethlehem, 2009). The idea behind this phenomenon is to promote the market of "clean" coal. The biggest challenge faced by South Africa is that it does not have the financial, human, and technological resources required to meet the new environmental regulations (Bethlehem, 2009). If major constraints are placed on South Africa's ability to export coal as a result of environmental trade measures, this could have a serious impact on the country's economy, attributable to the fact that coal exports contribute more to the South African economy than coal used locally. In the Copenhagen Accord, South Africa made a voluntary commitment to reduce its GHG emissions below a business-as-usual scenario (Ground Work, 2011). South African coal-using industries could engage in the use of clean coal technologies so as to become environmentally responsible.

## 2.4 CLEAN COAL TECHNOLOGIES

Based on the scientific analysis, it is generally accepted that a link exists between climate change and the use of coal. As a consequence, the development of clean coal technologies (CCTs) has been practiced in many countries over the years. Clean coal technologies usually address atmospheric problems resulting from burning coal. Several generations of technological advances have led to more efficient combustion of coal with reduced emissions of $SO_x$ and $NO_x$. Clean coal technologies involve removal of pollutants before, during, and after utilisation of coal. Below is a brief description of most commonly used CCTs.

- *Coal beneficiation*, a method of chemically washing minerals and impurities from coal before utilisation, in order to concentrate the desired qualities for marketing purposes (Drbal *et al.*, 1996). Reduced minerals will result in

improved conversion efficiencies, and reduced ash handling. However, there is a greater amount of discard produced from the beneficiation process that requires management.

- *Carbon capture and storage (CCS),* a technology where $CO_2$, the main cause of global warming, is removed from the flue gases for storage in geologic formations or the ocean (World Bridge, 2010).
- *Underground Coal Gasification (UCG),* a technology that involves injection of air or oxygen into a coal seam to support an in-situ gasification process (Jones *et al*., 2005). This process converts an unmined coal into a combustible gas, which can be brought to the surface to be used for industrial heating or power generation (Jones, 2005). This technology minimises environmental impact due to limited ash management, and higher efficiencies.
- *Coal Bed Methane,* a method whereby methane ($CH_4$) is extracted from coal seams and combusted in boilers for power generation (Mitchell, 1991). Large quantities of $CH_4$-rich gas are generated and stored within the coal on internal surfaces during coalification (Mitchell, 1991). Methane is a very efficient energy source.
- *Flue gas desulfurisation* is the method used to remove $SO_x$ and $SO_2$ from the flue gases produced in boilers at power plants (Shannon, 1997). It removes the pollutants before discharge to the atmosphere (Shannon, 1997)**.**
- *Fluidized-bed combustion* is a method whereby solid fuels such as coal are suspended in fluidized beds on upward-blowing jets of air during the combustion process. Fluidized bed combustion evolved from attempts to find a combustion process able to control pollutant emissions without external emission controls such as scrubbers (Shah *et al*, 2011).
- *Integrated gasification combined cycle* is a method that produces a clean coal gas (syngas), which fuels the combustion turbine (Armaroli and Balzani, 2011). Coal is combined with oxygen in the gasifier to produce the gaseous fuel, which is usually a mixture of hydrogen and carbon monoxide (syngas) (Armaroli and Balzani, 2011)**.**

- *Oxyfuel combustion* is a process where fossil fuels are burnt in pure oxygen instead of normal air (Man, *et al*., 2007). Almost all of the gas that is emitted is composed of $CO_2$ and water vapour. The vapour is condensed out and the $CO_2$ is then captured (Man, *et al.*, 2007).

A variety of technologies are being developed with a view of providing an environmentally satisfactory method of using coal as a basic fuel for power production in new plants. Some of these technologies are commercially available in a number of countries, supported by large-scale operating experience while others are still at the demonstration stage (IEA clean coal centre, 2010). A parallel approach is to build up more thermally efficient systems in order that less coal is used to generate the same amount of power, in the company of improved techniques for flue gas cleaning, for effluent treatment and for residues use or disposal. Historically, the primary focus was on $SO_2$ owing to its significant contribution to the formation of acid rain. Recently, the main focus is on $CO_2$ as a pollutant.

Unlike $NO_x$ and $SO_x$ which impact areas located near their point sources, the effect of $CO_2$ is manifested globally, and hence $CO_2$ is considered to be a global problem**.** Although there is a scientific consensus about the existence of global warming, there is no agreement about its exact cause (Nordell, 2003). The main cause of global warming is generally believed to be the release of GHGs from the burning of fossil fuels and the large-scale deforestation; leading to an increase in the greenhouse effect (Nordell, 2003). The greenhouse effect is an increase in the temperature of a planet as heat energy from sunlight is trapped by the GHGs in the atmosphere**.** Greenhouse gases are $CO_2$, methane ($CH_4$), water vapor, fluorocarbons, ozone, and nitrous oxide. Of all the GHGs, $CO_2$ is the most emitted due to anthropogenic activities**.**

Carbon dioxide is emitted in two of ways. It is emitted naturally through the carbon cycle and through human activities. Natural sources of $CO_2$ occur within the carbon cycle where billions of tons of atmospheric $CO_2$ are removed from the atmosphere by

oceans and growing plants (sinks), and are emitted back into the atmosphere annually through natural processes such as volcanic eruptions (sources) (Zeng, 2008). When in balance, the total amount of $CO_2$ emitted equals that of $CO_2$ removed from the atmosphere, and hence there is no net increase**.**

The largest anthropogenic source of $CO_2$ is the combustion of fossil fuels (mainly being coal) for power generation. Carbon dioxide concentrations in the atmosphere have increased from approximately 280 ppm in pre-industrial times to 392 ppm in 2006 (Conway, 2011), and are projected to rise to 625 ppm by 2050 should $CO_2$ emissions continue to increase in a business-as-usual scenario (Hawksworth, 2006). Increases in $CO_2$ concentration in the atmosphere have shown to be directly proportional to the global $CO_2$ emissions as well as the global temperature (Conway, 2011). Consequently, the relationship between global warming and atmospheric $CO_2$ levels attracted the attention of many researchers. For instance, as early as 1896, Svante August Arrhenius, a Swedish chemist and Nobel laureate, found that the $CO_2$ concentration in the atmosphere played an important role in allowing solar radiation to penetrate the atmosphere freely, while blocking a portion of the heat from escaping when it was re-radiated from the earth (Sun and Wang, 1996). Svante estimated, without the benefit of a computer, that doubling the concentration of $CO_2$ in the atmosphere could increase the global average surface temperature by 3.3 °C (Sun and Wang, 1996).

During the 20$^{th}$ century, the mean temperature of the Earth surface increased by approximately 0.4 – 0.8°C (Viola *et al*., 2010). Most of this increase occurred in two periods: from 1910 to 1945 (0.14 °C / decade), and since 1976 (0.17 °C / decade) (Viola *et al.,* 2010). The Intergovernmental Panel on Climate Change (IPCC) reported that, by the end of this century, there could be a global average temperature increase between 1.4 ˚C and 1.8 ˚C and sea level rise of 9 to 88 cm (Jadhav *et al*., 2007). The currently observed consequences of the global warming include rising sea

levels, melting glaciers, decreased snow cover in the Northern Hemisphere, and increased frequency of some extreme weather events**.**

As the global demand for energy increases, $CO_2$ discharge will continue to increase due to the overall dependence on coal. Since coal is the cheapest and most abundant fossil fuel available, it is unquestionable that its use shall perpetuate for years to come (Herzog and Golomb, 2004). Renewable-energy technologies have to be developed and established to be economically competitive with coal. However, the transition from coal utilisation to renewable energy is expected to take some time, and this is the period during which $CO_2$ emissions must be reduced (Herzog and Golomb, 2004). It therefore is necessary to develop processes that would capture and store $CO_2$ from the flue gas in combustion processes in order to mitigate the observed undesirable consequences of its emission. It is for this reason that research on CCS is receiving considerable attention recently.

### 2.4.1 Carbon Capture and Storage

Carbon capture and storage is a means of mitigating the contribution of fossil fuel emissions to global warming, based on capturing $CO_2$ from the atmosphere, and storing it in geologic formations or the ocean (World Bridge, 2010). Unlike other forms of sequestration, such as forestation and enhanced ocean uptake of $CO_2$, CCS technologies avoid atmospheric emissions altogether (Anderson and Newell, 2003). The currently available CCS technologies are amine-based absorption, membrane-based separation, adsorption and cryogenic separation (Figueroa *et al.*, 2008). These technologies can be applied to large point sources of $CO_2$, such as pre and post-combustion power plants, and in large industrial processes, for instance, separating $CO_2$ from flue gas, natural gas, coal bed methane, or biogas.

The CCS technology has already been implemented in areas such as Sleipner in Norway, and Otway in Australia (Surridge, 2009). South Africa, being a developing

country that has a range of technical and institutional strengths, and the highest dependence on coal in the continent, must employ CCS technologies to take responsibility for the $CO_2$ emissions it makes. An intense utilisation of coal translates into more $CO_2$ emissions. As illustrated in Figure 2.1, $CO_2$ emissions in South Africa are just as intense as the country's dependence on coal, thereby making South Africa a suitable country in which CCS technologies may be implemented.

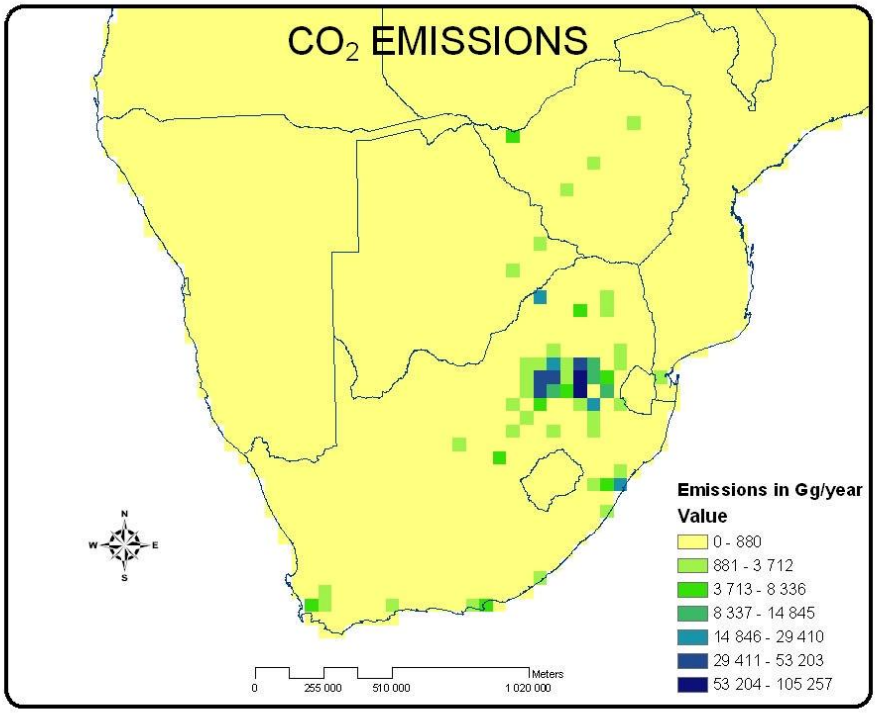


**Figure 2.1**: Carbon dioxide emissions in South Africa (Surridge, 2009).

South Africa is the 12$^{th}$ largest $CO_2$ emitter globally, producing 10.04 tons of $CO_2$ per person per year (Tomlinson *et al.*, 2010). 337.4 Mt (Million tons) is the total amount of $CO_2$ produced in South Africa, and this includes emissions from the automobiles, power stations, gasification plants, metallurgical plants, and other industries (IEA Statistics, 2010). Eskom, and Sasol are the biggest consumers of coal and hence are the leading emitters of $CO_2$ in the country. According to the annual report released by Eskom in 2010, 224.7 Mt of $CO_2$ was released from 12% concentrated gas steam

during the 2009/10 financial year (Eskom, 2010). Although Sasol uses the Benfield process to absorb and capture 90-98% of $CO_2$ produced, Sasol- Sasolburg and Secunda combined, are reported to emit 30 Mt of $CO_2$ annually (Engelbrecht, 2004). It was observed that approximately 39% of $CO_2$ emissions are non-sequestrable because of their diffuse nature (Surridge, 2009). About 65% of the $CO_2$ sequestrable emissions are linked to electricity generation, making Eskom the major source of $CO_2$ emissions in South Africa (Surridge, 2009).

Essential steps towards the establishment of the CCS technology have already begun in South Africa. The body, namely The South African Centre for Carbon Capture and Storage (SACCCS), which oversees all the CCS projects taking place in the country, was launched in 2009. The main objective of the Centre is to facilitate a suitable platform for the establishment and implementation of CCS projects. In 2010, the SACCCS launched an atlas, which highlighted that South Africa has about 150 Gigatons (Gt) of storage capacity for injected $CO_2$ (Cloete, 2010). The majority of the storage capacity is located offshore, which is a challenge for South Africa because there are high logistical costs associated with offshore storage.

The largest storage volume, representing about 98% of the total storage potential, is in the Mesozoic basins along the coast of South Africa (Cloete, 2010). This storage capacity is mainly in the capacity of saline formations in the Outeniqua, Orange, and Durban or Zululand basins (Cloete, 2010). It was estimated that the Outeniqua basin has a storage capacity of 48 Gt, the Orange basin could store 56 Gt, and the Durban/Zululand basin has 42 Gt of storage potential (Cloete, 2010). Less than 2% of the estimated storage capacity in South Africa occurs onshore (Cloete, 2010). Of the total onshore storage capacity, 0,46 Gt is in the Zululand basin, 0,40 Gt is in the Algoa basin, and 1,2Gt is in unmineable coal seams (Cloete, 2010). It is anticipated that a CCS demonstration plant in South Africa will be operational by the year 2020 (Surridge and Cloete, 2009).

Some researchers are looking at the feasibility of $CO_2$ sequestration by mineral carbonation in South Africa. Vogeli (2010) identified magnesium (Mg) and calcium (Ca) rich minerals (plagioclase, olivine, orthopyroxene, clinopyroxene) present in platinum mine tailings as good candidates for mineral carbonation because they mimic natural weathering processes where these minerals react with gaseous $CO_2$ to form Ca or Mg carbonates. Doucet (2010) also conducted research on $CO_2$ sequestration by steel furnace slags, phosphogypsum and mine tailings from different mine sectors.

## 2.5 COAL ASH

In addition to the environmental challenges presented by coal utilisation, further predicaments are faced with respect to the ash that forms as a result of the combustion of coal. The combustion of lignite, sub-bituminous, bituminous coal, and anthracite for power generation produces a range of coal combustion residues, also known as coal ash (Querol *et al.*, 2002**).** Coal combustion residues are solid wastes that remain behind in a combustion chamber as a result of the incombustible inorganic compounds bonded in the chemical structure of coal (Haynes, 2009)**.** Coal combustion residues include fly ash, bottom ash, and boiler slag. About 90% of the coal ash produced in South Africa is fly ash generated during combustion.

### 2.5.1 Fly Ash

Fly ash is defined as a fine-grained powder, which is mainly composed of spherical glassy particles, produced during the combustion of pulverized coal (Ahmaruzzaman, 2010)**.** It consists of small particles of mineral residue which are carried up and out of the boiler in the flow of exhaust gases. It is categorized as a pozzolan. Pozzolans are siliceous and aluminous materials that form cementitious products when combined with water and calcium hydroxide (CaOH) at ambient temperatures (Ahmaruzzaman, 2010)**.** The pozzolanic properties of fly ash, in addition to its lime binding capacity,

make it useful for the manufacture of cement, building materials, concrete, and concrete-admixed products. Fly ash may also be used in road constructions, and structural filling. The chemical composition of fly ash include silica ($SiO_2$), alumina ($Al_2O_3$), magnetite ($Fe_3O_4$), and hematite ($Fe_2O_3$) at varying percentages depending on the composition of the feed coal (Ahmaruzzaman, 2010)**.** Properties of fly ash also depend on such factors as pulverizing and combustion conditions, and conditions of deposition of fly ash. Hematite enables its use for the synthesis of zeolite, alum, and precipitated silica. The other important physicochemical characteristics of fly ash, such as bulk density, particle size, porosity, water holding capacity, and surface area, makes it suitable for use as an adsorbent (Yan *et al.,* 2002)**.**

Although certain amounts of fly ash are utilized by different industries, significant amounts are still being disposed of in lagoons and ash dumps. Fly ashes with high-unburned-carbon content, referred to as fly ash carbons, are an increasing problem for the utility industry, since they cannot be marketed as a cement extender and, therefore, have to be disposed. The current annual production of coal ash worldwide is estimated around 600 Mt, with fly ash constituting about 500 Mt (75–80% of the total ash produced) (Yan *et al.,* 2002)**.** Consequently, the amount of fly ash, released by coal using industries and power plants is increasing throughout the world, and the disposal of large amounts of fly ash has become a serious challenge as far as environmental regulations are concerned (Yan *et al.,* 2002)**.** The present day utilisation of coal ash on worldwide basis varies widely from a minimum of 3% to a maximum of 57%, yet the world average only amounts to 16% of the total ash (Yan *et al.,* 2002)**.**

### 2.5.2 Bottom Ash

Bottom ash consists of agglomerated ash particles, formed in pulverized coal furnaces or gasifiers that are too large to be carried in the flue gases, and impinge on the furnace walls or fall through open grates to an ash hopper at the bottom of the furnace (U.S. Environmental Protection Agency, 2010). Physically, bottom ash is typically grey to black in colour, is quite angular, and has a porous surface structure. It is a coarse material of surface texture and size ranging from fine gravel to fine sand (U. S. Department of Transportation, 2011). It is composed of $SiO_2$, $Al_2O_3$, and Fe with small amounts of Ca, Mg and sulphate ($SO_4^{2-}$) (U. S. Department of Transportation, 2011). The quality of bottom ash is governed by the coal source and not by the type of furnace (U.S. Environmental Protection Agency, 2010).

### 2.5.3 Boiler Slag

Boiler slag is the molten bottom ash collected at the base of slag tap and cyclone type furnaces that is quenched with water. When the molten slag comes in contact with the quenching water, it fractures, crystallizes, and forms pellets (Centre for Applied Energy Research, 2010). This boiler slag material is made up of hard, black, angular particles that have a smooth, glassy appearance.

Boiler slag particles are uniform in size, hard, and durable with a resistance to surface wear. In addition, the permanent black colour of this material is desirable for asphalt applications. Since boiler slag is angular, dense and hard, it is often used as a wear-resistant component in surface coatings of asphalt in road paving (Centre for Applied Energy Research, 2010). Finer-sized boiler slag can be used as blasting grit and is commonly used for coating roofing shingles. Other uses include raw material for the manufacture of cement and in colder climates, it is spread onto icy roads for traction control.

### 2.5.4 Coal Ash in South Africa

South Africa currently produces more than 40 Mt of coal ash per annum, of which only about 5.6 % of it is utilized for different purposes, such as backfilling of mines, soil stabilisation in geotechnical applications, a pozzolan for cement and concrete applications, and an adsorbent for inorganic wastes (Bada and Potgieter-Vermaak, 2008). The remaining coal ash is disposed in ash dumps and heaps.

Sasol and Eskom are the biggest consumers of coal and hence the biggest coal ash producers in South Africa. Sasol utilized about 40 Mt of coal for its gasification process in 2009 (Bada and Potgieter-Vermaak, 2008). No information about the ash produced in 2009 was given, however 7 million tons and 1.5 million tons of ash were generated in Secunda and Sasolburg respectively in 2005 (Bada and Potgieter-Vermaak, 2008**).** According to the Eskom annual report released in 2010, 122.7 Mt of coal was utilized to generate power, and 36.01 Mt/yr of ash was produced, whilst 2 Mt/yr of it was sold (Bada and Potgieter-Vermaak, 2008). This poses a huge ash disposal and management problem, and it demonstrates that, although attempts are made to utilize ash, a substantial amount of it is still disposed of on ash dumps**.** The destructive effects this practice has on the environment include wind and water pollution, and the leaching of salts and heavy metals into the groundwater (Yan *et al.*, 2002). Utilisation of coal ash is, for this reason, encouraged worldwide in order to reap the economic and environmental benefits of coal ash.

**Research on South African Coal Ash**

In South Africa, many researchers have carried out the studies of different aspects on coal-ash, such as its utilization, economic benefits, health effects, and its environment-related issues. Matjie *et. al.* (2005) conducted research on gasification ashes and steam station ashes to provide a detailed characterisation of these ashes and

to study its health effect with regards to toxic metals. The preliminary results indicated that CCSEM (Computer-Controlled Scanning Electron Microscopy) and X-ray diffraction spectroscopy (XRD) are able to identify and describe the minerals and phase proportions in gasification ash, fly ash and clinker samples. ICP-MS (Inductively Coupled Plasma Mass Spectroscopy) and ICP-OES (Inductively Coupled Plasma Optical Emission Spectroscopy) analyses of the ash leachates showed that none of the analysed leachates exceeded the United States Environmental Protection Agency regulatory limits for As, Ag, Ba, Cd, Cr, Pb, Hg and Se. As result, these ashes were classified as non-hazardous materials.

Kruger (1997) showed that beneficiation of fly ash in South Africa may be used as a means to create new opportunities in the market-place, and hence contributing to the advancement of the South African economy. Kruger (n. d.) further illustrated that apart from being used as a cement-extender, coal ash may be used as a filler in polymer industries, as a neutraliser to acidic soils, and as a support for underground gold mine cavities. Leslie *et al.,* (2003) demonstrated that South African fly ash may be used to treat acid mine drainage and to produce high quality zeolites from the residual solids. Mlambo *et. al.*, (2011) showed that injecting fly ash slurries in deep geological reservoirs could improve the reservoir integrity and the safety of $CO_2$ sequestration in South Africa.

## 2.6 ADSORPTION

Adsorption is a process that occurs when a gas or liquid solute accumulates on the surface of a solid or a liquid (adsorbent), forming a molecular or atomic film (the adsorbate) (Jaradat, 2009). The surface of solids tends to attract and retain other molecules when brought in contact with a gas or solution. This is due to imbalanced forces of attraction from molecules on the surface of the adsorbent and in the bulk phase of the adsorbate (Krkljuš, 2011). Molecules on the surface of the adsorbent

have higher energy than those in the bulk. This results in a higher concentration of adsorbate molecules on the surface of the solid. It is different from *absorption*, whereby a substance diffuses into a liquid or solid to form a solution. The term *sorption* encompasses both adsorption and absorption, while *desorption* is the reverse process. Similar to surface tension, adsorption is a consequence of surface energy (Jaradat, 2009).

Depending on the nature of the forces between an adsorbate and an adsorbent, adsorption may occur in two ways namely:

1) Physisorption: weak forces of attraction, known as Van der Waals interactions, which attach gas or solution molecules to the surface of the solid (Jaradat, 2009).
2) Chemisorption: strong forces of attraction hold an adsorbate and an adsorbent together, driven by a chemical reaction occurring at the exposed surface (Jaradat, 2009). Adsorption is governed by formation of electronic bonds, either ionic or covalent, depending on the type of reactive chemical species involved (Jaradat, 2009).

### 2.6.1 Factors Affecting Adsorption of Gases on Solids

The factors affecting adsorption of gases on solids are:

- *Nature of the gas to be adsorbed* – Physisorption is non-specific in nature, therefore, every gas can adsorb on any solid to a lesser or greater extend (Keller and Robens, 2003). Under given conditions of temperature and pressure, easily liquefiable or water soluble gases such as $CO_2$, $NH_3$, and HCl are adsorbed to a greater extent than permanent gases such as $O_2$, $N_2$, $H_2$ (Keller and Robens, 2003).

- *Nature of the adsorbent* - It has been discovered that different solids adsorb the same gas to different extents at the same temperature. This is attributable to the porosity and surface area that different adsorbents have. Since adsorption occurs on the surface of the adsorbent, the chemical composition and the geometry of the adsorbent are very important. The geometry of an adsorbent includes: specific surface area, pore size distribution, specific pore volume, particle size distribution and density (Keller and Robens, 2003).
- *Temperature* - Since adsorption is exothermic in nature, an increase in temperature decreases adsorption. Adsorption is very dependent on temperature.

- *Pressure* – At constant temperature, the adsorption of a gas increases with pressure.

- *Surface area / porosity of the adsorbent* – The notion of certain materials being porous dates back to ancient times (Tien, 1994). Conventionally, porous materials are either amorphous or crystalline compounds that contain pores for the reversible passage of gas or fluid (Jacobs, 2007). These compounds are categorized on the basis of pore size diameter: macroporous (>500 Å), mesoporous (15-500 Å) and microporous (<15 Å) (Jacobs, 2007). The higher the surface area, the higher the adsorption. This is because higher surface area implies that more of the adsorbent molecules are exposed, and hence a larger platform for adsorption to take place. The surface area of the adsorbent may be increased or improved in one of the following ways:

    - by making the surface of the adsorbent rough through mechanical rubbing or by depositing finely dispersed metals on the surface of the adsorbent via electroplating;
    - by crushing the sample. This is however to be carefully practiced because particles crushed too finely will result in blockage of the

pores of the adsorbent, thereby decreasing the surface area as opposed to increasing it;

- by degassing the sample. This ensures that unwanted gases are removed in order to increase the adsorption sites on which the gas in question is to adsorb.

In the context of this research, an adsorbate is $CO_2$ gas and adsorbent is coal ash. According to the theory proposed by Dubinin, a carbonaceous material, such as coal ash, contains some adsorption centers, called primary sites (Li, 2002). When a molecule of the adsorbate adsorbs on a primary site, the adsorbed molecule can then act as a secondary center for the adsorption of more molecules (Li, 2002). The primary sites on the carbon surfaces could be any spots that have a high affinity for $CO_2$ molecules, where the molecules are attached to the carbonaceous material through weak Van der waals interactions. These primary sites may be enriched with oxygen-containing and nitrogen-containing functional groups in order to amplify the adsorption potential (Li, 2002).

A suitable adsorbent to be used in the adsorption process for CCS must be cheap, selective for $CO_2$ despite the process temperature, have high surface area and pore volume, enable quick diffusion of $CO_2$ between the adsorbent particles, and enable reversible adsorption especially during pressure swings (Jacobs, 2007). Such characteristics must be constant throughout a large number of adsorption-desorption cycles in the long run to ensure a prolonged usability of the adsorbent (Jacobs, 2007). Activated carbons, zeolites, pillared clays, metal oxides and their surface modifications have been widely reported for $CO_2$ capture (Guo, 2006; Lee, 2002; Ramis, 1991). These adsorbents may retain $CO_2$ via weak physisorption and/or strong chemisorption interactions.

Adsorption is a potentially attractive alternative to capturing $CO_2$ from stationary sources in the context of CCS technologies. Activated carbon and zeolites are state-

of-art adsorbents which may be used for $CO_2$ adsorption, however it is beneficial for other much cheaper adsorbents to be explored and manufactured.

### 2.6.2 Adsorption Methods

There are four typical methods used to measure the adsorption potential of materials, namely; 1) volumetric adsorption method, 2) gravimetric adsorption method, 3) pulse adsorption method, and 4) dynamic adsorption method (Bel, 2007).

#### Volumetric Adsorption Method

The volumetric adsorption method consists of pressure sensors, valves, and vacuum system. The inner volume is calibrated before measuring the amount of gas adsorbed by the material. The amount of the adsorbed gas is calculated by subtracting the pressure of the adsorptive gas at equilibrium from the initial pressure of the adsorptive gas, using the ideal gas equation (Bel, 2007). The advantage of the volumetric adsorption method is that, it could achieve the high throughput measurement of surface area and porosity. However, its disadvantage is that, it is difficult to account for the non-ideal gas behavior for high density gas and thermal transpiration for the low pressure measurement (Bel, 2007).

#### Gravimetric Adsorption Method

The gravimetric adsorption method consists of a balance and a pressure sensor. This method is useful when measuring adsorption at high pressures and when water vapor is an adsorptive gas. To calculate the amount of gas adsorbed, it is necessary to correct for the buoyancy during the measurement (Bel, 2007). Since it is difficult to maintain the temperature stability at low temperatures, the gravimetric method is commonly used in measurements carried out at temperatures above room temperature.

**Pulse Adsorption Method**

The pulse adsorption method is used when stable gases, such as $H_2$ or CO, adsorb on rare metals like Pt and Pd to evaluate the active surface area. A thermal conductivity detector is commonly used as a detector (Bel, 2007). Before the adsorption measurement, the sample needs to undergo pre-treatment by oxidation and reduction in order to clean the surface. The carrier gas such as He then flushed over the sample, followed by the doses the adsorptive gas as pulses (Bel, 2007).

**Dynamic Adsorption Method**

The dynamic adsorption method is used in BET 1-point method and TPD (Temperature Programmed Desorption) spectroscopy (Bel, 2007). It also uses a thermal conductivity detector to detect the change in the gas concentration after going through the sample (Bel, 2007). The dynamic method can measure the amount of gas adsorbed quickly compared to other methods and is useful for the quality control. However, the most commonly used adsorption methods are the volumetric and the gravimetric adsorption systems.

### 2.6.3 Previous Research on $CO_2$ Sequestration by Adsorption

The biggest challenge faced by existing commercial CCS plants is that chemical adsorption processes, based on aqueous alkanomine solvents, are very expensive in terms of capital and running costs due to large amounts of water needed (Gray *et al.*, 2004). Consequently, the development of a low-cost means of capturing $CO_2$ is very crucial when applied on an industrial scale (Arenillas *et al.*, 2005). Some of the research done on the fabrication of $CO_2$ adsorbents is given below.

Plaza *et al.* (2009) prepared a series of carbon adsorbents from a low-cost biomass residue (olive stones). Two different approaches were studied: 1) activation with $CO_2$,

and 2) heat treatment with gaseous ammonia. The results showed that both methods are suitable for the production of adsorbents with a high $CO_2$ adsorption capacity, and their potential application in post-combustion $CO_2$ capture. It was found that the presence of nitrogen functionalities enhances $CO_2$ adsorption capacity, especially at low partial pressures.

Gray *et al.* (2004) developed amine-enriched sorbents based on a fly ash carbon concentrate. The initial fly ash carbon sorbents were generated by the chemical treatment of carbon-enriched fly ash concentrates with a 3-chloropropylamine-hydrochloride solution at 25˚C. It was observed that these amine-enriched fly ash carbon sorbents performed at a 9% $CO_2$ capture capacity based on commercially available sorbents.

Maroto-Valer *et al.* (2008) also developed activated fly ash derived sorbents for $CO_2$ capture. The samples were steam activated at 850˚C, resulting in a significant increase of the surface area (1075 $m^2/g$). The activated samples were impregnated with different amine compounds, and the resultant samples were tested for $CO_2$ capture at different temperatures. It was discovered that the impregnation process resulted in a decrease in surface areas, which indicated blockage of the pores. The highest adsorption capacity was observed at 30˚C and 70˚C for the amine impregnated activated carbons, attributable to a combination of physical adsorption inherent from the parent sample and chemical adsorption of the loaded amine groups.

Montes-Hernandez *et al.* (2009) conducted an experiment to capture $CO_2$ by aqueous carbonation of fly ash. The carbonation reaction was carried out in two successive chemical reactions: the irreversible hydration of lime and the spontaneous carbonation of calcium hydroxide suspension. 82% of the $CaO–CaCO_3$ chemical transformation was estimated by pressure-mass balance after 2 hours of the reaction at 30˚C. In addition, the qualitative comparison of X-ray diffraction spectra for reactants and products revealed a complete $CaO–CaCO_3$ conversion. The carbonation

efficiency of CaO was independent on the initial pressure of $CO_2$ (10, 20, 30 and 40 bar) and it was not significantly affected by reaction temperature (room temperature 20–25˚C, 30˚C and 60˚C) and by fly-ash dose (50g, 100g, 150 g). This experimental study demonstrated that 1 ton of fly-ash could sequester up to 26 kg of $CO_2$, which confirmed the possibility of using this alkaline fly-ash for $CO_2$ mitigation.

Muriithi, *et al.* (2011) studied the carbonation of brine-impacted fractionated coal fly ash as an implication of $CO_2$ sequestration. Controlled carbonation reactions were carried out in a reactor set-up to evaluate the effect of fractionation on the carbonation efficiency of fly ash. Chemical and mineralogical characteristics of fresh and carbonated ash were evaluated using X-Ray Fluorescence spectroscopy (XRF), Scanning Electron Microscopy (SEM), and XRD. Brine effluents were characterized using ICP-MS and IC. A factorial experimental approach was employed in testing the variables. The 20-150 mm size fraction was observed to have the highest $CO_2$ sequestration potential of 71.84 kg of $CO_2$ per ton of fly ash while the >150 mm particles had the lowest potential of 36.47 kg of $CO_2$ per ton of fly ash. Carbonation using brine resulted in higher degree of calcite formation compared to the ultra-pure water carbonated residues.

## 2.7 CHAPTER SUMMARY

The reduction of $CO_2$ emissions in South Africa, and globally, is vital in terms of reducing the predicted trend of global warming. Carbon capture and storage technologies are at various stages of development and deployment globally, but limited work has been done in South Africa to date. Owing to the fact that coal ash is abundant, cheap, porous, and may pose some unburnt carbon content and metal oxides (e,g, CaO, MgO) that could form stable carbonate compounds with $CO_2$, it may have potential as a $CO_2$ adsorbent.

In spite of the abundant literature on $CO_2$ adsorption, very few studies have been conducted on South African ash as a $CO_2$ adsorbent. South African ash is likely to

differ from Northern Hemisphere ash due to the conditions which prevailed during the formation of the parent coals, the boiler design and operation. Thus, research on $CO_2$ adsorption still needs to be conducted using South African ash. The University of Western Cape currently has a research group that studies coal ash, and so does the Coal and Carbon Research Group at the University of the Witwatersrand.

Fly ash and bottom ash samples from different industries were tested in a volumetric adsorption system. The ash samples were not treated by any solvent during this research; that is, raw ash was tested.

# CHAPTER 3

# EXPERIMENTAL METHOD

This chapter describes the sample preparation and the adsorption experimental work. The four ash samples used in this study were obtained from three different industries, all of which use coal, namely; 1) a coal power station, 2) a petrochemical industry, and 3) a metallurgical plant. These industries were chosen as a representation of different ways in which coal is used in South Africa.

## 3.1 THE PULVERISED FUEL ASH SAMPLE

More than 36 Mt of ash are produced by the South African power plants each year, the greater part of which is fly ash (Bada and Potgieter-Vermaak, 2008). All the operational coal power stations in South Africa utilise pulverised fuel (PF) technology.

The pulverised fuel ash (PF ash) sample was received as a homogenous, finely grained, grey powder, as illustrated in Figure 3.1. The total amount of the sample obtained from the power plant was 12 kg. The particle size range of the sample was 38 µm – 90 µm. The essential physicochemical characteristics of fly ash, such as bulk density, particle size, porosity, water holding capacity, and surface area, make it suitable for use as an adsorbent (Yan *et al.,* 2002**).**

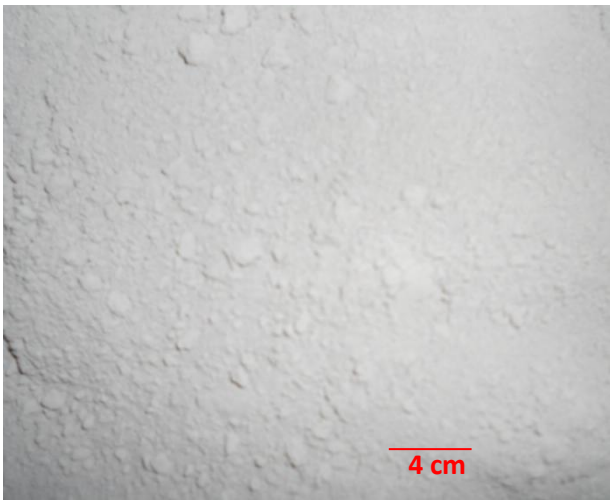


**Figure 3.1**: An optical image of the PF ash sample.

## 3.2 THE GASIFICATION ASH SAMPLE

Over 8.5 Mt of coal ash is produced in South Africa via the coal-to-liquid gasification technology each year, mostly as coarse ash (Matjie and Van Alphen, 2008). The bulk gasification ash (coarse and fine ash) particles are formed at elevated temperatures and pressures by the transformation of included minerals in the coal and in the extraneous rock fragments (Matjie and Van Alphen, 2008). The ash particles are removed from the gasifier and either disposed of on ash dumps or beneficiated and used as a feed product in the cement industry or for road construction.

The gasification ash (G ash) sample was received as a mixture of course ash and fine ash, consisting of white to grey stone in a black glassy matrix as shown in Figure 3.2. About 30 kg of the ash sample was obtained from the gasification plant, with a particle size range of 45 µm - 40 000 µm (4 cm).


**Figure 3.2**: An optical image of the G ash sample.

## 3.3 THE METALLURGICAL PLANT SAMPLES

Some of the South African refining operations use coal-fired water-tube boilers to generate saturated steam (Implats, 2011). The steam is used as a primary heat source to process operations in reactors (autoclaves) and heat exchangers (crystallisers and evaporators). The amount of coal ash produced from this process is about 21,000 tons/year (Implats, 2011).

The metallurgical plant ash samples were collected from two different boilers at the refinery: (1) the chain grate boiler (rated at 22 tons/hr capacity), and (2) the spreader stoker boiler (rated at 45 tons/hr). The samples collected from the chain grate and the spreader stoker boilers were named chain grate ash (CG ash) and spreader stoker ash (SS ash), respectively. Both of the CG ash and SS ash samples had fine, homogeneous texture and were black in colour as demonstrated in Figures 3.3 and 3.4. The quantity of the samples obtained from each boiler was 6 kg. The particle size range was 38 µm - 1000µm for both samples.

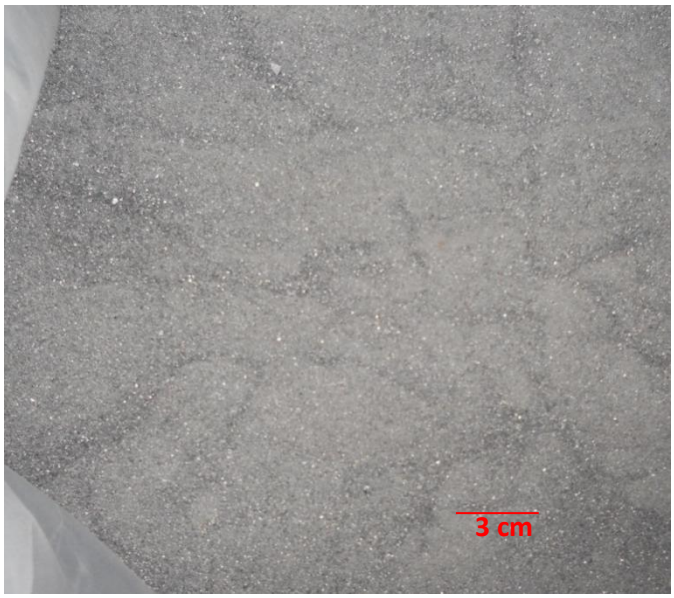


**Figure 3.3**: An optical image of the CG ash sample.

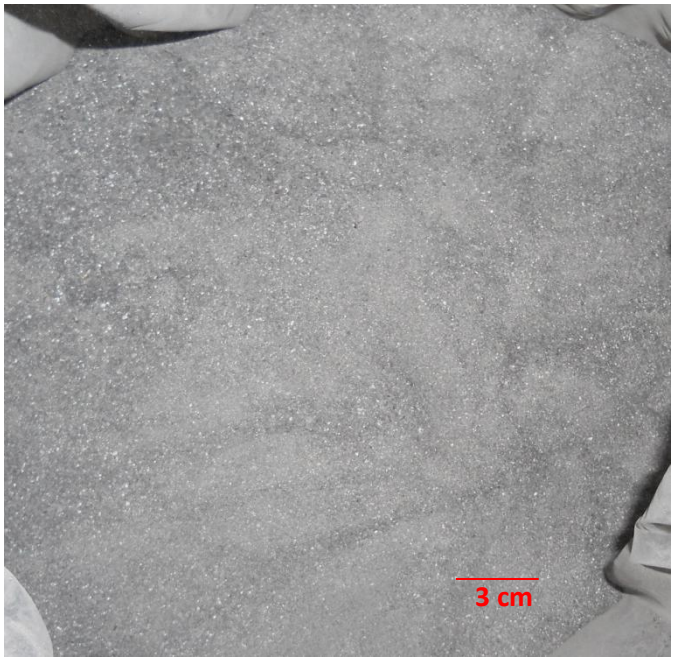


**Figure 3.4**: An optical image of the SS ash sample.

## 3.4 SAMPLE PREPARATION

Each of the samples was dried for 24 hours at room temperature to remove ambient moisture, split representatively using the cone and quartering method and ground to a homogenous texture of a particle size of 75 μm. Following grinding, the samples were split for characterisation by different techniques and for the adsorption process. The samples were further dried in an oven at 105 °C to remove residual moisture. Each of the samples was divided into 5 segments for the adsorption process and for analysis by various techniques. The experiment and characterisation techniques that were employed in this project are as follows:

- The adsorption experiment
- BET technique
- X-ray diffraction technique
- Thermogravimetric analysis
- Petrography

The entire sample preparation procedure was carried out at the School of Chemical and Metallurgical Engineering, at the University of the Witwatersrand. A summarized technical programme is given in Figure 3.5.

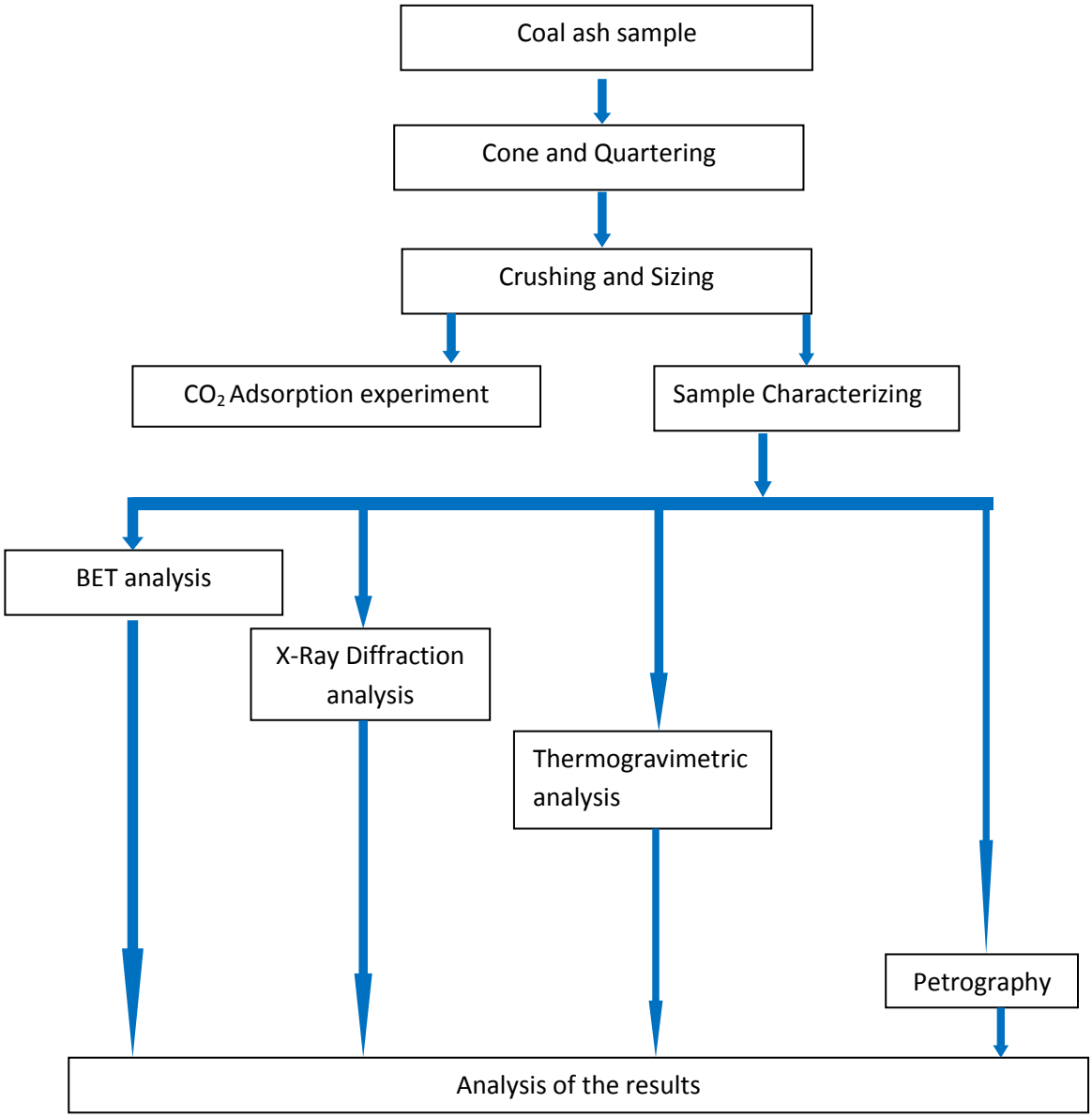


**Figure 3.5**: A summary of a technical programme for this research project.

### 3.4.1 The Cone and Quarter Technique

Each of the ash samples were divided into four sections using the cone and quarter technique. This is a technique that is carried out to ensure a homogeneous and representative separation of the sample particles. The sample is piled into a cone

shape with a flattened top, and the cone divided into quarters, as illustrated in Figure 3.6. The opposite quarters are kept aside while the remaining quarters are mixed together to form a second cone. The process is repeated until a desired sample size is reached.

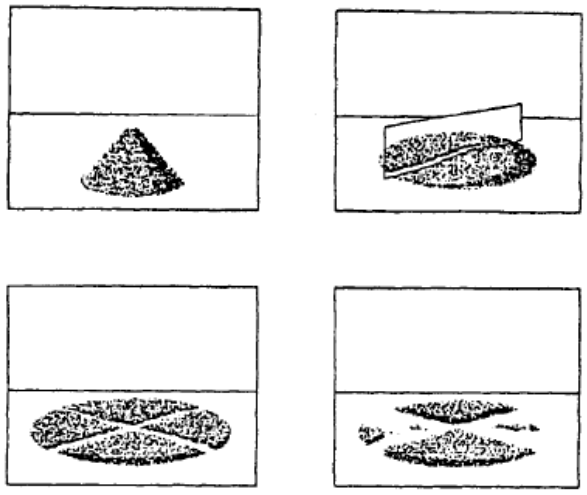

**Figure 3.6**: The cone and quarter technique (Schumacher *et al.*, 1990).

### 3.4.2 Milling and Sieving

Following the cone and quartering technique, the samples were sieved to prevent over milling of the small-sized particles, using test sieves. A vibrating sieve shaker was used to enable efficient separation of the particles. The particles with sizes smaller than 75 μm were kept aside while bigger particles were crushed to a particle size of 75 μm using a Reutsch ZM centrifugal mill. Particles larger than 2 mm were crushed using a hammer before being introduced to the grinder because it can only take the maximum sample size of 2 mm**.** The samples were split into representative sub-samples with an 8-test-tube centrifugal splitter.

### 3.4.3 Drying

After a desired particle size was achieved, the samples were dried at 105 °C for 30 minutes in a Labcon oven to drive off the moisture. The samples were then kept in a tightly closed vial and placed in a refrigerator.

## 3.5 THE VOLUMETRIC ADSORPTION METHOD

The volumetric adsorption method is one of the methods mostly used in the adsorption experiments, hence was used in the undertaking of this research project. In the volumetric method, the amount of the gas adsorbed is calculated from state equation of gas.

### 3.5.1 The Volumetric Adsorption Equipment

The volumetric adsorption system (VAS) used in this project consists of two chambers A and B (Figure 3.7), with volumes $V_A$ and $V_B$ respectively. Each chamber incorporates its own pressure transducer to measure the gas pressures $P_A$ and $P_B$ respectively. The chambers are separated from each other and from the surroundings by the valves $V_1$, $V_2$ and $V_3$, shown in Figure 3.8. The valves $V_1$ and $V_3$ connect the system to high pressure $CO_2$ cylinder and a vacuum, respectively. The instrument is situated inside a Labcon air heated oven in order to ensure isothermal conditions during the experiment.

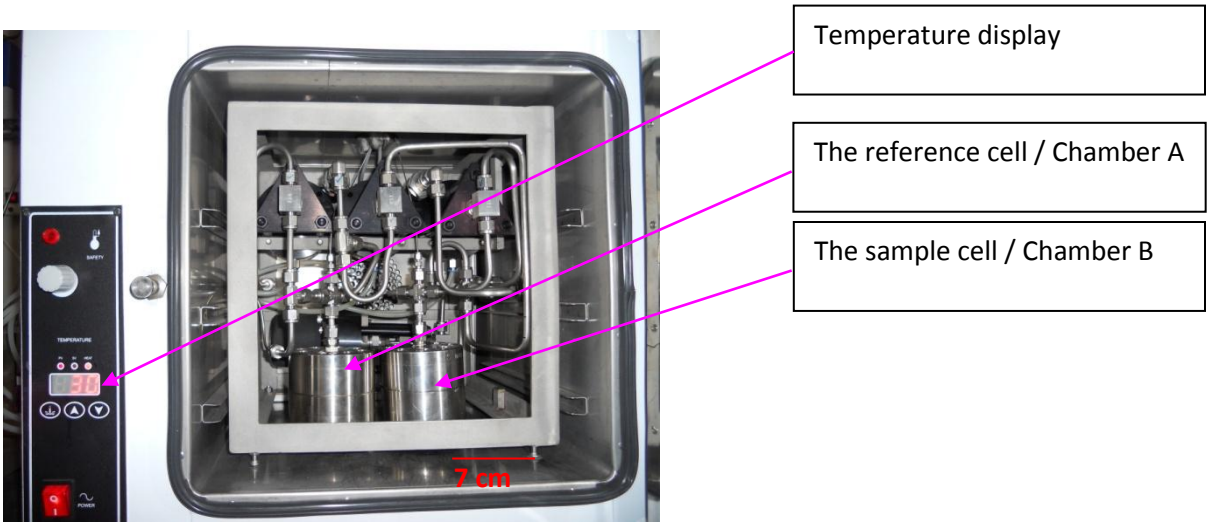


**Figure 3.7**: Inside the VAS equipment.

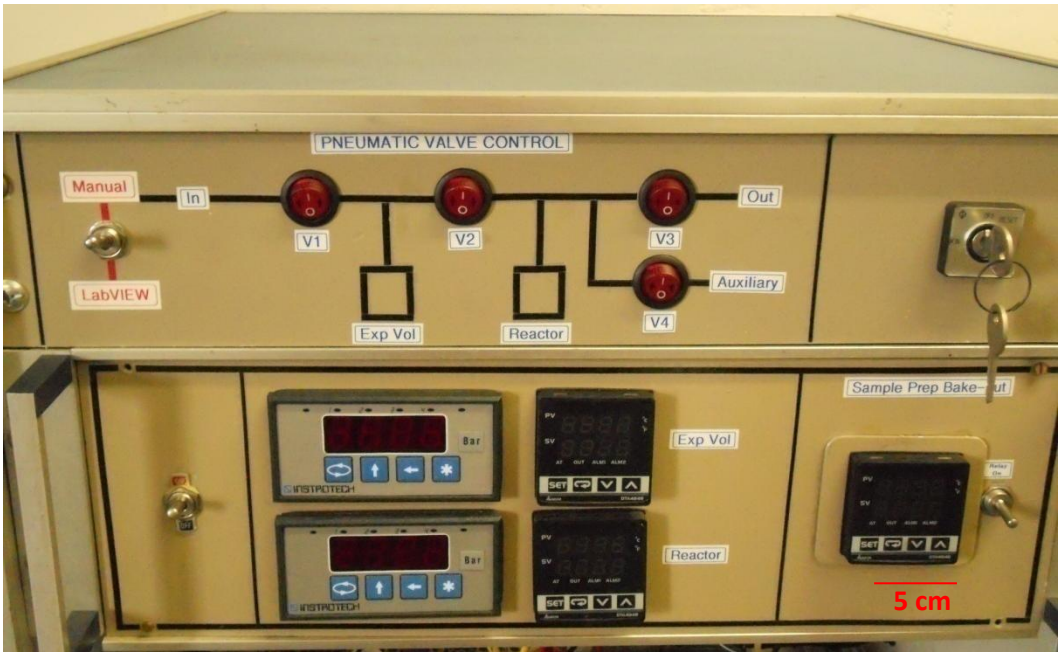


**Figure 3.8**: An optical image of a pneumatic valve control.

Figure 3.9 shows a sample cell connected to the vacuum pump during the degassing procedure. This process is undertaken prior to the adsorption process in order to

remove the gasses which might have adhered on the surface of the sample. Degassing the sample is important because it unlocks the pores of the sample, and it ensures that the only gas in the sample is that being tested ($CO_2$). The vacuum-pump pumps the air from the sample vessel to the outside via the volatile-trapping zeolite bed.

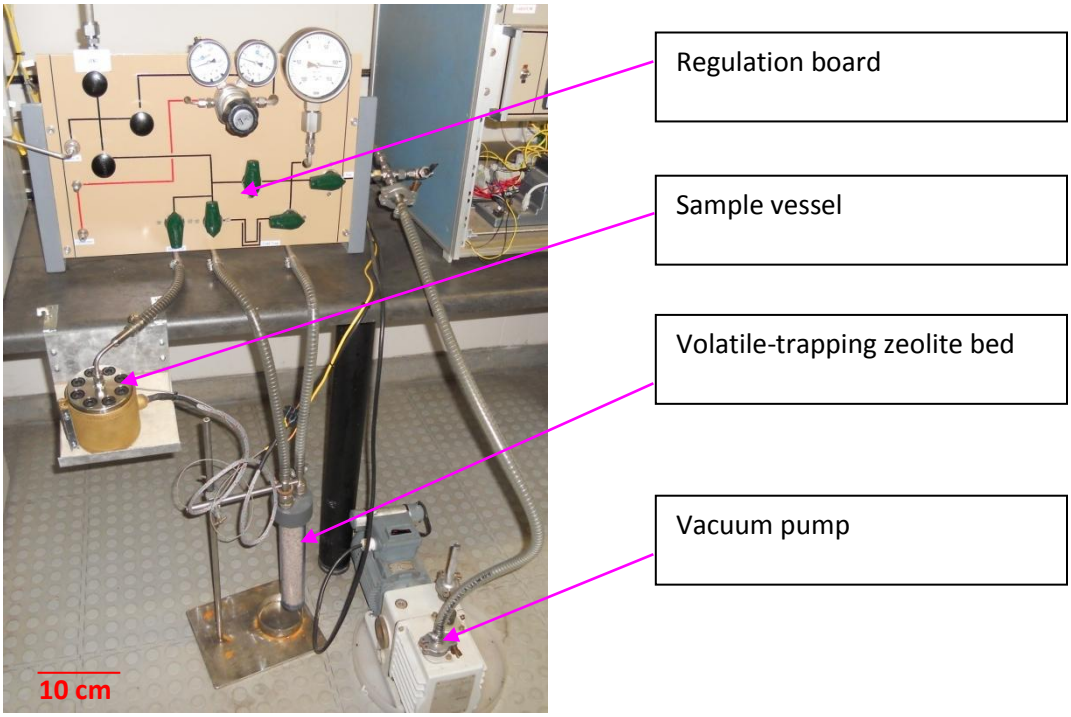


**Figure 3.9**: A sample vessel connected to the vacuum pump during the degassing process.

All the procedures carried out during the adsorption process were followed in real-time using a computer interface (Figure 3.10) that allows the user to monitor various physical conditions (i.e. temperature and pressure) during the adsorption experiment.

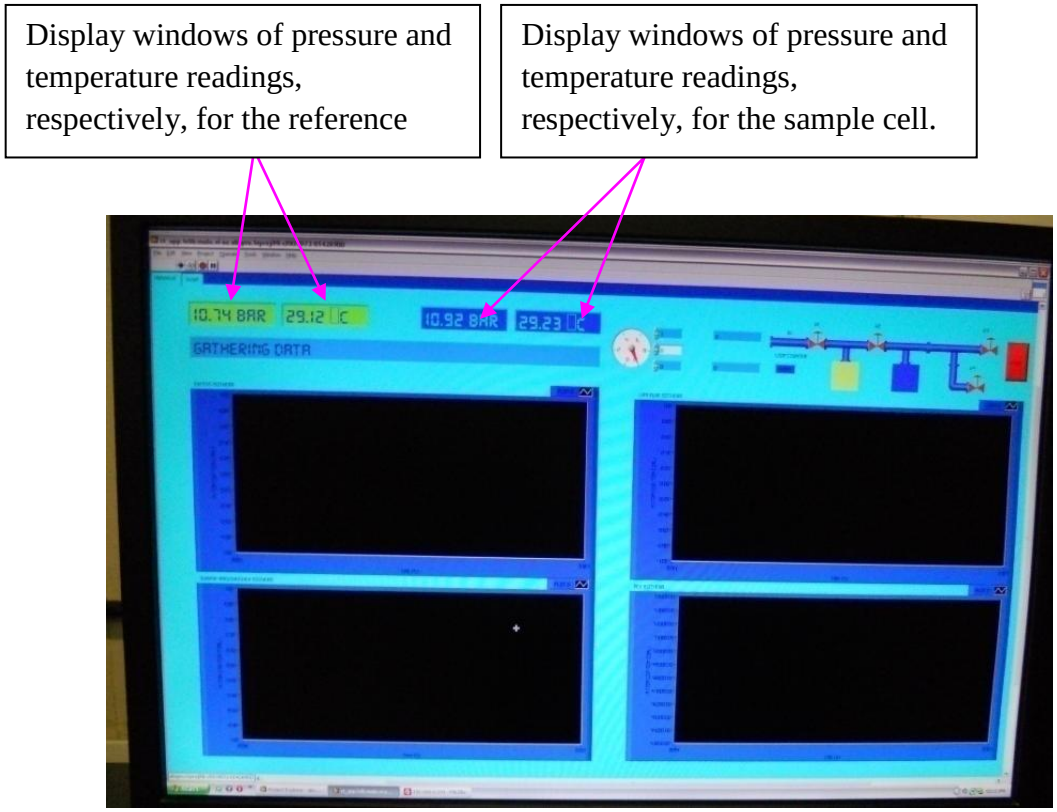


**Figure 3.10**: The computer interface showing the temperature and pressure readings taken during the course of a typical adsorption experiment.

### 3.5.2 The Adsorption Process

The sample under study is placed in chamber B (also referred to as the sample cell) and the chamber is evacuated using a vacuum pump to prevent air from adsorbing on the sample. Chamber A (the reference cell) is filled with the $CO_2$ gas, while keeping the sample cell under vacuum. By briefly opening and closing $V_2$ as shown in Figure 3.11, the amount of gas in the reference cell will decrease, while that in the sample cell increases. This process proceeds until the pressure in both chambers is equal, which is when the two chambers are at equilibrium. The amount of gas supplied to the sample cell can be monitored *in situ* using the LABVIEW software, which records changes in pressure at 1 second intervals. If the sample is either porous or has

reactive sites, the pressure in the sample cell will drop further, indicating that some of the $CO_2$ molecules have adsorbed on the sample. The amount of $CO_2$ (in moles) adsorbed by the sample is determined using the equation of state called the van der Waals equation, given in Eq. 3.1.

$$\left(P + \frac{n^2 a}{V^2}\right)(V - nb) = nRT \qquad \text{Eq. 3.1}$$

Where *a* and *b* are constants specific to the gas employed.

*a* - is a measure of the attraction between particles

*b* - is the volume excluded by a mole of the specific gas particles

*n* - is the number of moles

*V*- is the total volume of the container containing the gas

*R*- is the universal gas constant

*T*- is the absolute temperature

*P*- is the pressure of the gas

It is worth noting that '*a*' for $CO_2$ is 3.640 $L^2$ bar/$mol^2$, while *'b'* for $CO_2$ is 0.04267 L/mol.

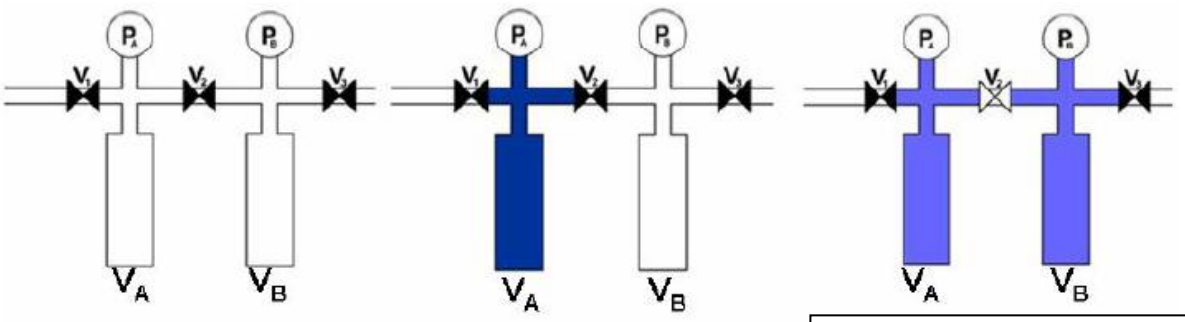


Chambers A and B before $CO_2$ introduction.

Chamber A filled with $CO_2$ while chamber B remains under vacuum.

Chambers A and B after equilibrium. Both chambers have equal pressures of $CO_2$.

**Figure 3.11**: A schematic representation of a VAS experiment (Marais, 2008).

In a sorption reaction, the temperature and volume must be kept constant to mathematically relate the pressure to the number of moles, *n*. For this reason, it is very important to regulate the temperature of the VAS equipment and to accurately determine the volumes $V_{A,}$ $V_B$ and the volume of the sample ($V_S$).

### 3.5.3 Determination of Sample Volume

The volume of the sample ($V_S$) was determined by use of density values obtained from an He-stereopycnometer (Figure 3.12).


**(a)** **(b)**

**Figure 3.12**: An optical image of (a) the outward appearance and (b) the sample container of the He-Stereopycnometer.

The sample of a known weight is placed in a sample holder and the helium gas is let into the sample vessel. Instructions are followed and at the end, two values ($P_2$ and $P_3$) are displayed on the Stereopycnometer screen. The $P_2$ and $P_3$ values are entered in

the Microsoft excel sheet that is especially designed to calculate the density and volume values. This procedure has to be done 3 times so as to get 3 sets of $P_2$ and $P_3$ values. The average density and average volume of the sample are then calculated from the 3 sets of results. The displayed density datasheet obtained after determining the density of a typical sample is shown in Figure 3.13.

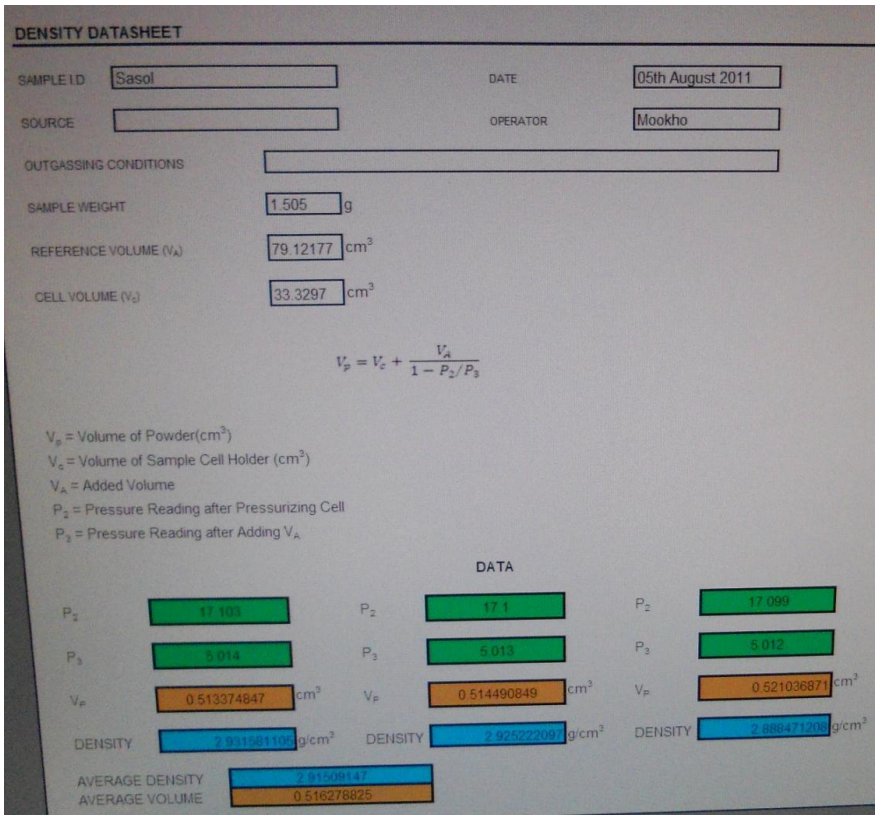


**Figure 3.13**: A density datasheet of the density of a typical sample.

### 3.5.4 Determination of Volumes of the Reference Cell and Sample Cell

To determine the volume of the reference cell ($V_A$) and the sample cell ($V_B$), the temperature was set at 27 °C. Both cells were evacuated using a vacuum pump, and the valves were all closed. $V_1$ was opened and $CO_2$ was introduced into the reference cell. The system was allowed to stabilize before recording the pressure reading from $P_A$. Once the system had stabilized, $V_1$ was closed and the pressure was recorded as $P_1$. Valve $V_2$ was then opened, allowing the $CO_2$ gas to fill both cells, as illustrated in Figure 3.11. The pressure reading, which should be the same for both cells, was then recorded as $P_2$. This is depicted by Eq. 3.2 below:

$$P_1 V_A = P_2 (V_A + V_B) \quad \text{Eq. 3.2}$$

which upon rearrangement becomes:

$$\frac{V_B}{V_A} = \frac{P_1}{P_2} - 1 \quad \text{Eq. 3.3}$$

When a sample of known volume ($V_S$) is placed in the sample cell, the pressures in the reference cell and the sample cell recorded as $P_3$ and $P_4$ may be given as follows in Eq. 3.4**:**

$$P_3 V_A = P_4 (V_A + V_B + V_S) \quad \text{Eq. 3.4}$$

Upon rearrangement, the equation becomes:

$$V_A = V_S \left[\frac{P_3}{P_4} - \left(1 + \frac{V_A}{V_B}\right)\right]^{-1} \quad \text{Eq. 3.5}$$

Since $P_3$, $P_4$, $V_S$ and $\frac{V_A}{V_B}$ are known, $V_A$ can be calculated using Eq. 3.5, following which $V_B$ can then be calculated using Eq. 3.2. The procedure is repeated three times so that a standard deviation of the volumes is determined. As determined earlier, the

volume of the reference cell was found to be 15.8290 mL while that of a sample cell was found to be 29.0370 mL (Maphada, 2011).

When performing an experiment with a sample in chamber B, it is imperative to subtract the volume of the sample ($V_S$) from the calculated volume ($V_B$) in order to arrive at a value for the dead volume, $V_D$, of the chamber. A dead volume is a space which is not occupied by a sample (Figure 3.14). This is because once the sample chamber $V_B$ contains a solid sample, the pressure $P_B$ monitors the pressure in the volume $V_D$ as opposed to $V_B$. $V_D = V_B - V_S$.

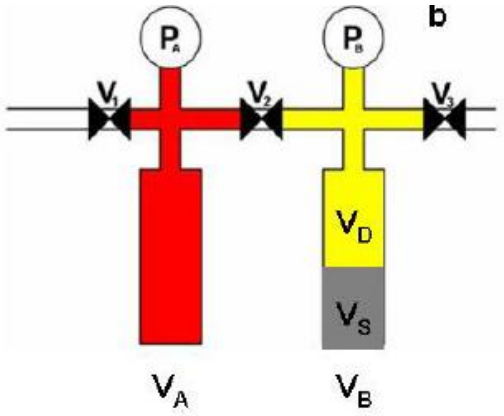


**Figure 3.14**: $V_A$ represents the volume of a reference cell while $V_B$ represents the volume of a sample and the dead volume (Marais, 2008).

The experimental method rests upon two important assumptions:

- that $CO_2$ gas behaves as an ideal gas for the accurate volume determination,
- that the sample volume remains constant throughout the experiment.

Generally, for any volumetric adsorption experiment to be accurate, there are a number of parameters that the device must comply with, namely:

1. The accurate determination of $V_A$ and $V_B$. The van der Waals equation (Eq. 3.1) requires the parameter $V_B$ .
2. The accurate determination of $V_S$.

3. The accurate determination of the $V_D$.

4. The temperature of the device should be kept constant. This ensures that the gas in different modular parts is at the same temperature.

5. Accurate pressure measurements.

6. Long-term stability of the instrument with regard to all electronic and physical components as a typical sorption reaction can take several hours before it can reach equilibrium.

### 3.5.5 Calculating the Number of Moles

The most sensitive and accurate adsorption measuring device can still yield meaningless results if the theoretical model used to fit the experimental data is incorrect. As a result, the equation of state used to relate pressure, temperature, volume and the number of moles becomes important. In this study, the van der Waals equation of state was used.

Recall Eq. 3.1 ……$\left(P + \frac{n^2 a}{V^2}\right)(V - nb) = nRT$

Upon re-arrangement, the equation becomes:

$$\boldsymbol{n^3}ab - \boldsymbol{n^2}aV + \boldsymbol{n}(RT + bP)V^2 - PV^3 = 0 \qquad \text{Eq. 3.8}$$

which is a cubic equation. The values for all the parameters except for *n* are known. Microsoft Excel and Matlab software were used to solve for the number of moles given in Eq. 3.8. As with all the cubic equation calculations, three possible values of *n* were obtained for each calculation, where one of them was a positive-real number, while the other two values were complex numbers. This simplified the process of selecting the correct value of *n*. The cubic equations were solved using the MATLAB software. Once the *n* values were calculated from the van der Waals Equation of state, it becomes feasible to calculate the number of moles of the gas introduced to the sample as depicted in Eq. 3.9.

$$n_{intro} = n(P_{Astart}) - n(P_{Aend}) \qquad \text{Eq. 3.9}$$

where ;

$n(P_{Astart})$ - is the number of moles of $CO_2$ calculated by using the initial pressure recorded in the reference cell / chamber A.

$n(P_{Aend})$ - is the number of moles of $CO_2$ calculated using the final pressure recorded after the gas from the reference cell has escaped to the sample cell / chamber B, due to the opening of the $V_2$ valve.

$n_{intro\ -}$ is the number of moles of $CO_2$ introduced to the sample.

Thus, the total number of moles of $CO_2$ adsorbed by the sample at a particular equilibrium loading pressure is given by Eq. 3.10.

$$n_{total} = n_{intro} - n_{(PBeq)} \qquad \text{Eq. 3.10}$$

where;

$n_{total}$ – is the total number of moles of $CO_2$ adsorbed by the sample

$n_{(PBeq)}$ – is the number of moles of $CO_2$ calculated by using a specific pressure where equilibrium in the sample cell / chamber B was reached.

## 3.6 THE EXPERIMENTAL PROCEDURE

A thorough leak test was performed prior to loading each of the samples into the sample cell. This was conducted by running the He gas through the system and monitoring the pressure changes in the reference cell and in the sample cell. 1.5 g of each of the samples was placed in the VAS sample cell for 7½ hours in total, to allow the adsorption process to take place. The temperature was kept constant at 30 °C. During the first hour, the sample was exposed to $CO_2$ at a pressure of 5 bar. The pressure was increased to 10 bar after an hour. The process was repeated until the 36 bar pressure was achieved (Table 3.2**)**. The intention was to leave the samples for 36 hours in the VAS to allow enough time for the adsorption process to occur. However, it was apparent that system could only acquire data for the maximum time of 7½ hours due to the script encoded in the LABVIEW software. The maximum pressure

that could be attained in the sample cell was 36 bar as opposed to the anticipated 40 bar, hence the pressure increased by 6 bars between the runs 4 & 5, instead of 10 bar.

**Table 3.1**: The pressure increments at 1 hour intervals during a typical adsorption experiment

| **Time/hours** | **$CO_2$ Pressure in the sample cell / bar** |
|---|---|
| 0 - 1 | 5 |
| 1 - 2 | 10 |
| 2 - 3 | 20 |
| 3 - 4 | 30 |
| 4 - 5 | 36 |
| 5 - 7½ | 36 |

The experimental procedure is followed in real-time using a computer interface that allows one to monitor various physical conditions (i.e. temprerature and pressure) of the adsorption experiment.

## 3.7 SAMPLE CHARACTERISATION

Each of the samples were characterised using a variety of techniques as listed in Figure 3.5**.** The intention was to determine the surface area and porosity, mineral content, the carbon content, and char content of the samples using BET, XRD, TGA and petrography techniques.

### 3.7.1 BET Isotherms

The BET isotherm was developed by Brauner, Emmett and Tellet, hence BET. Unlike the Langmuir isotherm, BET type adsorption corresponds to multilayer adsorption (Gökcekus et al, 2011). This isotherm indicates that more than one layer of adsorbate can accumulate at the surface, that is, the first adsorbed layer serves as a site for adsorption of a molecule onto the second and so on (Gökcekus et al, 2011). BET isotherms estimate the surface area, pore volume and pore size distribution of a sample.

The types of adsorption isotherms are shown in Figures 3.15. These types are labeled I, II, III, IV, V and VI according to the classification developed by de Boer (Condon, 2006). These classifications are widely used in the literature on physisorption and normally have the interpretations listed in Figure 3.16.

The first step in analysis of the isotherm is to classify the isotherm. A further recommendation is to determine the classification of the isotherm according to the standard curve representation or the $\chi$ plot representation. This used to be more difficult than present since each adsorbent – adsorbate combination had its own standard curve that was numerically obtained (Condon, 2006). There is now a universal representation of the standard curve based upon a quantum mechanical theory of adsorption. This representation is referred to as the chi, $\chi$, representation. A $\chi$ plot is a plot of the amount adsorbed vs the quantity $P/P_0$. In general, the $\chi$ plot of a non-porous adsorbent for which there is only one energy of adsorption for a particular adsorbent-adsorbate combination is a straight line (Condon, 2006). In type VI, an initial adsorption step may be observed if chemisorption occurs along with physisorption, however the chemisorption portion should be somewhat irreversible and subsequent isotherms will differ from the first measured isotherm (Condon, 2006).

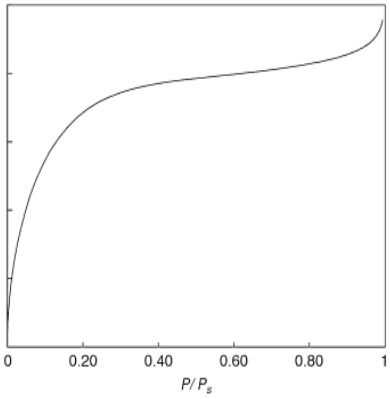


Type I Isotherm

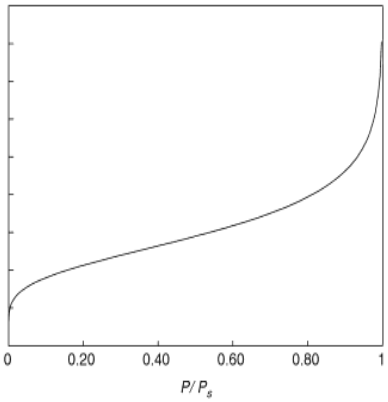


Type II Isotherm

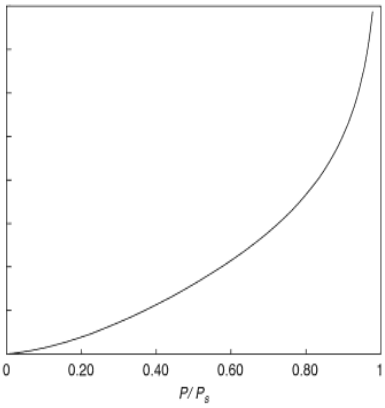


Type III Isotherm

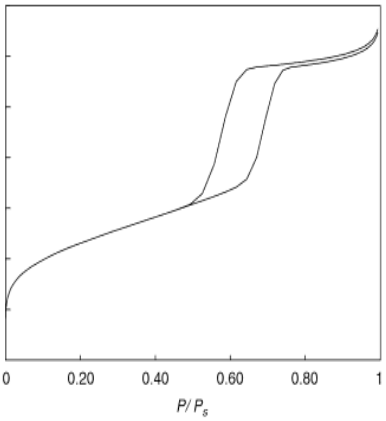


Type IV Isotherm

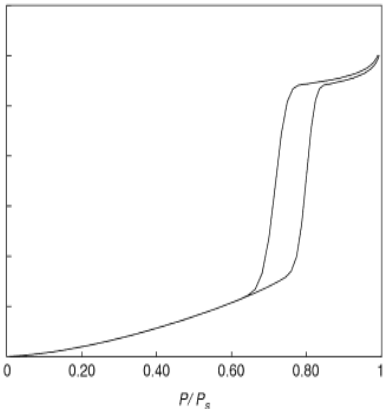


Type V Isotherm

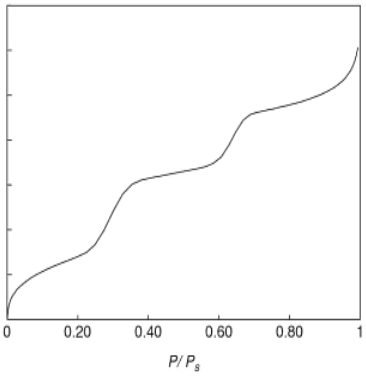


Type VI Isotherm

**Figure 3.15**: Types of adsorption isotherms (Condon, 2006).

**Table 3.2**: Classification and interpretation of the adsorption isotherms (Condon, 2006).

| **Type** | **Interpretation** |
|---|---|
| I | This is characteristic of either a chemisorption isotherm (in which case the final upswing at high pressures may not be present or physisorption on a material that has extremely fine pores (micropores) |
| II | This is characteristic of a material, which is not porous. or possibly macroporous, and has a high energy of adsorption |
| III | This is characteristic of a material, which is not porous. or possibly macroporous, and has a low energy of adsorption |
| IV | This is characteristic of a material, which contains mesoporosity and has a high energy of adsorption. These often contain hysteresis attributed to the mesoporosity |
| V | This is characteristic of a material, which contains mesoporosity and has a low energy of adsorption. These often contain hysteresis attributed to the mesoporosity |
| VI | This type of isotherm is attributed to several possibilities the most likely being, if the temperature is below the adsorptive triple point, that the adsorbate is more like a solid forming a structured layer. i.e. epitaxial growth. Other possible explanations include multiple pore sizes. If the steps are at the low- pressure portion of the isotherm, then the steps may be due to two or more distinct energies of adsorption. If the steps are at the high pressure part of the isotherm, then the steps might he due to sharp steps on the adsorbate surface |

The type of the BET instrument used in this project was Micrometrics ASAP 2020 Surface Area and Porosity analyser, housed in the School of Chemical and Minerals Engineering, Northwest University, Potchefstroom Campus. Carbon dioxide was used as an adsorbing gas.

### 3.7.2 X-Ray Diffraction Spectroscopy

X-ray diffraction spectroscopy is a versatile, non-destructive technique that reveals detailed information about the chemical composition and crystallographic structure of natural and manufactured materials (Lee, 2005). It provides direct information on the mineralogical composition of a sample as each crystalline compound produces a unique diffraction pattern (Stutzxnan and Centeno, 1995). The XRD technique requires a sample of the material to be placed in a holder, where the sample is illuminated with x-rays of a fixed wavelength and the intensity of the reflected radiation is recorded using a goniometer. Diffraction occurs, and the sample scatters radiation coherently, producing concerted constructive interference at specific angles (Speakman, 2010). The data is analysed for the reflection angle to calculate the inter-atomic spacing (D value in Angstrom units - $10^{-8}$ cm). The intensity (I) is measured to discriminate (using I ratios) the various D spacings and the results are compared to the large database from the software used to identify possible matches (Lee, 2005).

The following procedure was used in preparation and analysis of the samples:

After addition of 20 % Si (Aldrich 99.9%) for quantitative determination of amorphous compounds, and micronising in a McCrone micronizing mill, the samples were prepared for XRD analysis using a back loading preparation method. This method was carried out 3 times for each sample in order to obtain reproducible results. The samples were analysed using a PANalytical X'Pert Pro powder diffractometer with X'Celerator detector, variable divergence and fixed receiving slits with Fe filtered Co-K radiation. The phases were identified using X'Pert Highscore

plus software. The relative phase amounts (weight %) were estimated using the Rietveld method (Autoquan Program). Errors are on the 3 sigma level. Under the assumption of normality, the 3 sigma quality level translates to a process yield of 99.73%. The XRD analysis was conducted at XRD Analytical and Consulting Company in Pretoria.

### 3.7.3 Thermogravimetric Analysis

The thermogravimetric analyser (TGA) is an instrument used to measure the loss of mass of a sample over time during heating, and can be used to determine certain characteristics in coal and carbon samples. Proximate analysis is an evaluation of the moisture, ash, volatile matter and fixed carbon in a given sample, as determined by the series of standard test methods (Donahue and Rais, 2009). It was developed as a simple means of determining the distribution of products obtained when a sample is heated under specified conditions. Moisture, volatile matter, and ash are all determined by subjecting the sample to prescribed temperature levels for prescribed time intervals. The losses of weight are, by stipulation, due to loss of moisture and volatile matter at the higher temperature. The residue remaining after ignition at the final temperature is called ash (Speight, 2005). Fixed carbon is the difference of these three values summed and subtracted from 100. In low-volatile materials such as coke and anthracite coal, the fixed-carbon value equates approximately to the elemental carbon content of the sample.

The TGA analyses were performed using Perkin ElmerSTA6000 TGA equipment and the following TGA programme was used:

The nitrogen gas tap was switched on at 40 mL/min to flush the furnace. A small quantity of the sample was placed in a crucible and heated from 30 ˚C to 110 ˚C at 50 ˚C/min in a furnace. The temperature was held for 3 min at 110 ˚C. From 110 ˚C the

temperature was increased to 900 ˚C at 30 ˚C/min. The $O_2$ gas tap was then switched on at 40 mL/min. The temperature was held at 900 ˚C for 1 min.

### 3.7.4 Petrography

Coal petrography is a standard method for characterising the organic (maceral) and inorganic (mineral) constituents of coal. Two types of data can be derived from this method: rank (defined by vitrinite reflectance) and composition (maceral proportions). Under incident light, vitrinites appear to be dark grey, light grey or white as the coal rank increases. Liptinites appear dark grey or grey while inertinites are bright to extremely bright (Karr, 1978). Petrography analyses are used by geologists to gain an understanding of coal deposition, by coal technologists to evaluate coals for coking potential, and by coal quality personnel to monitor the quality of mine product or shipment coal (O'Brien et al, 2003). These analyses also provide a powerful forensic tool for monitoring coal blending and for detecting and identifying contamination. An incident light Leica DMP 4500 microscope with an oil immersion lens and total magnification of x500 was used for the analysis. The analysis was conducted at the School of Chemical and Metallurgical Engineering, University of the Witwatersrand.

## 3.8 CHAPTER SUMMARY

The morphological appearance of the as-received samples were different, attributable to the way their respective parent coal were utilised. A detailed description of the equipment and characterising techniques used during the experiment was given. The duration of the experimental procedure is $7^1/_2$ hours, the period during which the pressure shall be increased from 5 bar to 36 bar at 5 bar or 10 bar increments, at 1 hour intervals. The van der Waals equation was found to be a suitable equation of state to use to calculate the number of moles of $CO_2$ adsorbed by the samples.

# CHAPTER 4

# RESULTS AND DISCUSSION

The results discussed in this chapter are based on the as-recieved ash samples obtained from various industries as discussed in Section 3.1. The adsorption results are obtained from the adsorption experiments, where the pressure data acquired by the VAS system are used to calculate the number of the adsorbed moles using Matlab software. The adsorption results are then interpreted using isotherm plots. The plots of all the ash samples are compared against each other to determine which ash sample has the greatest adsorption potential. The results from TGA, XRD, BET, and petrography analyses were compared with the adsorption results and discussed to further understand the adsorption behaviour of the samples.

## 4.1 INTEPRETATION OF EXPERIEMNTAL RESULTS

### 4.1.1 Temperature Change with Introduction of $CO_2$ Gas in the Chambers

During an adsorption experiment (see Figure 4.1), the temperature in the reference cell is characterised by two sharp decreases. The first decrease is due to the introduction of cool $CO_2$ gas into the reference cell, and as a result this cooled the thermometer in the cell. The second decrease occurs when the valve between the two cells was then opened to allow the gas into the sample cell. The reason for this observation is unknown; however, it could be due to a transient behaviour usually observed in temperature sensors (Wyrsch, 2008; Daga *et al*., 2009).

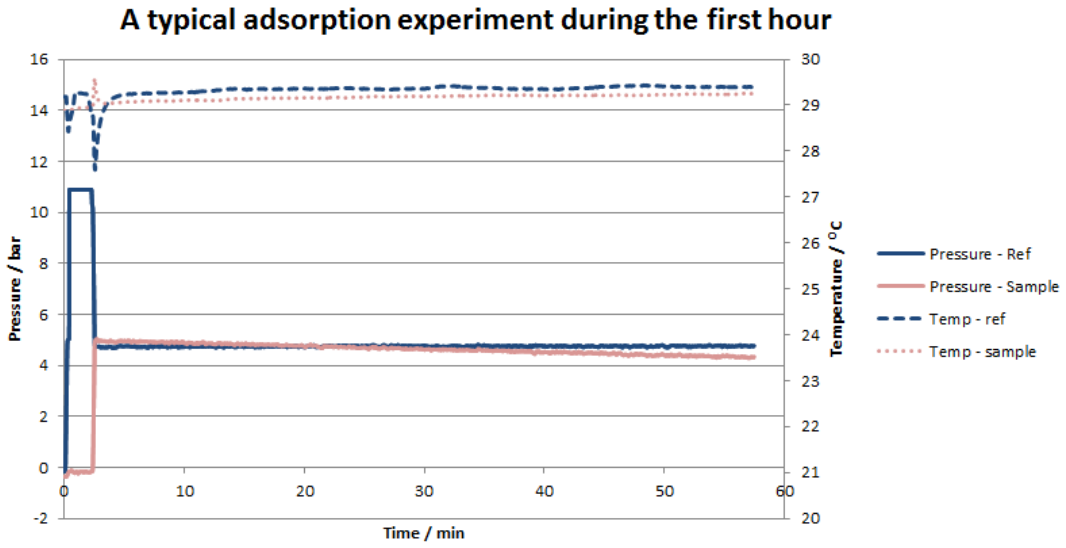


**Figure 4.1**: A typical Pressure-Temperature graph of a 1-hour run of the adsorption experiment.

The aspiration to keep the temperature in both cells constant was not achieved as there was always a slight gap between the two temperature graphs through-out the first hour. The two lines should have merged into one line, illustrating that the temperature in the reference cell and in the sample cell were the same. This slight temperature difference may be due to an off-set error in the calibration of the temperature sensors. However, the temperature in the individual cells remained fairly constant throughout the experiments regardless of the two cells not being at the exact temperature. As a result, the adsorption experiment will not be affected.

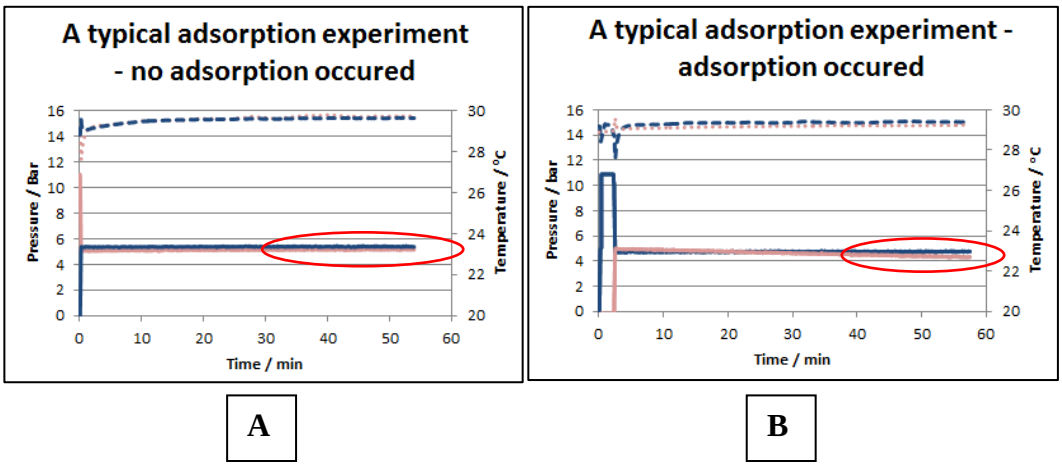


**Figure 4.2**: In plot A, adsorption did not occur while in plot B adsorption occurred.

### 4.1.2 Pressure Change with Introduction of the $CO_2$ Gas in the Cells

In a typical adsorption experiment, the reference cell is first filled with $CO_2$ gas. Once a desired pressure is reached, the valve between the reference cell and the sample cell is opened to allow the pressure in the reference cell to flow into the sample cell until an equilibrium state is reached.

The solid lines in Figures 4.2 A and 4.2 B represent pressures in the reference cell and sample cell. As the pressure in the reference cell decreases, that in the sample cell increases and the two pressures reach equilibrium. Depending on the nature of the adsorption experiment, the two pressure lines may either remain constant, in which case adsorption has not occurred (as in Figure 4.2 A), or the sample cell line may deviate from that of the reference cell, illustrating that adsorption has occured (as in Figure 4.2 B).

As stated in Section 3.6, the samples were left in the adsorption equipment to allow enough time for the adsorption process to take place. The pressure was increased by 5 bars and sometimes by 10 bar increments at one hour intervals. A graph that depicts an entire run is given in Figure 4.3**.**

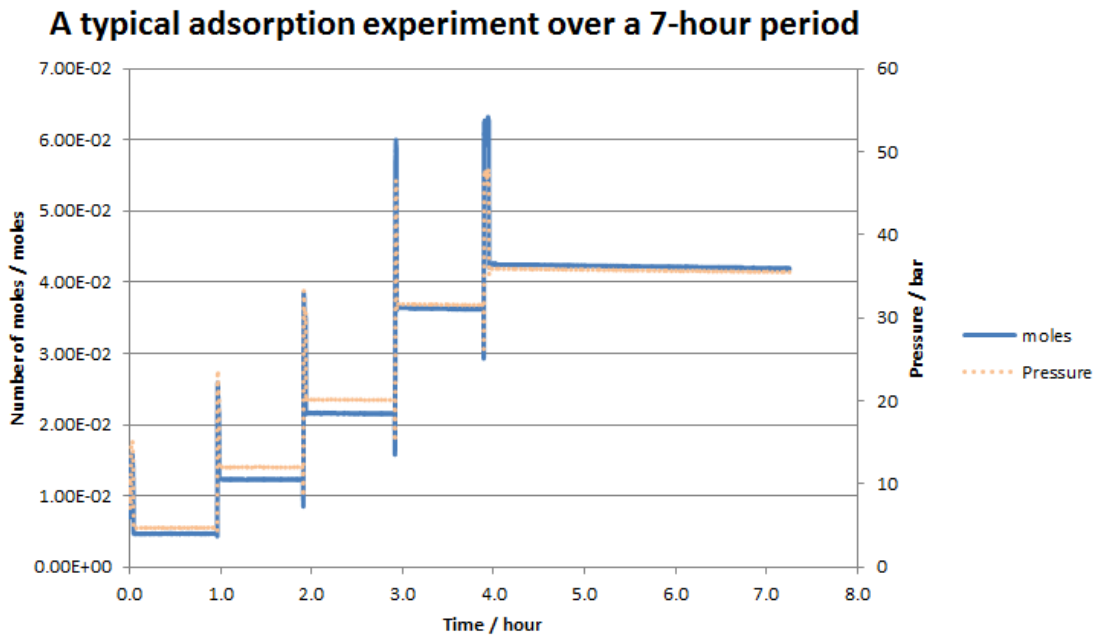


**Figure 4.3**: A typical 7-hour adsorption experiment plot.

As shown in Figure 4.3, the number of moles of $CO_2$ increased as the pressure increased. For the first four hours, no adsorption was observed because the number of moles and the pressure in the sample cell remained constant. Adsorption was only observed at the highest pressure (37 bar), where the sample was left to adsorb continuously for 3 hours. There was a slight drop in the number of moles from the starting point to the end point (in the region 4 – 7 hours), and this was due to the adsorption process occurring.

In the case where the decrease in pressure or number of moles is vague, a pressure-time graph given in Figure 4.4 may be plotted; this depicts small changes more clearly than the mole-time graph given in Figure 4.3. Figure 4.4 clearly indicates the instances where adsorption occurred, and where it did not occur. Two straight overlapping lines show that there was no decrease in the number of moles, and hence adsorption did not occur. Two diverging lines show that there was a decrease in the number of moles in the sample cell. The decrease in the number of moles causes the

plot of the pressure in the sample cell to deviate from that of the reference cell, hence illustrating that adsorption occurred.

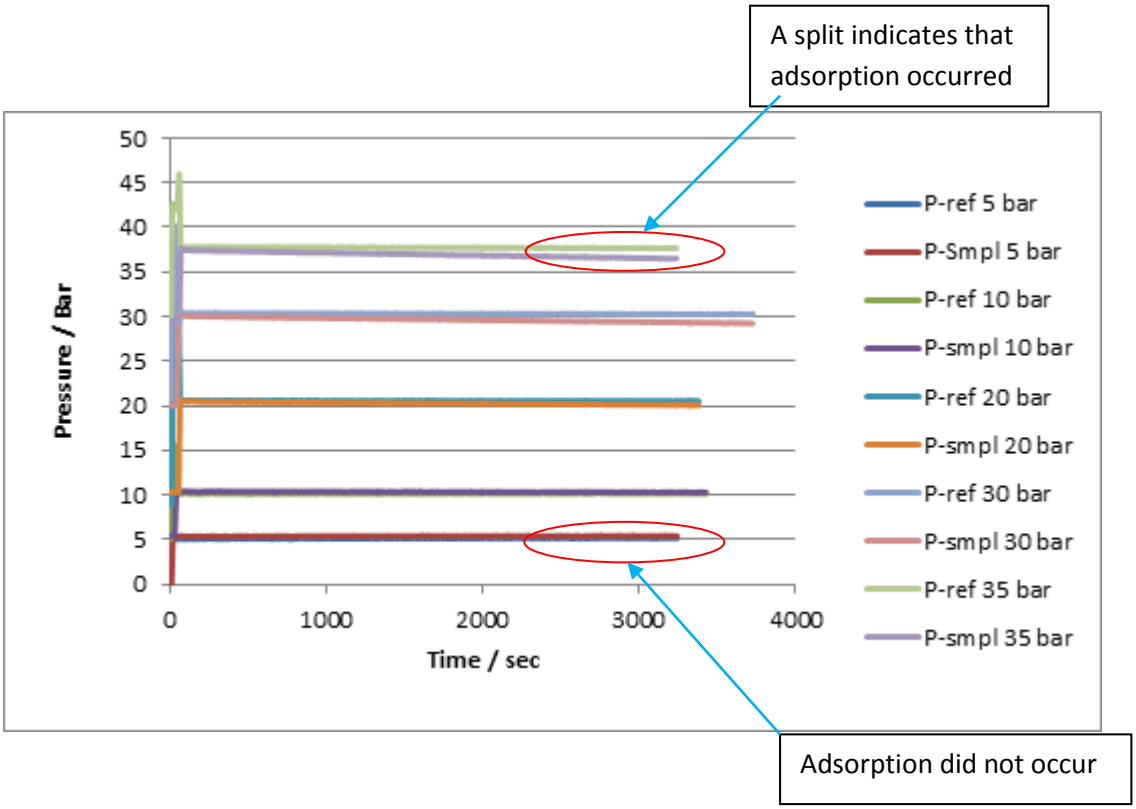


**Figure 4.4**: A Pressure-Time graph showing instances where adsorption occurred and where it did not occur.

### 4.1.3 Calculating the Adsorbed Moles of $CO_2$

To calculate the number of moles adsorbed for each 1-hour session, the number of moles at the end point of the interval is subtracted from that at the starting point as illustrated in Figure 4.5, also given by Eq 3.10 in Chapter 3.

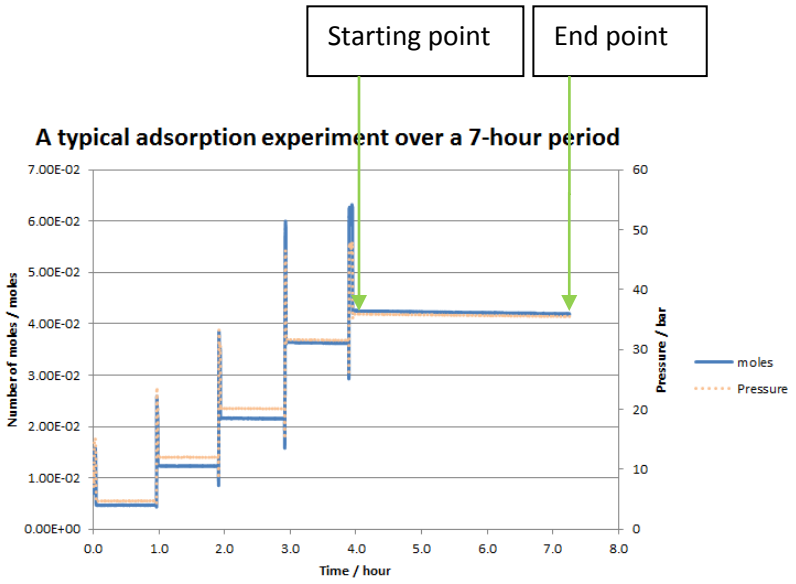


**Figure 4.5**: A plot showing the starting and end points used to calculate the number of adsorbed moles in a typical adsorption experiment.

Once the number of moles of the adsorbed $CO_2$ is calculated, a plot given in Figure 4.6 may be drawn. This graph depicts the most essential part of this research as it explains the adsorption potential of a sample.

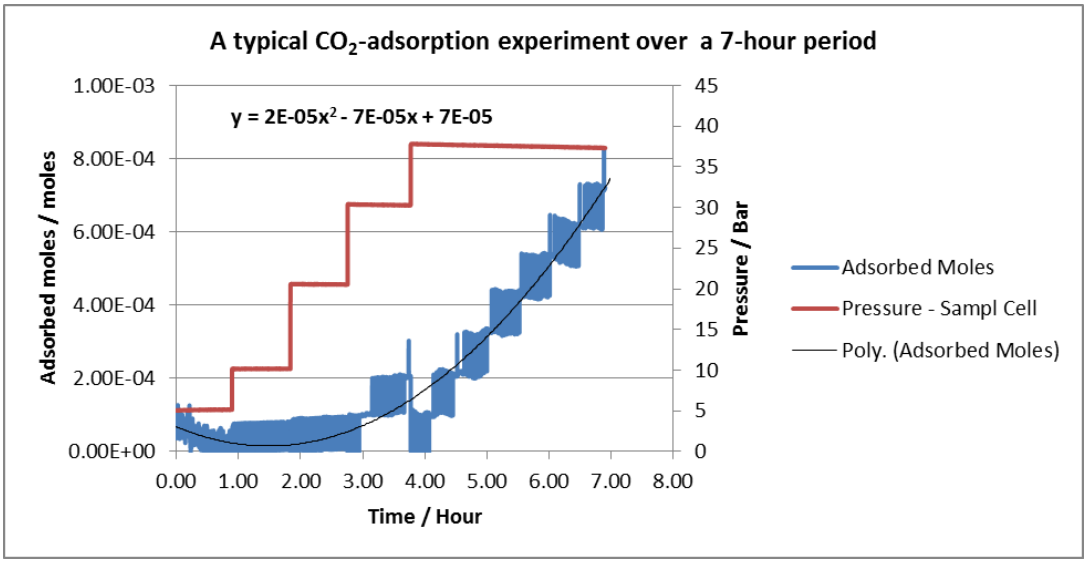


**Figure 4.6**: A typical $CO_2$-adsorption graph during a 7-hour period.

## 4.2: ADSORPTION RESULTS

The adsorption results for each ash sample are discussed based on increases in the number of the adsorbed moles, and the graphs are also compared against each other. The adsorption graphs of the individual samples are discussed and given in Figures 4.7-4.10 for comparison.

### 4.2.1: Chain Grate Ash Sample

Figure 4.7 shows the adsorption behaviour of the CG ash sample.

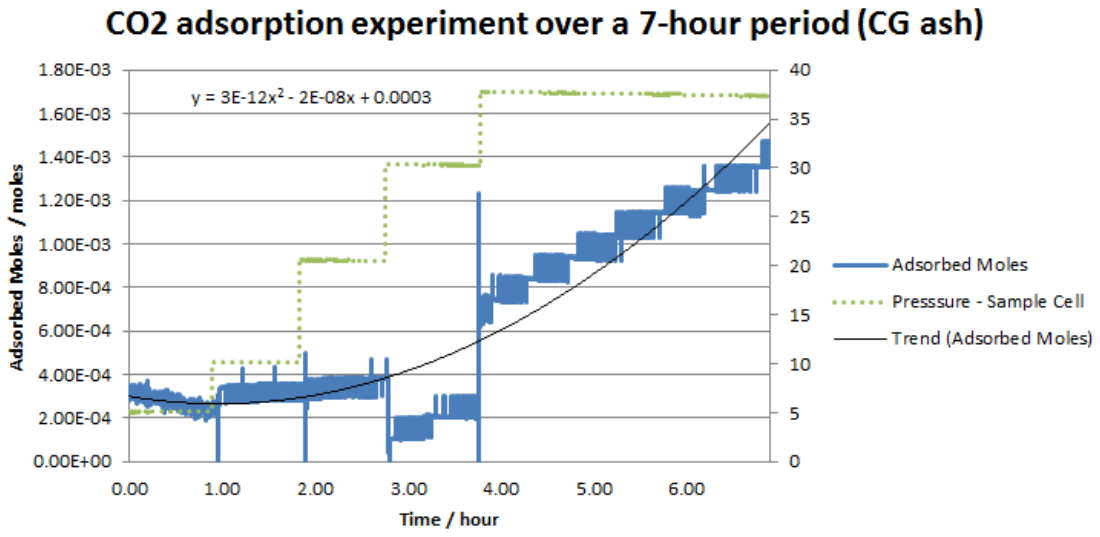


**Figure 4.7**: The adsorption behavior of the CG ash sample.

**The *first* hour of the experiment (at 5 bar)**: There was a decrease in the number of the adsorbed moles during the first hour. The cause for the decrease remains unknown as no leakage was detected, however the extent of the decrease was fairly small.

**The *second* hour of the experiment (at 10 bar)**: There was a slight increase in the number of the adsorbed moles attributable to the 5-bar pressure increase. The number of moles increased from $2.60 \times 10^{-4}$ moles to $2.57 \times 10^{-4}$ moles. Although a couple of outliers were observed on the graph, the number of the adsorbed moles remained fairly constant.

**The *third* hour of the experiment (at 20 bar)**: Pressure increase from 10 bar to 20 bar did not make a notable difference as far as the number of the adsorbed moles is concerned. There was a slight increase from $2.57 \times 10^{-4}$moles to $3.48 \times 10^{-4}$ moles.

**The *fourth* hour of the experiment (at 30 bar)**: The number of the adsorbed $CO_2$ moles, were observed to have decreased significantly from $3.48 \times 10^{-4}$moles to $1.10 \times 10^{-4}$moles. The cause for the decrease is unknown. However, there was an increase from $1.10 \times 10^{-4}$ to $2.03 \times 10^{-4}$ moles.

**The *last 3- hour* interval of the experiment (at 37 bar)**: Upon a pressure increase from 30 bar to 37 bar, the number of the adsorbed moles increased exponentially from $2.03 \times 10^{-4}$ moles to $1.47 \times 10^{-3}$ moles. The 37 bar pressure seems to increase the adsorption rate quite significantly.

**Overall summary**: The overall behavior shown by the adsorption behavior of the CG ash sample is an exponential increase, where during the first 2 hours, the number of the adsorbed moles was constant and from the 3rd hour to the 7th, an exponential increase was observed. The quadratic equation that was drawn from the trend shown by the data is as follows:

$$y = 3 \times 10^{-12}x^2 - 2 \times 10^{-8}x + 0.0003 \qquad \text{Eq. 4.1}$$

### 4.2.2: Gasification Ash Sample

Figure 4.8 shows the adsorption behaviour of the G ash sample.

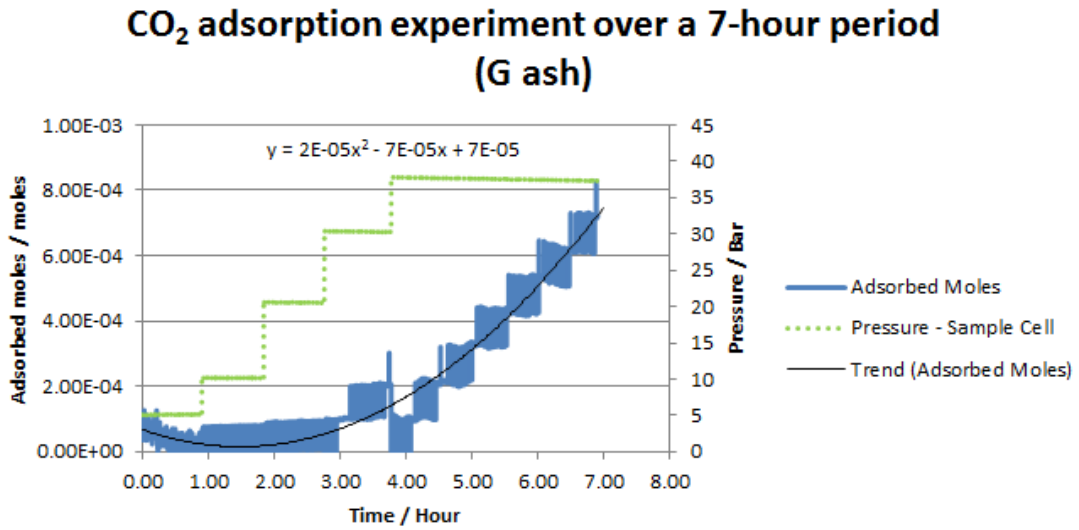


**Figure 4.8**: The adsorption behaviour of the G ash sample.

**The *first* hour of the experiment (at 5 bar)**: The number of the adsorbed $CO_2$ moles seemed to decrease during the first hour of the experiment. This behaviour could not be accounted for, because there were no leaks in the sample cell.

**The *second* hour of the experiment (at 10 bar)**: Upon an increase of the pressure from 5 bar to 10 bar, the number of the adsorbed $CO_2$ moles (N-ads $CO_2$ moles) increased from $1.02 \times 10^{-6}$moles to $1.67 \times 10^{-6}$moles, which was very little. After the increase, the graph remained constant with no significant change through-out the 1-hour experiment.

**The *third* hour of the experiment (at 20 bar)**: An insignificant difference was observed after the pressure increase from 10 bar to 20 bar. The number of the adsorbed moles increased form $1.67 \times 10^{-6}$moles to $4.93 \times 10^{-6}$moles, which is

inconsequential. The small increase indicates that the sample was almost fully saturated with $CO_2$ from the previous 10-bar experiment and thus could not take any more $CO_2$ molecules, irrespective of the 10 bar pressure increase. The number of the adsorbed $CO_2$ moles further increased, although inconsequentially, from $4.93 \times 10^{-6}$molesto $7.63 \times 10^{-6}$moles.

**The *fourth* hour of the experiment (at 30 bar)**: The number of the adsorbed moles increased significantly and immediately from $7.63 \times 10^{-6}$moles to $2.00 \times 10^{-4}$moles upon an additional 10 bar pressure increase. The number of the adsorbed moles remained fairly constant. However, there was outlier point which was observed towards the end of the run.

**The *last 3- hour* interval of the experiment (at 37 bar)**: The number of the adsorbed $CO_2$ moles increased exponentially from $2.00 \times 10^{-4}$moles to $7.28 \times 10^{-4}$ moles.

**Overall summary**:

The number of the adsorbed $CO_2$ moles showed a decrease during the first hour of the experiment, a steady increase during the subsequent 2 hours, and an exponential increase from the 4th hour to the 7th hour. The quadratic equation that was extracted from the trend in the data is as follows:

$$y = 2 \times 10^{-5}x^2 - 7 \times 10^{-5}x + 7 \times 10^{-5} \qquad \text{Eq. 4.2}$$

### 4.2.3: Pulverised Fuel Ash Sample

Figure 4.7 shows the adsorption behaviour of the PF ash sample.

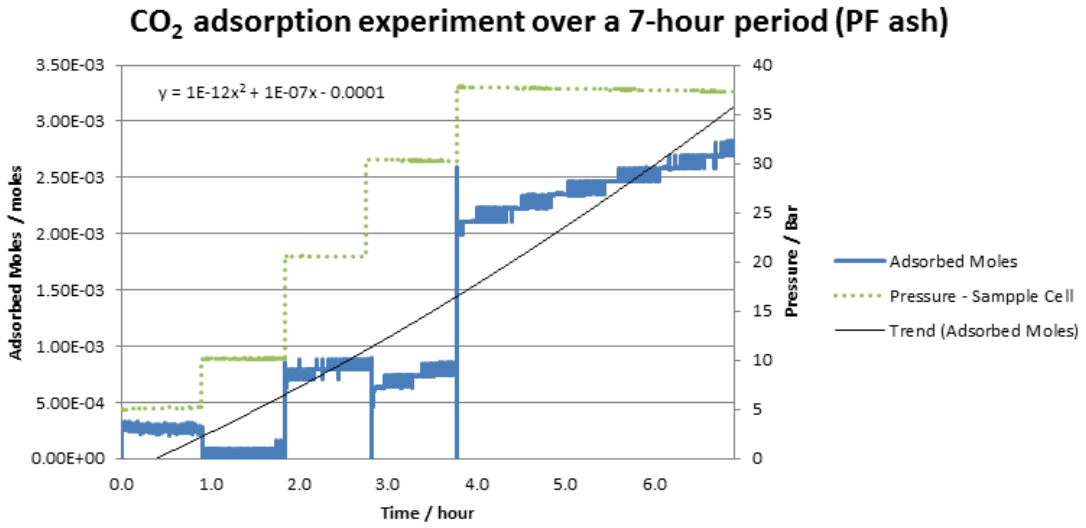


**Figure 4.9**: The adsorption behaviour of the PF ash sample.

**The *first* hour of the experiment (at 5 bar)**: The number of the moles of $CO_2$ adsorbed by the sample appears to be constant, with an average of $6.21 \times 10^{-5}$adsorbed moles. This shows that adsorption did not occur at significant levels. At the boundary between the first and second hour experiments, the adsorption graph shows a presence of a peak. This peak is attributable to the sudden increase in the pressure in the sample cell, which occurred when the pressure was increased from 5 bar to 10 bar. The same phenomenon is observed at the boundaries at the third and fourth hours.

**The *second* hour of the experiment (at 10 bar)**: the number of the adsorbed moles remained constant, at approximately the same level to that of the first hour (i.e. $8.54 \times 10^{-5}$adsorbed moles). Thus, an increase in pressure from 5 bar to 10 bar did not meaningfully change the adsorption capacity of the sample.

**The *third* hour of the experiment (at 20 bar)**: The adsorbed $CO_2$ increased at the beginning of the experiment and plateaued throughout the rest of the experiment. There was a significant change in the number of the adsorbed $CO_2$ moles during this period. This showed that an increase of pressure from 10 bar to 20 bar successfully increased the adsorption potential of the sample. The average number of the adsorbed moles increased from $8.54 \times 10^{-5}$ to $1.63 \times 10^{-4}$ moles.

**The *forth* hour of the experiment (at 30 bar)**: After the pressure had increased from 20 bar to 30 bar, the graph shows a sudden increased in the adsorbed moles from $1.63 \times 10^{-4}$ to $6.14 \times 10^{-4}$ moles. The number of the adsorbed moles further increased constantly until it reached $8.47 \times 10^{-4}$ moles. This shows that the adsorption capacity of the sample increased fundamentally.

**The *last 3-hour* interval of the experiment (at 37 bar)**: The adsorbed number of moles increased profoundly from $8.47 \times 10^{-4}$ to $2.03 \times 10^{-3}$ moles upon increasing the pressure from 30 bar to 35 bar. Of interest is the fact that although the pressure was increased by only 5 bar, the increase in the adsorbed moles was highest. Following the sudden increase was a constant steady increase to $2.81 \times 10^{-3}$ moles over a period of three hours. This shows that the ash-adsorption experiments require high pressures.

**Overall summary**:

The overall experimental graph showed a trend-line which almost resembles a straight line as opposed to a curved line. This shows that the rate of adsorption on the PF ash sample was almost constant with changing pressures. The quadratic equation that was drawn from the trend in the data is as follows:

$$y = 1 \times 10^{-12}x^2 + 1 \times 10^{-7}x - 0.0001 \qquad \text{Eq. 4.3}$$

### 4.2.4: Spreader Stoker Ash Sample

Figure 4.10 shows the adsorption behaviour of the SS ash sample.

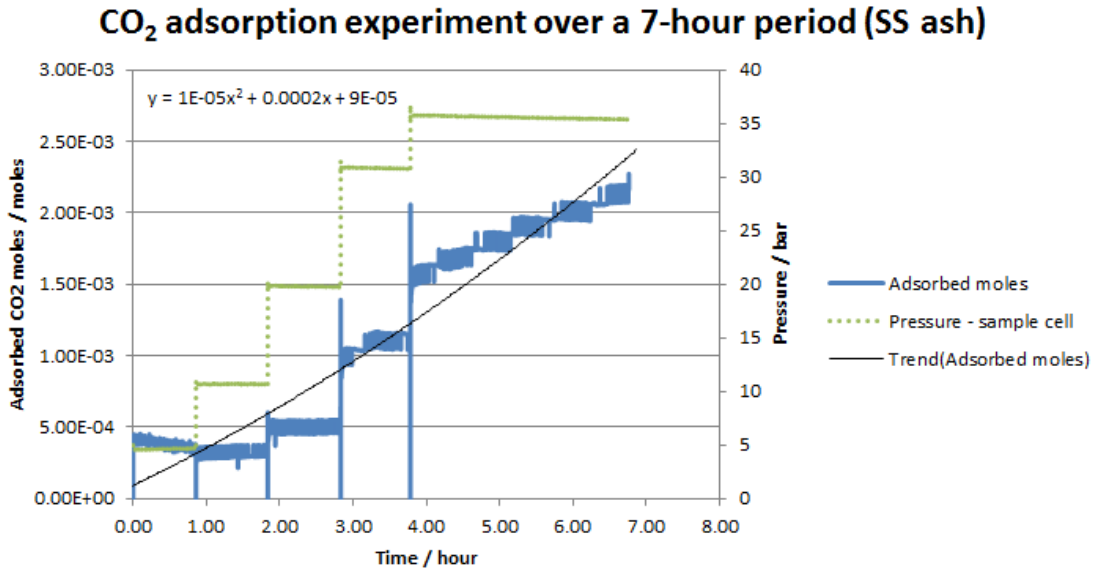


**Figure 4.10**: The adsorption behaviour of the SS ash sample.

**The *first* hour of the experiment (at 5 bar)**: A slight decrease in the number of the adsorbed moles was observed during the first hour. The moles decreased from $4.07 \times 10^{-4}$ moles to $3.38 \times 10^{-4}$ moles.

**The *second* hour of the experiment (at 10 bar)**: During this hour of the experiment, the adsorbed $CO_2$ moles remained fairly constant at $2.96 \times 10^{-4}$ moles.

**The *third* hour of the experiment (at 20 bar)**: The adsorbed moles increased from $2.96 \times 10^{-4}$ moles to $5.50 \times 10^{-4}$ moles and remained constant at that level.

**The *fourth* hour of the experiment (at 30 bar)**: The adsorbed $CO_2$ moles increased fundamentally from $5.50 \times 10^{-4}$ moles to $1.04 \times 10^{-3}$ moles, and continued to increase steadily until reaching $1.16 \times 10^{-3}$ moles.

**The *last 3- hour* interval of the experiment (at 37 bar)**: The number of the adsorbed moles increased constantly from $1.16 \times 10^{-3}$ moles to $2.07 \times 10^{-3}$ moles.

**Overall summary**:

The SS ash sample graph showed that adsorption took place even at lower pressures because the general trend almost resembles that of the PF ash sample with a linear behavior. The quadratic equation that was drawn from the trend in the data is as follows:

$$y = 1 \times 10^{-5}x^2 + 0.0002x + 9 \times 10^{-5} \quad \text{Eq. 4.4}$$

### 4.2.5 A Compilation of the Adsorption Graphs for All the Samples

The adsorption potential graphs of all the four samples were compiled in Figure 4.11 and compared against each other in order to determine which sample had the highest adsorption capacity at 29˚C, and at pressures 5 bar, 10 bar, 20 bar, 30 bar and 37 bar.

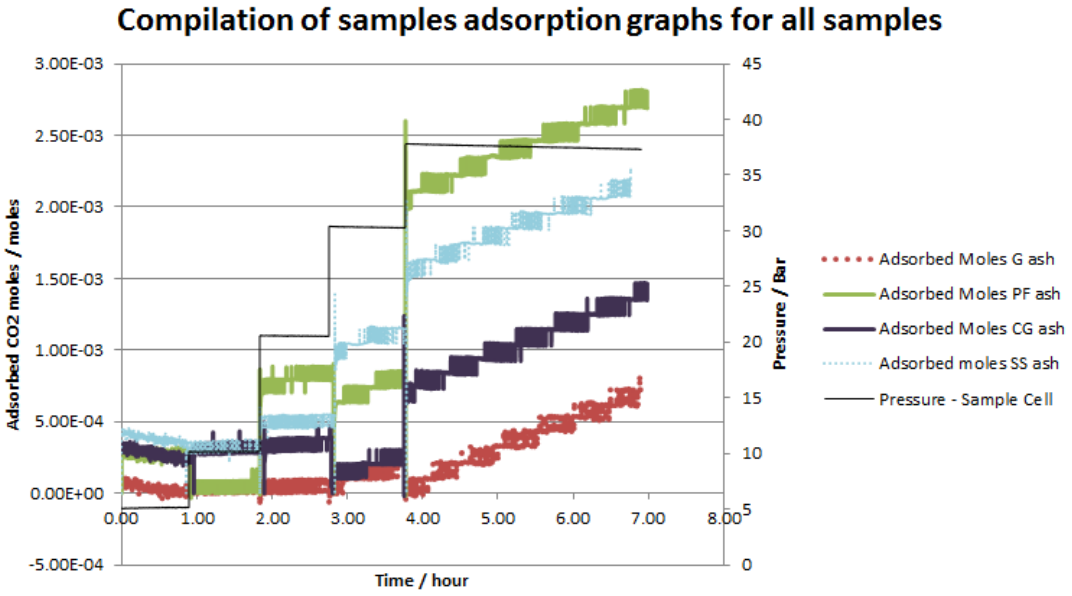


**Figure 4.11**: A compilation of the adsorption potential graphs for all four samples.

**First hour of the experiment (At 5 bar):** Comparing the graphs of the samples during the first hour of the experiment, it is observable that the SS ash sample had the highest starting adsorption potential of all the samples. However, all graphs showed a decrease in the number of the adsorbed $CO_2$ moles over the hour, which was unexpected. This shows that adsorption is possibly not favourable at low pressures, and that the samples are possibly "acclimatising".

**Second hour of the experiment (At 10 bar):** During the second hour of the experiment, the graphs of all the samples showed a constant behaviour, where the number of the adsorbed moles remained constant. CG ash and SS ash samples were in the lead in terms of the adsorption potential, while the PF ash and G ash samples were at the bottom. The arrangement of the samples in order of decreasing adsorption potential is as follows:

CG ash = SS ash > PF ash = G ash

**At 20 bar (3$^{rd}$hour):** A general trend shown by the samples is that the CG ash, SS ash, and the G ash sample remained fairly constant, with no significant increase in the

number of the adsorbed $CO_2$ moles, while the PF ash sample demonstrated an increase. The PF ash sample had the highest number of the adsorbed $CO_2$ moles, while the G ash sample had the lowest. The samples are listed below in order of decreasing adsorption potential:

PF ash > SS ash > CG ash > G ash

**At 30 bar (4$^{th}$ hour):** Generally, the samples showed a tendency to increase the number of the adsorbed moles, with SS ash as the sample with the highest adsorption capacity, and G ash as the sample with the lowest adsorption capacity. The samples are listed below in order of decreasing adsorption potential:

SS ash > PF ash > CG ash > G ash

**At 37 bar (5$^{th}$, 6$^{th}$ and 7$^{th}$ hours):** The samples showed a similar tendency of having an increase in the number of the adsorbed moles, such that the adsorption graphs showed a resemblance to each other. The PF ash sample had the highest adsorption capacity, while G ash had the lowest capacity. The samples are arranged below in order of decreasing adsorption potential:

PF ash > SS ash > CG ash > G ash

**Summary:** The G ash sample proved to have the lowest adsorption capacity of all the samples at all 4 different pressure levels. The CG ash sample generally appeared to be the sample with the second lowest adsorption capacity.

It was a bit difficult to decide which sample, between the PF ash and SS ash sample, generally had the highest adsorption capacity because the adsorptivity of the two samples was almost comparable, with the two samples trading positions in the number one spot at different pressures.

The trend lines obtained from the two samples (the PF ash and SS ash samples) are almost linear because the coefficients of $x^2$ (refer to Eqs. 4.1 and 4.4) are much smaller than those of x (smaller by 4 orders of magnitude). Consequently, the $x^2$ parameters may be ignored and a linear equation may be assumed as opposed to a quadratic equation. A comparison of the two gradients (coefficients of x) indicates that the PF ash sample (with 0.0005) had a higher rate of adsorption than that of SS ash sample (with 0.0002). Thus, in this regard the PF ash sample has the higher adsorption capacity than the SS ash sample, and the rest of the samples. Given the same sample mass, pressure and time of adsorption, the PF ash sample adsorbs the largest quantity of $CO_2$.

Therefore, the overall arrangement of the samples in order of decreasing adsorption capacity is as follows:

PF ash > SS ash> CG ash > G ash

When the second order polynomial trend-lines are added to the graphs as shown in Figure 4.12, it becomes easier to compare the adsorption potential of the samples.

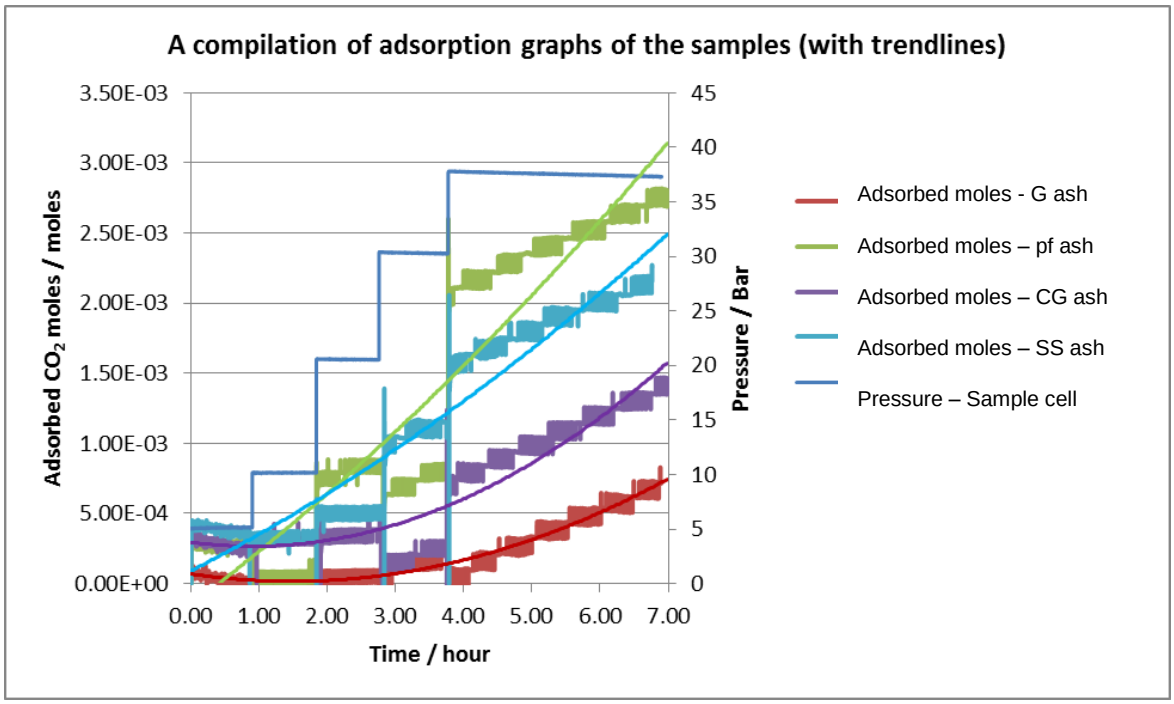


**Figure 4.12**: A comparison on the second order polynomial trend-lines of the sample data.

The total amount of $CO_2$ adsorbed by the respective samples is given below.
1.5g of the PF ash sample adsorbed $2.81\times 10^{-3}$ moles of $CO_2$, which translates into:

$$\frac{0.00281\ moles}{1.5g} = \mathbf{0.00187333333\ mol/g}$$

$$\mathbf{\sim 1873\ mol/ton}$$

Converting mol/ton to ton of $CO_2$/ton of ash, the amount of $CO_2$ moles adsorbed by the PF ash sample becomes:

1873 mol/ton ×44 g/mol = 82 430 g/ton,
rewritten as **0.08243 ton $CO_2$/ton ash**

The amount of the $CO_2$ molecules adsorbed by the rest of the samples is included in Table 4.1.

**Table 4.1**: Adsorption capacity values of the ash sample.

| Sample name | Adsorbed amount of $CO_2$ | | |
|---|---|---|---|
| | In mol/g | In mol of $CO_2$/ton of Ash | In ton of $CO_2$/ton of ash |
| CG ash | 0.00098 | 980 | 0.04313 |
| G ash | 0.000487 | 487 | 0.02143 |
| PF ash | 0.001873 | 1873 | 0.08243 |
| SS ash | 0.00154 | 1540 | 0.06777 |

In order to determine the range in which $CO_2$ may be adsorbed by different types of South African coal ash, the amount of $CO_2$ that could be uptaken by 1) the sample with the highest adsorption capacity (PF ash sample), and 2) the sample with the lowest adsorption capacity (G ash sample) were calculated.

**Highest Adsorption Capacity: Calculations of the amount of $CO_2$ that could be adsorbed by PF ash sample**

The total amount of PF ash produced by coal power stations in South Africa in 2010 was 36 Mt (Eskom, 2010). Since 5.6 % of the ash produced in South Africa is used for different purposes such as cement making and backfilling of mines (Bada and Potgieter-Vermaak, 2008), it means that 33.98 Mt of PF ash could be used for $CO_2$ sequestration.

i.e. $\frac{5.6}{100} \times 36\ \text{Mt} = 2.016\ \text{Mt}$

Therefore, 36 Mt – 2.016 Mt = 33.98400 Mt

If 33.98 Mt of the ash produced by coal power stations in the country is used in $CO_2$ adsorption, up to 2 801 301ton of $CO_2$ could be captured at 37 bar and 30˚C.

i.e. 0.08243 ton$CO_2$/ton ash × 33.98 Mt

= 0.08243 ton$CO_2$/ton ash × 33 984 000 ton ash

= 2 801 301 ton of $CO_2$

= 2.80 Mt $CO_2$

**Lowest Adsorption Capacity: Calculations of the amount of $CO_2$ that could be adsorbed by G ash sample**

The total amount of ash produced by gasification plants in South Africa was reported as a total of 8.5 Mt in 2005 (Bada and Potgieter-Vermaak, 2008). Since 5.6 % of the ash produced in South Africa is used for different purposes such as cement making and backfilling of mines (Bada and Potgieter-Vermaak, 2008), it means that 8.024 Mt of PF ash could be used for $CO_2$ sequestration.

i.e. $\frac{5.6}{100} \times 8.5\ \text{Mt} = 0.476\ \text{Mt}$

Therefore, 8.5 Mt – 0.476 Mt = 8.024 Mt

If 8.024 Mt of the ash produced by gasification plants in the country is used in $CO_2$ adsorption, up to 2 801 301 ton of $CO_2$ could be captured at 37 bar and 30˚C.

i.e. 0.02143 ton$CO_2$/ton ash × 8.024 Mt

= 0.02143 ton$CO_2$/ton ash × 8 024 000 ton ash

= 171 954 ton of $CO_2$

= 0.17 Mt $CO_2$

Therefore, $CO_2$ may be adsorbed in a range, **0.17 Mt $CO_2$ – 2.8 Mt $CO_2$**, by South African ash. It is worth noting that the amount of both the PF and G ash produced annually is far more than the amount of SS and CG ash produced from metallurgical industries. This is because coal power plants and gasification plants are the leading coal utilization industries in South Africa (Bada and Potgieter-Vermaak, 2008). Thus, the above given range of ton of $CO_2$ is plausible.

Out of the 337.4 Mt of the total $CO_2$ produced in South Africa (IEA Statistics, 2010), 65% is sequestrable (Surridge, 2009), therefore 219.31 Mt could be sequestered.

i.e. $\frac{65}{100} \times 337.4$ Mt = 219.31 Mt of $CO_2$

Since the maximum amount of $CO_2$ that could be adsorbed by raw untreated ash is 2 801 301 ton (2.801 Mt), it means that at most 1.28 % of the sequestrable $CO_2$ could be sequestered using all of the ash produced annually at the South African power stations.

i.e. $\frac{2.801\ \text{Mt}}{219.31\ \text{Mt}} \times 100\% = 1.28\ \%$

1.28 % is fairly little. However treatment of the ash samples with amines, acids, brine or steam could significantly improve the adsorption capacity of coal ash (Gray *et al.*, 2004; Maroto-Valer *et al.*, 2008; Muriithi *et al.*, 2001). Other means of adsorbents also need to be explored in order to help capture and store all of the sequestrable $CO_2$ in South Africa.

These calculations are based on the following assumptions:

- Ash produced by the South African power stations is 36 Mt/yr. However, this is the quantity that was produced in 2010, and it is likely to increase with time

as more coal power stations are built and/or more coal is combusted to generate more power.

- Only 5.6 % of the ash is used for other purposes. This value is however, liable to change depending on the demand of ash by the cement and mine industries.
- $CO_2$ sequestration conditions to be used at an industrial scale will be the same as those used during the undertaking of this research project.
- Raw, untreated ash is used.

## 4.3 BET RESULTS

Figure 4.13 shows the type of an isotherm depicted by the CG ash sample and the rest of the samples. The graph also illustrates the adsorption behaviour of $CO_2$ on the ash samples with increasing pressure. BET isotherms for the rest of the samples, together with detailed full-set reports are given in Appendix A.

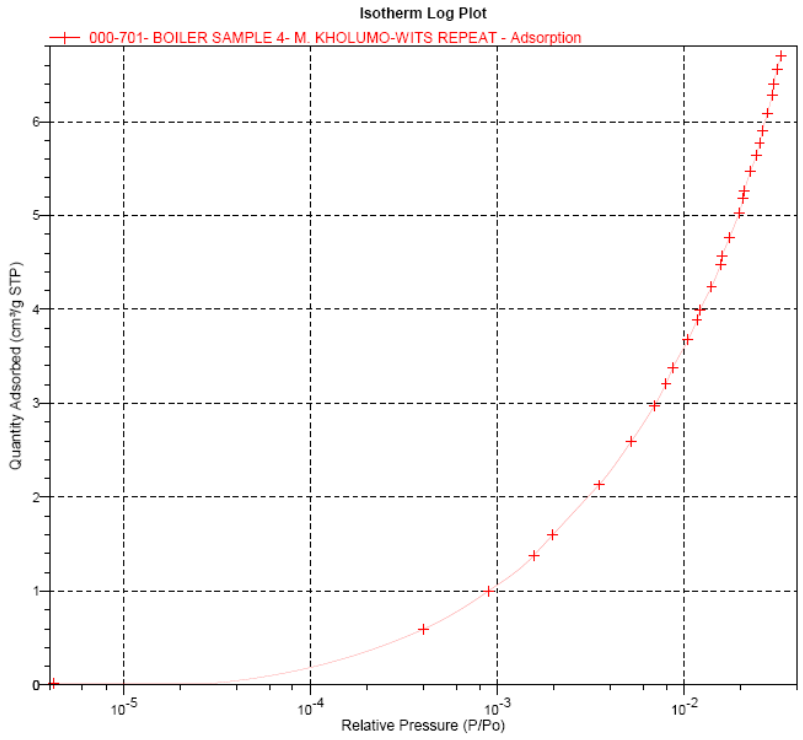


**Figure 4.13**: The CG ash isotherm log plot.

According to the values of the quantity adsorbed, given in Figure 4.13 and Appendix A, the CG ash sample would be expected to have the largest adsorption potential, while the PF ash sample would have the lowest adsorption capacity. The predicted adsorption trend is given below in order of decreasing adsorption capacity:

CG ash > SS ash > G ash > PF ash

However the arrangement of the samples in order of decreasing adsorption capacity, as determined in Section 4.2.5, is:

PF ash > SS ash > CG ash > G ash

An isotherm log plot of a CG ash sample in Figure 4.13 shows that the quantity of $CO_2$ adsorbed by a gram of the sample is 6.2 $cm^3$ at standard temperature and pressure.

Converting 6.2 $cm^3$/g of $CO_2$ to moles:

$$\mathbf{Mass}_{CO2} = \mathbf{Density}_{CO2} \times \mathbf{Volume}_{CO2}$$

$$= 1.562 g/cm^3 \times 6.2\ cm^3$$

$$= 10.7778 g$$

$$\text{Moles} = \frac{\text{Mass}}{\text{Molecular weight}}$$

$$= \frac{10.7778\ g}{44.02\ g/mole}$$

$$= 0.2448 \text{ moles}$$

This implies that 0.2448 moles of $CO_2$ were adsorbed by 1 gram of the ash sample, hence may be re-written as 0.2448 mole/g. The predicted numbers of moles adsorbed by the rest of the samples are given in Table 4.2, and are compared with the actual numbers of moles of $CO_2$ adsorbed, as determined from the VAS.

**Table 4.2**: The predicted and actual number of moles adsorbed by the samples.

| Sample Identity | Number of moles of $CO_2$ adsorbed | |
|---|---|---|
| | Predicted by BET (mole / g) | Actual amount adsorbed (mole / g) |
| CG ash | 0.245 | 0.00098 |
| G ash | 0.085 | 0.000487 |
| PF ash | 0.071 | 0.00187 |
| SS ash | 0.213 | 0.00154 |

With reference to the adsorption isotherm-types given in Figure 3.15, it can be concluded that the type of isotherm depicted by all the samples as per BET results is a Type III isotherm. As discussed in Section 3.7.1, a Type III isotherm is characteristic of a material that is not porous, or possibly macroporous, and has a low energy of adsorption. As a result, all isotherms obtained are categorized as unfavourable, hence no significant adsorption is expected to take place at low pressures with BET Type III materials, unless the pressure of the adsorbate is increased significantly.

Previous research has shown that the adsorption capacity of coal ash can be improved by treatment with polyethyleneimine (PEI), ammonia ($NH_3$) and nitric acid ($HNO_3$), via introduction of active nitrogen and oxygen functional groups (Tang *et al.*, 2004). Polyethyleneimine and $NH_3$ treatments introduce nitrogen groups on the surface of

the ash while $HNO_3$ treatment introduces both oxygen and nitrogen functional groups, where the oxygen groups are mainly carboxylic (COO-) (Tang *et al.*, 2004). However, extensive research needs to be conducted on the sorbent itself before treatment with various solvents.

According to the results given in Table 4.1, the adsorption capacity values obtained are indeed very small, except for the PF ash sample. The PF ash sample has an adsorption capacity of 1873 mole/ton (~ 1873 µmol/g), which is comparable to the commercially available sorbents. The commercially available sorbents with surface areas of 1000–1700 $m^2/g$ normally have $CO_2$ capture capacities of 1800–2000 µmol/g (Gray, 2004). This shows that treating the samples with acids and amines could essentially improve the adsorption capacity of the PF ash sample to levels much higher than the currently existing commercial sorbents. The SS ash sample, with an adsorption capacity of 1540 mole/ton, could also show an adsorption capacity comparable to that of the commercial adsorbents after being treated with acids and/or amines.

According to the pre-adsorption results given in Table 4.3, the surface area of the PF ash sample is not in the range, 1000–1700 $m^2/g$, normally exhibited by the commercially available sorbents, instead, it is 17.1 $m^2/g$, which is very small. This shows that the PF ash sample has a fairly high adsorption rate even at low surface areas. This is a very important factor especially in the industries, where space is a crucial factor.

**Table 4.3**: BET analyses conducted before and after the adsorption process.

| Sample Description | Surface area / $m^2/g$ | | Maximum Pore Volume / $cm^3/g$ | | Median pore width / Å | |
|---|---|---|---|---|---|---|
| | **Before adsorption** | After Adsorption | **Before adsorption** | After Adsorption | **Before adsorption** | After Adsorption |
| CG ash | **34.7** | 42.9 | **0.011816** | 0.015608 | **4.018** | 0.000 |
| G ash | **13.0** | 17.4 | **0.004413** | 0.004956 | **4.306** | 3.894 |
| PF ash | **17.1** | 19.2 | **0.003666** | 0.004344 | **4.433** | 4.055 |
| SS ash | **29.8** | 37.0 | **0.0111945** | 0.013719 | **4.005** | 3.52 |

Table 4.3 shows that the CG ash sample has the highest pre-adsorption surface area, while the G ash sample has the lowest surface area. The sequence of the samples in order of decreasing surface area is;

CG ash > SS ash > PF ash > G ash

It would be expected that the CG ash sample would have the highest adsorption capacity while the G ash would have the lowest adsorption capacity. This is because an increase in surface area leads to an increase in adsorption capacity. However, prediction only holds for the G ash sample because it does have the lowest adsorption capacity according to the VAS adsorption results. This observation shows that surface area does play an important role in adsorption, although to a certain extend. There are other factors which contribute to the adsortion capacity of coal ash.

According to the pre-adsorption pore volume results in Table 4.3, it would be expected that the adsorption potential of the samples would decrease with the

decrease in pore volume, owing to the fact that larger pore volume implies a largest space to accommodate $CO_2$ molecules. This would make CG ash sample the one with the largest adsorption capacity, and PF ash the sample with the smallest adsorption potential. This is understandable as ash from PF ash was very fine. This is due to the fact that the coal used in power plants is usually pulverised to a very fine particle size in order to speed up the combustion process. Crushing the samples to a very small particle size could cause blockage of the pores, hence leading to a decrease in the surface area and hence the adsorption capacity. However, according to the actual adsorption results obtained from the VAS, the opposite was observed. The PF ash sample is the one with the highest adsorption capacity, while the CG ash sample comes in the third place . This observation illustrates that pore volume does not play a crucial role in the adsorption potential of the samples although it could be of importance to some degree.

All the samples had the median pore width that is greater than 3.230 Å, which is the pore width of the adsorptive molecule ($CO_2$). For this reason, the $CO_2$ molecules are not expected to encounter diffusion problems with regards to diffusing through the sample. High surface area and open pore structure increases the adsorption rate, and decreases the overall energy requirements of the adsorption process. The PF ash sample had the highest median pore width while the SS ash had the lowest pore width. This shows that the pore width of the sample could play a significant role in the adsorption potential of the samples. The adsorption capacity of the samples as per pore width results would be in the decreasing order;

PF ash > G ash > CG ash > SS ash

As this series differs from that obtained from the adsorption results, it suggests that there are other factors that play a role in the adsorptivity of the samples apart from the pore width.

comparison between pre-adsorption and post-adsorption results (regarding surface area, pore volume and pore width) in Table 4.3 was made. It shows that the adsorption of $CO_2$ on the samples increased the surface area of all the samples. This observation is sensible because the alignment of the $CO_2$ molecules on the ash surface would increase the surface area of the sample, especially if the $CO_2$ molecules followed a multiple layer model as in Figure 4.14 (b), as opposed to formation of a monolayer given in Figure 4.14(a).

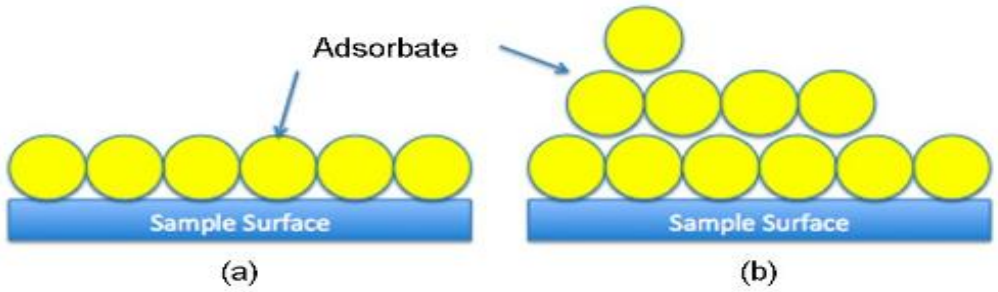


**Figure 4.14**: Schematic of the adsorption of gas molecules onto the surface of a sample showing (a) monolayer adsorption model and (b) multilayer adsorption model (Barron, 2011).

Table 4.3 illustrates that the pore volume of the samples increased after the adsorption process. This observation is due to the fact that applying pressure to the sample causes the pores to stretch, hence increasing the volume of the pores. The pore width of the samples decreased after the adsorption process. This is attributable to the $CO_2$ molecules that align themselves on the walls of the pores, hence constricting the width of the pores.

## 4.4 X-RAY DIFFRACTION SPECTROSCOPY

The samples were prepared for XRD analysis using a back loading preparation method, in order to conduct a quantitative study of the minerals. Table 4.4 shows a quantitative list of the minerals present in the samples as per XRD analysis. A detailed table is given in Appendix C.

**Table 4.4**: A summary of XRD results[1].

| MINERALS | CG ASH / % | G ash / % | PF ash / % | SS ASH / % |
|---|---|---|---|---|
| Akermanite $Ca_2MgSi_2O_7$ | 0.12 | 1.62 | 0.05 | 0.00 |
| Amorphous | 71.09 | 44.48 | 47.6 | 68.64 |
| Anhydrite$CaSO_4$ | 1.44 | 0.51 | 1.63 | 1.10 |
| Lime $CaO$ | 0.08 | 0.02 | 0.33 | 0.56 |
| Corundum$Al_2O_3$ | 1.55 | 1.64 | 1.65 | 1.22 |
| Hematite $Fe_2O_3$ | 2.13 | 0.25 | 2.20 | 1.53 |
| Magnetite $Fe_3O_4$ | 2.59 | 0.75 | 1.11 | 2.53 |
| Mullite $Al_6Si_2O_{13}$ | 13.64 | 20.14 | 31.54 | 18.00 |
| Periclase $MgO$ | 0.72 | 0.63 | 0.70 | 0.82 |
| Plagioclase$NaAlSi_3O_8$ to $CaAl_2Si_2O_8$ | 4.15 | 12.29 | 1.18 | 3.27 |
| Pyrite $FeS_2$ | 0.08 | 0.16 | 0.26 | 0.06 |
| Quartz $SiO_2$ | 2.42 | 12.96 | 11.72 | 2.25 |

In all samples, the majority of the minerals in the ash are quartz and aluminosilicates (plagioclase and mullite). The quartz may represent fragments of material from the original feedstock which passed without reaction through the respective combustion

[1]*Minerals of interest are highlighted in red.*

systems. The aluminosilicates were probably formed during combustion, possibly from kaolinite commonly present in raw coals, via a meta-stable phase such as metakaolin or sillimanite (Ram, 1992). The formation of Al-silicates might have been from the reaction of $Al_2O_3$ with free silica ($SiO_2$). However, since $Al_2O_3$ is not very common in coal, the formation of Al-silicates might have happened via the formation of an intermediate product ($Al_2Si_2O_5$) (van Dyk, 2006). The formation of Al-silicates could have also been due to the solid phase reactions between quartz and liberated oxides of K/Na/Ca via the formation of silicates phases and their transformation to specific Al-silicates at high temperatures (Vassileva and Vassilev, 2006). Some of the minerals might have been already present in coal even before the combustion or gasification process. Due to extremely high temperatures and pressures at which they were formed, it might be that they did not change their chemical structures when heated due to high stability.

Not all the minerals listed in Table 4.4 are of relevance to this project. The minerals of interest are periclase (MgO), and lime (CaO).This is because they are alkaline metal oxides. The alkaline metal oxides (MgO and CaO) react with $CO_2$ to produce calcite ($CaCO_3$) and magnesite ($MgCO_3$). This is a naturally occurring rock weathering process, the chemical equations of which is given below:

$$2\ CaO + 3\ CO_2 \longrightarrow 2\ CaCO_3 \qquad \text{Eq. 4.5}$$

$$2\ MgO + 3\ CO_2 \longrightarrow 2\ MgCO_3 \qquad \text{Eq. 4.6}$$

Carbonate has a lower energy-state than carbon, and carbonation reactions are highly exothermic. However, a downfall of the carbonation processes is that they require the oxides to be aqueous. CaO and MgO readily and rapidly sequester $CO_2$ under moist conditions (Herzog, 2002).

### 4.4.1 Expected Adsorption Capacity through Mineral Carbonation

To calculate the amount of $CO_2$ that could be sequestered through mineral carbonation, the CG ash sample was chosen as an example.

#### i) Adsorption by CaO

According to the XRD analysis in Table 4.4, 1.5 g of CG ash sample has 0.08 % CaO

Therefore: CaO in the sample = $\frac{0.08}{100} \times 1.5$ g

= 0.0012 g

Converting mass to moles

Moles of CaO = $\frac{\text{Mass of CaO}}{\text{Molecular Weight of CaO}}$

= $\frac{0.0012\text{g}}{56\text{g/mole}}$

= $2.14\times 10^{-5}$ moles

The ratio of CaO to $CO_2$ is 2:3 (refer to Eq. 4.1), therefore the number of moles of $CO_2$ expected to be adsorbed is:

$\frac{3}{2} \times 2.14\times 10^{-5}$ moles = $3.21\times 10^{-5}$ moles

Therefore CaO could adsorb **$3.21\times 10^{-5}$ moles** of $CO_2$. Since the mass of the sample used was 1.5 g, the number of moles adsorbed becomes:

$\frac{3.21\times 10^{-5}\ moles}{1.5g}$ **= $2.14\times 10^{-5}$ moles/g**

#### ii) Adsorption by MgO

According to the XRD results in Table 4.4, 1.5 g of CG ash sample 0.72 % of MgO.

Therefore: MgO in the sample = $\frac{0.72}{100} \times 1.5$ g

= 0.0108 g

Converting mass to moles;

$$\text{Moles of MgO} = \frac{\text{Mass of CaO}}{\text{Molecular Weight of CaO}}$$

$$= \frac{0.0108\ \text{g}}{40.3045\ \text{g/mole}}$$

$$= 2.68 \times 10^{-4}\ \text{moles}$$

The ratio of MgO to $CO_2$ is 2:3 (refer to Eq. 4.1), therefore the number of moles of $CO_2$ expected to be adsorbed is:

$$\frac{3}{2} \times 2.68 \times 10^{-4}\ \text{moles} = 4.02 \times 10^{-4}\ \text{moles}$$

Therefore MgO could adsorb **$4.02 \times 10^{-4}$ moles** of $CO_2$. Since the mass of the sample used was 1.5 g, the number of moles adsorbed becomes:

$$\frac{4.02 \times 10^{-4}\ moles}{1.5\ g} = \mathbf{2.68 \times 10^{-4}\ moles/g}$$

The numbers of moles of $CO_2$ expected to be adsorbed by the samples through mineral carbonation are given in Table 4.5**,** together with the actual amount adsorbed as per VAS results, for comparison purposes.

**Table 4.5**: The expected numbers of moles of $CO_2$ to be adsorbed by the individual samples.

| Sample | The predicted amount of $CO_2$ that could be adsorbed through mineral carbonation based on | | | Actual amount adsorbed (mole/g) |
|---|---|---|---|---|
| | CaO (mole/g) | MgO (mole/g) | Total amount expected to be adsorbed (mole/g) | |
| CG ash | $2.14\times 10^{-5}$ | $2.68\times 10^{-4}$ | $\mathbf{2.89\times 10^{-4}}$ | $\mathbf{9.80\times 10^{-4}}$ |
| G ash | $5.36\times 10^{-6}$ | $2.34\times 10^{-4}$ | $\mathbf{2.40\times 10^{-4}}$ | $\mathbf{4.87\times 10^{-4}}$ |
| PF ash | $8.84\times 10^{-5}$ | $2.61\times 10^{-4}$ | $\mathbf{3.49\times 10^{-4}}$ | $\mathbf{1.87\times 10^{-3}}$ |
| SS ash | $1.50\times 10^{-4}$ | $3.05\times 10^{-4}$ | $\mathbf{4.55\times 10^{-4}}$ | $\mathbf{1.54\times 10^{-3}}$ |

Comparing the predicted total amount of $CO_2$ with the actual amount adsorbed, it is perceived that the actual amount adsorbed by the samples is much larger than the predicted amount, based mineral carbonation. This shows that the amorphous portion of the samples, which is larger than the mineral content in all samples (according to the XRD results given in Table 4.4), plays the major role in the adsorption potential of the samples. Obviously, these results are only theoretical as the time for mineral carbonation to occur is predicted to be in the order of years, and the experiments were only conducted over $7\frac{1}{2}$ hours.

## 4.5 THERMOGRAVIMETRIC ANALYSIS

The samples were characterized using a TGA to determine their thermal stability and dehydration characteristics. The measurements were performed using *Perkin Elmer STA6000* TGA equipment as outlined in Section 3.7.3. CG ash sample is used as an example for interpreting the TGA data. The TGA analysis graph of the CG ash

sample is given in Figure 4.15, while those for other samples are attached in Appendix B.

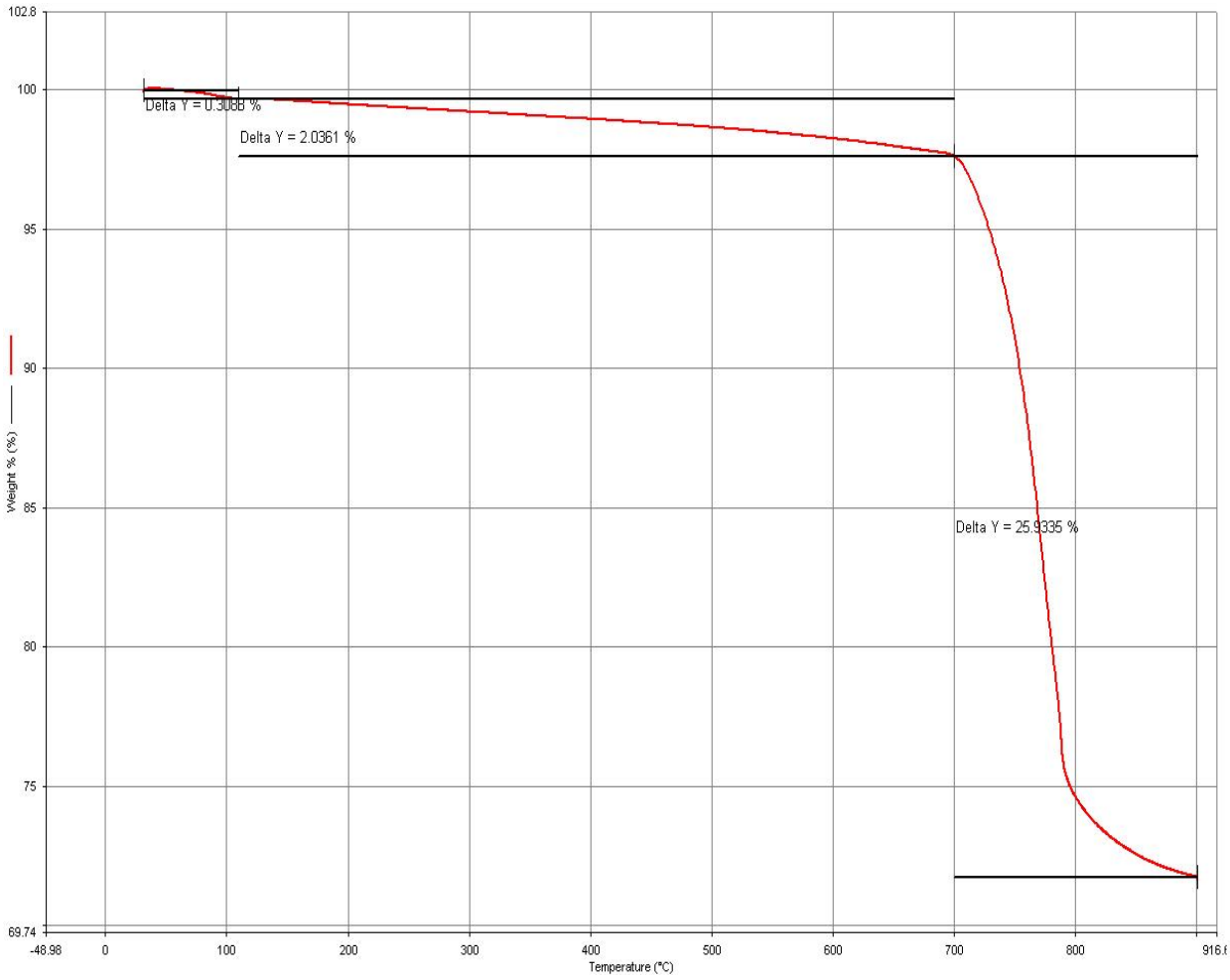


**Figure 4.15**: CG ash sample TGA graph.

**First heating step** (30ºC – 110ºC): This is the first heating step where the sample was heated from room temperature (30ºC) to 110°C. During this step, only water is expected to be released due to the fact that water changes to a gaseous state at 100°C while other ash components vaporize at much higher temperatures. Figure 4.14 shows a mass loss of 0.3088%, meaning that the CG ash sample was fairly dry. Therefore, inhibition of adsorption of $CO_2$ molecules by water molecules is not a significant factor for this sample.

**Second heating step** (110°C to 700°C): During this temperature regime, the volatile matter disengages from the ash. Figure 4.14 shows that only 2.0361% of the CG ash sample mass was lost, suggesting that the volatile matter in this sample was significantly low. This is attributable to the fact that the ash sample is combustion product.

**Third heating step** (700°C to 900°C): During this heating regime, the nitrogen gas is switched to oxygen gas, as a result the remaining carbon reacts with the oxygen and is combusted. Figure 4.14 depicts that 25.9335% of the CG ash sample is fixed carbon. Since over a quarter of the sample was fixed carbon, this suggests that to a considerable extent, adsorption may have occurred through interaction of $CO_2$ with the unburned carbon.

The ash percentage is determined by adding the moisture percentage to that of volatile matter and fixed carbon. The sum of the three is then subtracted from 100% and the difference is the ash content of the sample. For the CG ash sample, the ash content is given as:

Fixed carbon = 100% - (Moisture % + Volatile % + Ash %), hence

Ash content = 100% - (Moisture % + Volatile % + Fixed carbon%)

= 100% - (0.3088% + 2.0361% + 25.9335%)

= 100% - 28.2784%

= 71.7216%

The ash content of the CG ash sample is 71.7216% and is comprised of incombustible inorganic minerals as depicted by the XRD results in Table 4.4. The TGA results of the rest of the samples are summarized in Table 4.6.

**Table 4.6**: A summary of the TGA results.

| Sample Identity | Moisture content (%) | Volatile matter content (%) | Fixed carbon Content (%) | Ash content (%) |
|---|---|---|---|---|
| CG ash | 0.31 | 2.04 | 25.93 | 71.72 |
| G ash | 0.41 | 3.22 | 5.77 | 90.60 |
| PF ash | 0.21 | 2.92 | 3.99 | 92.87 |
| SS ash | 0.35 | 1.50 | 30.56 | 67.59 |

The moisture content for all the samples seems to be fairly low as expected, and therefore there is no fear that the $CO_2$ molecules may have competed with water molecules for the adsorption sites (in addition the sample was evacuated before testing). The volatile matter is also observed to be fairly low, as expected. The G ash sample has the largest content of volatile matter, while SS ash has the smallest amount. High volatile matter is associated with high adsorption capacity (Soares *et al.*, 2007), therefore the G ash sample would be expected to have the highest adsorptivity. However, since the content of volatile matter is fairly low (3.22%), the influence of volatile matter on adsorption is likely to be insignificant.

CG ash and SS ash samples have high fixed carbon contents, which may increase the adsorption capacity of the sample as carbon is possibly a more suitable site for adsorption than mineral matter. Fixed carbon content may increase the adsorption potential of ash by virtue of interacting with the $CO_2$ via weak carbon-carbon dipole moments. This explains why the SS ash sample had a high adsorption capacity. However the PF ash sample, which also had high adsorption capacity, has the lowest fixed carbon content. This means that there are other factors apart from fixed carbon, which play an important role in the adsorption capacity of ash.

As with fixed carbon content, the ash content is also another manner by which the efficiency of the boilers may be determined. The higher the ash content in coal ash,

the higher the efficiency of the boiler. Ash mainly consists of incombustible inorganic matter, such as the minerals outlined in Table 4.4. Some of these minerals were already integrated within the matrix of coal, and for them to have not reacted even at high combustion temperatures implies that it is very unlikely for them to be affected by the adsorption process, and hence will remain inactive through-out the adsorption experiment. Some of the minerals were formed at high combustion temperatures, meaning that they are in an inactive glassy phase and hence would need a much higher temperature to be reactive.

## 4.6 PETROGRAPHY RESULTS

The coal ash samples were prepared for petrography. Observations were made with regards to char particles and minerals.

### 4.6.1 Char Morphology

The petrographic images (Figures 4.16 – 4.19) showed that the CG ash sample had the highest observed proportion of chars, while PF ash had the lowest amount of char. The trend in order of the decreasing char particle size as was observed is as follows:

CG ash > SS ash > G ash> PF ash.

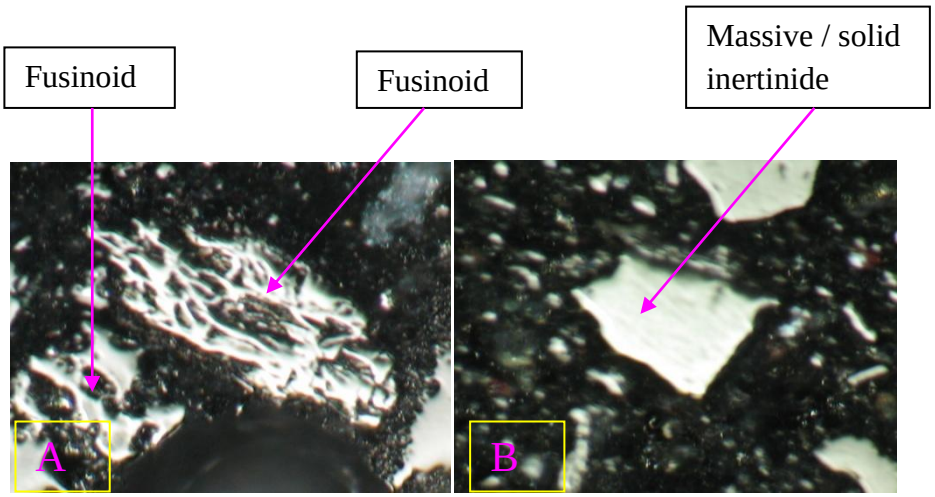


**Figure 4.16**: CG ash char particles showing A) fusinoid char B) a solid/massive inertinitic char.

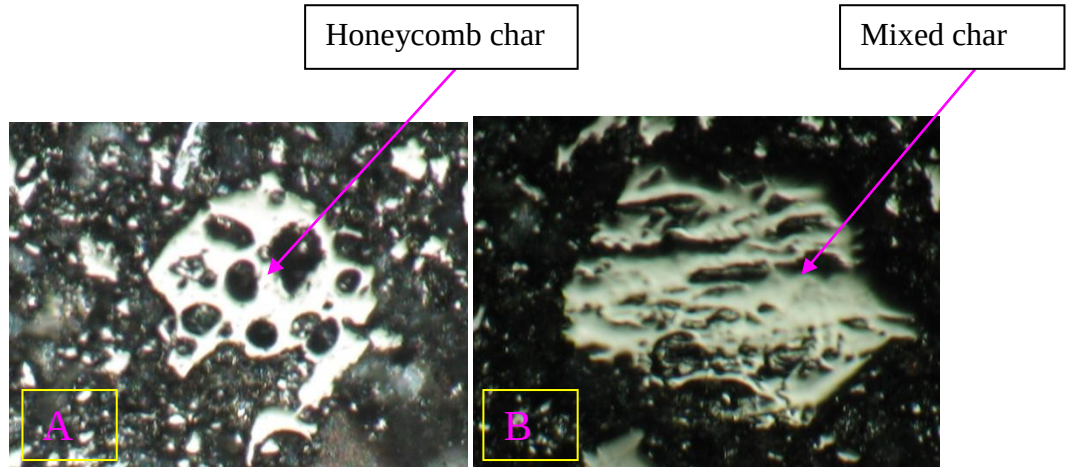


**Figure 4.17**: SS ash char particles showing A) a vesicular, honeycomb char and B) a mixed char particle showing porous and non-porous bands.

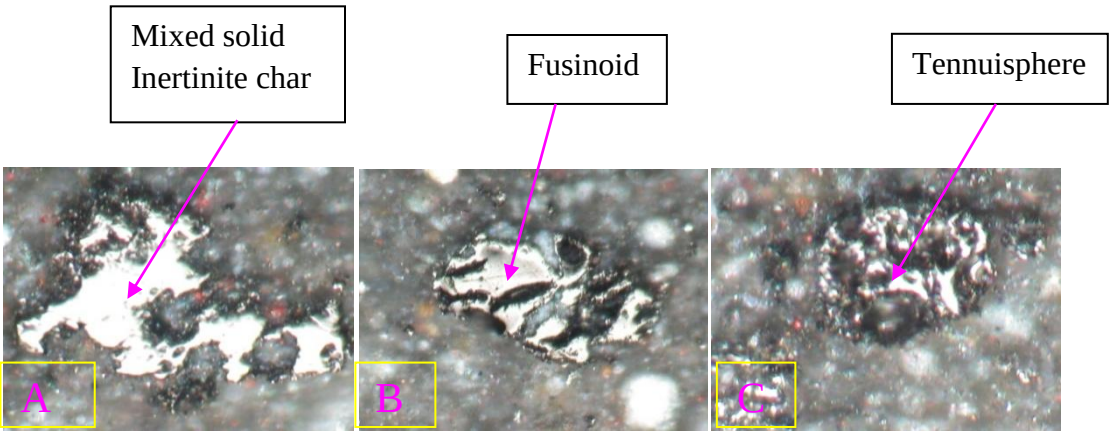


**Figure 4.18**: PF ash char particles of A) a mixed solid inertinite char, B) a fusinoid char and C) tennuisphere.

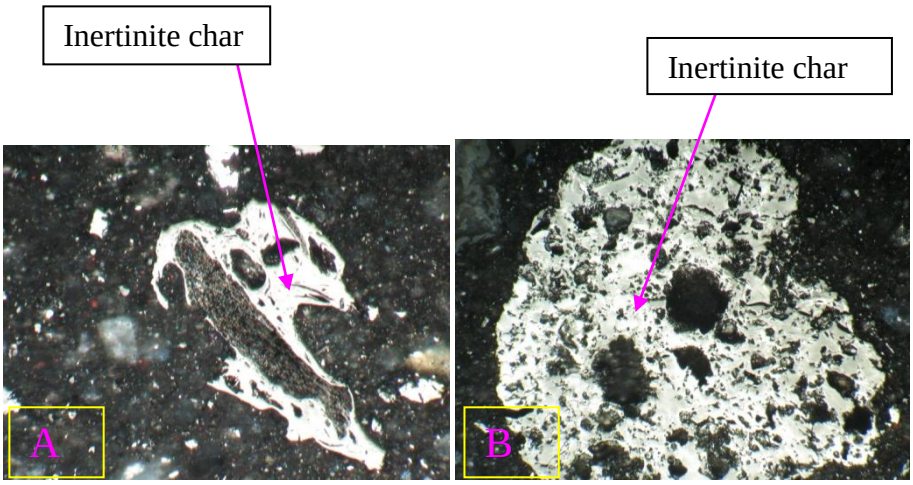


**Figure 4.19**: Sasol char images of A) an inertinite char B) inertinide char derived from inertodetrinile.

While some of the chars may be isotropic, they are most likely to be anisotropic carbonized products due to severe process conditions used during coal combustion (Hower and Mastalerz, 2001).

### 4.6.2 Ash Minerals

Combustion ash residues from coal minerals such as clay, other silicates, carbonates, quartz, pyrite and iron oxides were observed in some of the samples. Some images are given in Figures 4.20 – 4.23.

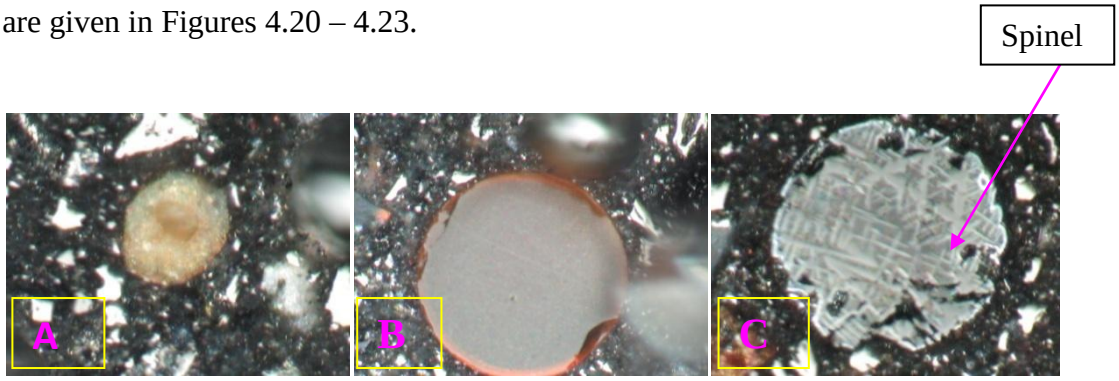


**Figure 4.20**: CG ash mineral particles: A) glassy phase sphere B) glassy phase sphere C) spinel ferrospheres indicate the presence of iron oxides.

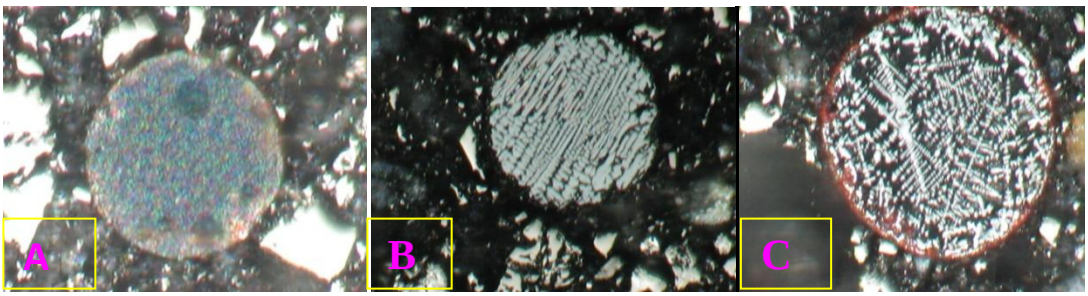


**Figure 4.21**: SS ash mineral particles showing different types of spinel in images A, Band C.

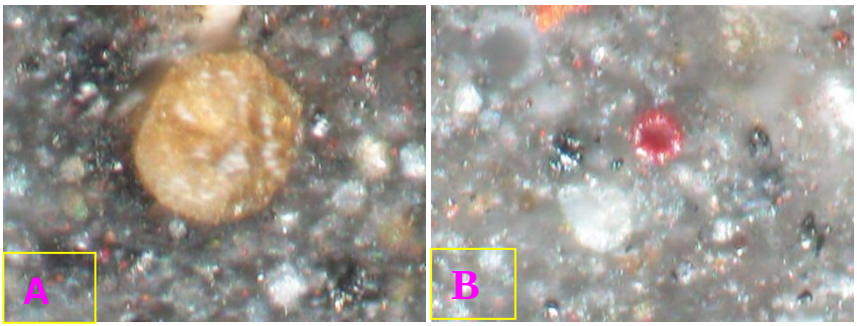


**Figure 4.22**: Images A and B show different PF ash mineral particles.

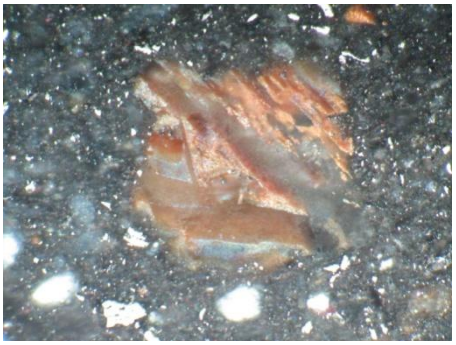

**Figure 4.23**: An unidentified mineral form the G ash sample.

Petrographic images confirmed presence of minerals and char particles in the samples.

## 4.7 CHAPTER CONCLUSIONS

The ranking of the samples based on their adsorption capacity as predicted by different characterizing techniques is given in Table 4.7. The predicted rankings were also compared against the actual adsorbed $CO_2$. The samples are ranked in such a way that $1^{st}$ refers to the sample with the highest expected adsorption capacity while $4^{th}$ refers to the lowest adsorption capacity.

**Table 4.7**: A summary of the rankings drawn from different techniques on the basis of samples' $CO_2$ adsorption capacities.

| Sample | Ranking based on | | | |
|---|---|---|---|---|
| | Fixed carbon content - (TGA results) | Surface area and pore volume - (BET results) | minerals carbonation - (XRD results) | **Actual adsorption results** |
| CG ash | 2nd | 1st | 3rd | **3rd** |
| G ash | 3rd | 3rd | 4th | **4th** |
| PF ash | 4th | 4th | 2nd | **1st** |
| SS ash | 1st | 2nd | 1st | **2nd** |

Based on Table 4.7, it is very difficult to decide on the number one factor that solely contributes most to the adsorption capacity. However, pore volume, pore width, and surface area seemed to agree more with the adsorption results than most of the characterising techniques. Therefore, adsorption of $CO_2$ on coal ash is likely to have occurred via physisorption and not through both physisorption and chemisorption as was initially anticipated. XRD results showed that the amount of minerals that were expected to react with $CO_2$ (CaO and MgO) constitute about 1% of the total samples, which is very small. Apart from that, these minerals would require high temperatures and pressures for them to be active, the conditions which were not applied during the undertaking of this project. Hence, it is very unlikely that chemisorption could have contributed to the overall adsorption capacity of the samples. Petrography analysis confirmed presence of some of the minerals.

TGA results agreed with XRD in that, both techniques showed that the G ash and PF ash samples had higher quantities of ash content than the CG ash and SS ash samples. These techniques also showed that CG ash and SS ash samples had higher carbon content and amorphous content than G ash and PF ash samples. The amount of $CO_2$ that may be adsorbed by coal ash ranges between 0.17 Mt $CO_2$ and 2.8 Mt $CO_2$.

# CHAPTER 5

## CONCLUSIONS AND RECOMMENDATIONS

### 5.1 PROJECT SUMMARY

Coal continues to play a significant role as a major energy source in the advancement of economic activity in South Africa. However, coal combustion emits various gases that negatively affect the environment, particularly the ground-level air quality. Recently, the main focus is on $CO_2$ as it is generally believed to cause global warming.

Much research is being conducted with the aim of fabricating suitable adsorbents for $CO_2$ in order to reduce its emissions. Ash is among the most widely used materials in the synthesis of $CO_2$ adsorbents because it has high porosity, high carbon content, and is highly abundant. This research project was intended to determine whether or not South African coal ash is a suitable adsorbent for $CO_2$ and to study the adsorption potential of a variety of ash types.

The chemical and physical composition of four coal ash samples were assessed. The ash samples used in this study were obtained from three different coal-using industries namely: 1) a coal power station, 2) a petrochemical industry, and 3) a metallurgical plant. The characterisation techniques employed in this project were: BET, XRD, TGA, and petrography analyses.

The adsorption capacity of each sample was assessed using VAS experiment at varying pressure. Each of the samples were placed in the VAS sample cell for 7½ hours in total, to facilitate the adsorption process. During the first hour, the sample was exposed to $CO_2$ at a pressure of 5 bar. The pressure was increased to 10 bar after an hour. The process was repeated until the pressure reached 36 bar.

## 5.2 KEY FINDINGS AND CONCLUSIONS

The PF ash sample was found to have the highest $CO_2$ adsorption capacity with a value of 0.001873 mol/g, followed by the SS ash sample with 0.00154 mol/g. In the third place was the CG ash sample with 0.00098 mol/g and lastly the G ash sample with 0.000487 mol/g. The as-received coal ash was found to have a potential to uptake $CO_2$ in a range of 0.17 – 2.8 Mt $CO_2$. This means that at most 1.28% of annual sequestrable $CO_2$ produced could be captured using ash produced annually by coal power stations in South Africa.

Additional key findings are listed below:

- A marked difference was observed in the colour of the ash samples. The PF ash sample was a homogenous finely grained grey powder. The G ash sample appeared to be a mixture of course ash and fine ash, consisting of white to grey stone in a black glassy matrix. The CG ash and SS ash samples were black in colour, with a fine homogeneous texture. As confirmed by the XRD and TGA analyses, the CG ash and SS ash samples had more unburned carbon and amorphous content than the PF ash and G ash samples.

- Although mullite is the second most abundant mineral in the samples, it is not expected to have played any role in the adsorption experiment because it is a very stable compound. It is expected to be reactive only at extremely high temperatures. Other minerals, such as quartz and plagioclase, are also not expected to contribute to the adsorption capacity of the ash due to their high stability. Although all samples contained MgO and CaO, they contributed less that 1% of the samples' mineral content. Even if the quantity of the oxides had been more than 1%, they might have not reacted with $CO_2$ because CaO and MgO readily and rapidly sequester $CO_2$ under moist conditions (Herzog, 2002). Petrography confirmed presence of some of the minerals.

- Different factors appear to affect the adsorprtivity of the samples, and none of the factors considered during this research solely provided accurate predictions about the adsorption capacity of the samples. However, it could be concluded that adsorption of $CO_2$ on coal ash is mostly influenced by surface area, pore volume and pore width because the results obtained from BET analysis agreed with the actual adsorption results. Therefore, adsorption of $CO_2$ on coal ash is likely to have occurred through physisorption only and not through both physisorption and chemisorption as was initially anticipated. XRD results showed that the amount of minerals, which were expected to react with $CO_2$ (CaO and MgO) constitute about 1% of the total samples, which is very small. Furthermore, these minerals would require high temperatures and pressures for them to be active, the conditions which were not applied in this project. Hence it is very unlikely that chemisorption could have contributed to the overall adsorption capacity of the samples.

The aims and objectives stated in Section 1.3 were met in that the adsorption potential of $CO_2$ on coal ash was established and the type of coal ash with the most $CO_2$ adsorption capacity was determined. Since coal ash is cheap and abundantly available, it could be used to synthesise, or be used as a cost-effective $CO_2$ adsorbent in the future. The hypothesis stated in Section 1.4 was found to be true because South African coal ash is a suitable material for use as a $CO_2$ adsorbent. Based on the experimental results, South African coal ash could be considered as a suitable material to sequester $CO_2$, in order to reduce $CO_2$ emissions.

## 5.3 RECOMMENDATIONS

The 1.28 % of the annual sequestrable $CO_2$ adsorbable through untreated ash as established in this project is fairly little. However, its adsorption capacity could be improved by introducing active functional groups through treatment with acids, brine or amines. This could be further looked into as a follow-up project. In addition, the

reversibility of the isotherms, regenerability, stability, adsorption-desorption kinetics, operating windows and the diffusional aspects could also be investigated, using other characterising techniques such as Temperature Programmed Desorption (TPD), and SEM, in order to fully understand the adsorption properties of coal ash. It would be very beneficial to also examine the factors that could ultimately affect the adsorption capacity on a large industrial scale, because some of the aspects may work well at a laboratory scale but not necessarily at large scales. Other means of adsorbing $CO_2$ also need to be explored in order to help capture all of the sequestrable $CO_2$.

For future work, coal ash from UCG cavities could also be used in adsorption experiments in order to study the adsorption capacity of the UCG ash. This study will help to ultimately link UCG to CCS, which is an interesting research direction that should be undertaken globally.

# REFERENCES


Ahmaruzzaman, M., 2010, *A review on the utilisation of fly ash*, Progress in Energy and Combustion Science, Vol. 36, pp. 327–363.

Anderson, S., Newell, R., 2003, *Prospects of Carbon capture and storage technologies,* Resources for the future, RFF Discussion paper 2-68, Available at< http://www.rff.org/documents/RFF-DP-02-68.pdf>, [Accessed 19th June 2011].

Armaroli,N. and Balzani,V., 2011, *Energy for a Sustainable World: From the Oil Age to a Sun-Powered Future*, John Wiley & Sons, pp. 302.

Arenillas, A., Rubiera, F., Parra, J. B., Ania, C. O., Pis, J. J., 2005. APPLIED SURFACE SCIENCE: *Surface modification of low cost carbons for their application in the environmental protection.* Vol 3, pp 619-624.

ASME, 2009, *General position statement on technology and policy recommendations and goals for reducing carbon dioxide emissions in the energy sector,* American Society of Mechanical Engineers, Available at <http://www.asme.org>, [Accessed 20th July 2011].

Bada, S.O. and Potgieter-Vermaak, S., 2008, *Evaluation and Treatment of Coal Fly Ash for Adsorption Application*, Leonardo Electronic Journal of Practices and Technologies, Vol. 7, pp. 37-48.

Barron, A. R., 2011, *Physical Methods in Inorganic and Nano Chemistry*. Connections, Available at <http://cnx.org/content/col10699/1.12/> [Accessed 20th July 2011].

Bel, 2007, *Method of Adsorption Amount Measurement, BEL Japan Inc.*, Available at <http://www.nippon-bel.co.jp/tech/seminar03_e.html>, [Accessed 5th Dec 2011].

Bethlehem, L., 2009, *Catalysing change: International environmental pressures on South African exporters*, International Development research centre, Available at <http://www.idrc.ca/en/ev-138112-201-1-DO_TOPIC.html>, [Accessed 13th May 2011].

Cairncross, B., 2001, *An overview of the Permian (Karoo) coal deposits of Southern Africa*, African Earth Sciences, Vol. 33, pp. 529-562.

Centre for Applied Energy Research, 2010, *Boiler Slag*, Kentucky Ash Education Site, Available at <http://www.caer.uky.edu/kyasheducation/boilerslag.shtml>, [Accessed 13th May 2011].

Cloete, M., 2010, *Atlas on geological storage of carbon dioxide in South Africa*. Council of Geoscience, Pretoria, South Africa.

Condon, J.B**.,** 2006, *Surface Area and Porosity Determinations by Physisorption*, Elsevier, Amsterdam, Netherlands. pp. 6 – 9.

Conway, T. and Tans, P., 2011, *Trends in atmospheric carbon dioxide*, Earth System Research laboratory, [Last updated in February 2011], Available at <http://www.esrl.noaa.gov/gmd/ccgg/trends/global.html>, [Accessed 16th March 2011].

Daga, A., Ganesan, N. and Shankar, K., 2009, *Behaviour of magneto-electro-elastic sensors under transient mechanical loading*, Sensors and Actuators A: Physical, Vol. 150, pp. 46-55.

Donahue, C.J. and Rais, E.A., 2009, *Proximate analysis of coal*, Journal of Chemical Education, Vol. 86, pp. 222-224.

Doucet, F. J. 2010, *Effective $CO_2$-specific sequestration capacity of steel slags and variability in their leaching behaviour in view of industrial mineral carbonation.* Minerals Engineering, Vol. 23, pp. 262-269.

Drbal, L.F., Boston, P., and Westra, K.L, 1996: *Power plant engineering by Black & Veatch*.
Springer Science+Business Media, Inc., New York, USA, pp. 114.

Energy Information Administration, 2000, *National Energy Information Centre*, Available at <http://www.eia.doe.gov /cabs/sadc.html>, [Accessed 30th March 2010].

Engelbrecht,A., Golding, A., Heitkamp, S., Scholes,B., 2004, *The potential for CO2 sequestration in South Africa,* Council of Scientific and Industrial Research, Available at <http://www.docstoc.com/docs/68868291/THE-POTENTIAL-FOR SEQUESTRATION-OF-CARBON-DIOXIDE-IN-SOUTH-AFRICA>, [Accessed 12th April 2011].

Eskom, 2010, *Integrated report 2010,* Available at <http://www.eskom.co.za/annreport10/downloads/eskom_ar2010.pdf>, [Accessed 14th April 2011].

Falcon, R. and Ham, A.J., 1988, *The characteristics of Southern African coals*, Journal of The South African Institute of Mining and Metallurgy, Vol. 88, pp. 145-161.

Figueroa, J.D., Fout,T., Plasynski, S., McIlvried, H., Srivastava, R. D.,2008, *Advances in $CO_2$ capture technology—The U.S. Department of Energy's Carbon Sequestration Program*, International Journal of Greenhouse Gas Control, Vol. 2, pp. 9 – 20.

Gökcekus, H., 2011, *Survival and Sustainability: Environmental Concerns in the 21st Century*, Springer, New York, pp. 1049.

Guo, B., Chang, l., Xie, K., 2006, *Adsorption of carbon dioxide on activated carbon*, Journal of Natural gas Chemistry, Vol. 15, No. 3, pp. 223-229.

Gray, M.L, 2004, *$CO_2$ capture by amine-enriched fly ash carbon sorbents*, Separation and Purification Technology, Vol. 35, pp. 31–36.

GroundWork, 2011, *GroundWork submission on: National Climate Change Response White Paper 2011*. Available at <http://www.groundwork.org.za/Publications/Reports/groundWork%20Submission%20White%20Paper%20CC.pdf>, [Accessed 22nd November 2011].

Hawksworth, J., 2006, *The world in 2050: implications of global growth for carbon emissions and climate change policy*, Price waterhouse cooper, Available at <http://www.pwc.com/gx/en/world-2050/pdf/world2050carbon.pdf>, [Accessed 22nd November 2011]

Haynes. R. J., 2009, *Reclamation and revegetation of fly ash disposal sites – Challenges and research needs*, Journal of Environmental Management, Vol. 90. Pp.43–53.

Herzog, H., 2002, *Carbon Sequestration via Mineral Carbonation: Overview and Assessment,* MIT Laboratory for Energy and the Environment, Available at <http://sequestration.mit.edu/pdf/carbonates.pdf >, [Accessed 4th Dec 2011].

Herzog, H.J. and Golomb, D., 2004, *Carbon capture and storage from fossil fuel use*, In: C.J. Cleveland, ed., *Encyclopedia of energy*, Elsevier Science, New York, pp. 277–287.

Hower, J. C. and Mastalerz, M., *2001, An approach toward a combined scheme for the petrographic classification of fly ash,* Energy and Fuels, Vol. 15, pp.1319-1321.

Hu, Y., Naito, S., Kobayashi, N. 2000, *$CO_2$, $NO_x$ and $SO_2$ emissions from the combustion of coal with high oxygen concentration gases,* Fuel, Vol. 79. pp. 1925–1932.

IEA Clean Coal Centre, 2010, *The global resource on the clean use of coal*, Available at <http://www.iea-coal.org.uk/site/2010/database-section/clean-coal-technologies>, [Accessed 15th May 2010].

IEA statistics, 2010, *$CO_2$ emissions from fuel consumption: Highlights*, International Energy Agency, Paris Cedex. Available at< http://www.energyconf.ir/pdf/7.pdf > [Accessed 9th July 2011].

Implats, 2011, *Integrated Annual Report 2011,* Available at <http://www.implats.co.za/implats/downloads/2011/annual%20reports/Implats%20AR_Combined_LoRes.pdf>, [Accessed 4th Dec 2011].

Jacobs, T., 2007, *Design and construction of novel porous materials,* University of Stellenbosch.

Jadhav, P.D., Chatti, V., R., Biniwale, R., B., Labhsetwar, N., K., Devotta, s., Rayalu, S., S., 2007, *Monoethanol amine modified zeolite 13X for $CO_2$ adsorption at different temperatures*, Energy Fuels, Vol. 21, pp. 3555–3559

Jaradat, K.M.A., 2009, *Adsorption and Desorption Characteristics of Endosulfan Pesticide in Three soils in Palestine*, PhD Thesis, AN-Najah National University, Nablus, Palestine, Available at <http://www.najah.edu/thesis/5171721.pdf >, [Accessed 18th August 2011].

Jones, N.S., _Holloway, S., Creedy, D. P., Garner.K., 2005, *Can UK coal resources contribute to a gas renaissance?*, Petroleum Geology Conference series, Vol. 6, pp. 715 – 722.

Karr, C., 1978, *Analytical Methods for Coal and Coal Products Volume I*, Academic Press, New York.

Keller, J.U. and Robens, E., 2003, *A Note on Sorption Measuring Instruments*, Journal of Thermal Analysis, Vol.71, pp.37-45.

Krkljuš, I., 2011, *Correlation between the Microstructure of Porous Materials and the Adsorption Properties of $H_2$ and $D_2$*, PhD Thesis, Universität Stuttgart, Available at <http://elib.uni-stuttgart.de/opus/volltexte/2011/6348/pdf/I._Krkljus_PhD_Thesis.pdf> [Accessed 18th August 2011].

Kruger, R. A., 1997, *Fly ash beneficiation in South Africa: creating new opportunities in the market-place*, Fuel, Vol. 76, pp. 777-779.

Kruger, R. A., n.d., The *creation of a sustainable coal ash industry in South Africa*, Richonne Consulting, Available at <http://ccp.eapbe.ru/uploads/files/krugereng.pdf>, [Accessed 02th Dec 2011].

Lee, J-S., *et al.*, 2002, *Adsorption Equilibria of $CO_2$ on Zeolite 13X and Zeolite X/Activated Carbon Composite*, Journal of chemical and engineering data, Vol 47, No. 5, pp. 1237–1242.

Lee, C. T., 2005, *Microstructure evaluations and thermomechanical properties of spinel ($MgAl_2O_4$) dispersed molybdenum alloys*, PhD Thesis, West Virginia University, Available at <http://wvuscholar.wvu.edu:8881//exlibris/dtl/d3_1/apache_media/L2V4bGlicmlzL2R0bC9kM18xL2FwYWNoZV9tZWRpYS8yMDc3Mg==.pdf >, [Accessed 14th May 2011].

Li, Z., Hwang, J. Y., Sun, X., 2002, *Carbon from Fly Ash for Mercury Adsorption: II. Adsorption Isotherms and Mechanisms*, Journal of Minerals & Materials Characterisation & Engineering, Vol. 1, No.2, pp.79-96.

Man, C.K., Gibbins, J.R., Cashdollar, K.L., 2007, *Effect of Coal Type and Oxyfuel Combustion Parameters on Pulverised Fuel Ignition*, 2007 International Conference on Coal Science and Technology, Available at <http://www.cdc.gov/niosh/mining/pubs/pdfs/eocta.pdf >, [Accessed 17th June 2011].

Marais, C.G., 2008, *Thermodynamics and kinetics of sorption*. MSc Dissertation, University of Stellenbosch.

Maroto-Valer, M., lu, Z., Zhang, Y., Tang, Z., 2008. Waste management: *Sorbents for $CO_2$ capture from high carbon fly ashes*. Vol 28, pp 2320–2328.

Maphada, 2011, *Verification of an automated volumetric adsorption system*. M.Sc Dissertation, University of the Witwatersrand, Johannesburg.

Matjie R. H., Ginster, M., Van Alphen, C., Sobiecki, A., 2005, *Detailed Characterisation of Sasol Ashes*, 2005 World of Coal Ash (WOCA), Lexington, Kentucky, USA, 11-15 April 2005, Available at < http://www.flyash.info/2005/95mat.pdf>, [Accessed 19 September 2011].

Matjie, H. and van Alphen, C., 2008, *Mineralogical features of size and density fractions in Sasol coal gasification ash, South Africa and potential by-products*, Fuel, Vol. 87, pp.1439–1445.

Mbendi Information Systems, 2011, *Coal Mining in Africa – Overview*, Mbendi Information Systems, (Last updated on the 22nd Nov 2011), Available at: <http://www.mbendi.com/indy/ming/coal/af/p0005.htm> [Accessed 17th June 2010].

Mitchell, C., 1991, *Coal bed methane in the UK*, Energy Policy, Vol. 19, pp. 849-854.

Mlambo, T. K., 2011, *The injection of fly ash slurries in deep geological reservoirs for improved reservoir integrity and safe $CO_2$ sequestration*, World of Coal Ash (WOCA) Conference, 9-12 May, 2011, Denver, Colorado, USA.

Montes-Hernandez, G., R. Perez-Lopez, F. Renard, J.M. Nieto and L. Charlet, 2009. Journal of Hazardous Materials: *Mineral sequestration of $CO_2$ by aqueous carbonation of coal combustion flyash*. Vol 16, pp 1347-1354.

Muriithi, G. N., Gitari, W. M., Petrik L. F. Ndungu, P. G., 2011. Journal of Environmental Management: *Carbonation of brine impacted fractionated coal fly ash: Implications for CO2 sequestration*. Vol 92, pp 655-664.

Nordell, B., 2003, *Thermal pollution causes global warming*, Global and Planetary Change, Vol. 38, pp. 305-312.

O'Brien, G., Jenkins, B., 2003, *Coal characterisation by automated coal petrography*, Fuel, Vol. 82, pp. 1067-1073.

Palmer, B., 2007, *Household coal use in an urban township in South Africa,* Journal of Energy in Southern Africa, Vol. 18, No 3.

Petrik, L., White, R. A., Klink, M. J., Somerset, V. S., Burgers, C. S., fey, M. V., 2003. *Utilization of South African fly ash to treat acid coal mine drainage, & production of high quality zeolites from the residual solids*, Int. Ash Utilization Symposium, 20-22 October, 2003, Lexington, Kentucky.

Pires, J.C.M., Martins, F.G., Alvim-Ferraz, M.C.M., Simões, M. 2011. Recent developments on carbon capture and storage: An overview. *Chemical Engineering Research and Design*, Vol 89, Pages 1446-1460.

Plaza, M.G., Pevida, C., Arias, B., Fermoso, J., Casal, M.D., Martín, C.F., Rubiera, F.,Pis, J. J., 2009. Fuel: *Development of low-cost biomass-based adsorbents for postcombustion $CO_2$ capture*. Vol 88, pp 2442–2447.

Prevec, R., 2006. *The power of plants: how ancient forests drive SA's economy*, Science in Africa, Available at <http://www.scienceinafrica.co.za/2006/february/coal.htm>, [Accessed 22nd November 2011].

Prevost, X.M., 2004, *South African reserves and the Minerals Act*, Coaltrans South Africa, 1–2 March, 2004, Cape Town, 2004, pp. 6.

Querol, X., 2002, *Synthesis of zeolites from coal fly ash: an overview*, International Journal of Coal Geology, Vol. 50, pp. 413 – 423.

Ram, L.C., 1992. *Moessbauer Spectroscopic and Gamma Radiolytic Studies of Some Indian Coals.* PhD thesis, Banaras Hindu University, Varanasi, India.

Ramis, G., Busca**,** G. and Lorenzelli**,** V., 1991, *Low-temperature $CO_2$ adsorption on metal oxides: spectroscopic characterisation of some weakly adsorbed species*, Materials Chemistry and Physics ,Vol. 29, pp. 425-435.

Shah, S.A. PATEL, B. S., Gohel, V., Javiya, R., 2011. *Fluidized Coal Combustion IC Engine.* National Conference on Recent Trends in Engineering & Technology. Available at <http://www.bvmengineering.ac.in/docs/published%20papers/mechprod/mechprod/601023.pdf> [Accessed 22nd November 2011].

Shannon, L.D., 1997, *Beneficial Reuse of Lime Softening Residuals for Flue Gas Desulfurization*, American Water Works Association, pp. 4.

Schumacher, B. A., Shines, K. C., Burton, J. V., Papp, M. L., 1990, *A comparison of soil sample homogenization techniques*, U.S. Environmental Protection Agency, Available at <http://www.epa.gov/esd/cmb/research/papers/bs120.pdf> [Accessed 22nd July 2011].

Soares, J.L., 2007, *Carbon Dioxide Adsorption in Brazilian Coals*, Energy Fuels, Vol. 21, No. 1, pp. 209–215.

Speakman, S.A., 2010, *Basics of X-Ray Diffraction*, Available at <http://prism.mit.edu/xray>, Massachusetts Institute of Technology**, [**Accessed 14th May 2011].

Speight, J.G., 2005, *Hand book of coal analysis*, John Wiley and Sons.

Stutzxnan, P.E. and Centeno, L., 1995, *Compositional Analysis of Beneficiated Fly Ashes*, National Institute of Standards and Technology, Available at <http://www.fire.nist.gov/bfrlpubs/build95/PDF/b95010.pdf>, [Accessed 14th May 2011].

Sun, L. and Wang, M., 1996, Global Warming and Global Dioxide Emission: An Empirical Study, Journal of Environmental Management, Vol. 46, pp. 327–343**.**

Surridge, A. D., 2009, *Carbon capture and storage South African activities and plans*. South African National Energy Research Institute, Available at < http://www.un.org/esa/dsd/dsd_aofw_ene/ene_egm0907_presentations.shtml>, **[**Accessed 19 July 2010].

Surridge, A. D. and Cloete, M., 2009, *Carbon Capture and Storage in South Africa*, Energy Procedia, Vol. 1, No. 1, pp. 2741-2744.

Tang, Z., Zhang, Y. and Maroto-Valer , M.M., 2004, *study of the $CO_2$ adsorption capacities of modified activated anthracites*, Fuel, Vol. 49, Issue 1, pp. 308-309.

Thiruvenkatachari R., 2009, *Post combustion $CO_2$ capture by carbon fibre monolithic adsorbents*, Progress in Energy and Combustion Science Vol. 35, No. 5, pp. 438-455.

Tien, C, 1994, *Adsorption Calculations and modeling*, Butterworth – Heinemann.

Tomlinson, S., Araya, M., Mabey, N., Claire Langley, C., Ng, S.,

Zorlu, P., 2010, *Assessment of priority countries for climate action in 2010*, Third Generation Environmentalism, Available at <http://www.e3g.org/images/uploads/E3G_Priority_Country_Analysis.pdf> [Accessed 16th March 2011].

University of California College Prep, 2009, *Non-renewable energy sources*, University of California, Available at: <http://cnx.org/content/m16730/latest/>, [Accessed 16th March 2011]

U. S. Department of transportation, 2011, *Utilisation of Recycled Materials in Illinois Highway Construction* Available at <http://www.fhwa.dot.gov/pavement/recycling/recbash.cfm>, [Accessed 13th May 2011].

U.S. Environmental protection agency, 2010, *Bottom ash*, Available at <http://www.epa.gov/osw/conserve/rrr/imr/ccps/bottomash.htm>, [Accessed 13th May 2011].

Van Dyk, J.C., 2006, *Understanding the influence of acidic components (Si, Al, and Ti) on ash flow temperature of South African coal sources*, Minerals Engineering, Vol. 19, pp. 280–286.

Vassileva, C.G. and Vassilev, S.V., 2006, *Behaviour of inorganic matter during heating of Bulgarian coals*, Fuel Processing Technology, Vol 87, pp. 1095–1116.

Viola, F.M., Paiva, S.L.D. and Savi, M.A., 2010, *Analysis of the global warming dynamics from temperature time series*, Ecological Modelling, Vol. 221, pp. 1964–1978.

Vogeli, J., 2010, *Investigation of the potential for mineral carbonation of South African PGM tailings*, Masters Thesis, University of Cape Town, Cape Town, Available at<http://www.mineralstometals.uct.ac.za/Research_Projects/Investigation-of-the-potential-for-mineral-carbonation-of-South-African-PGM-tailings.html> [Accessed 22nd November 2011].

World Bridge, 2010, *Compressor $CO_2$ Removal Process*, Available at <http://worldbridge.com/compressor_co2_removal.html>, [Accessed 22nd November 2011].

Wyrsch, N., Franco, A., Riesen, Y., Despeisse, M., Dunand, S., 2008, *Performance and Transient Behavior of Vertically Integrated Thin-film Silicon Sensors*, Sensors, Vol. 8, pp. 4656-4668.

Yan, L., Gupta, R.P. and Wall, T.F., 2002, *A mathematical model of ash formation during pulverized coal combustion*, Fuel, Vol. 81, Issue 3, Pp. 337-344.

Zeng, N., 2008, *Carbon sequestration via wood burial*, Carbon Balance and Management, Vol. 3.

# APPENDIX A: BET RESULTS

## **A1:** BET Isotherm Log Plots

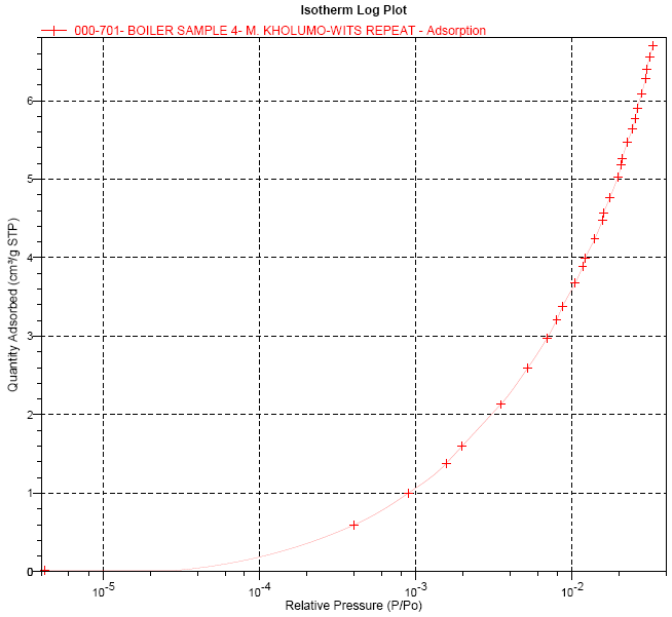


**Figure A1.1:** The CG ash isotherm log plot

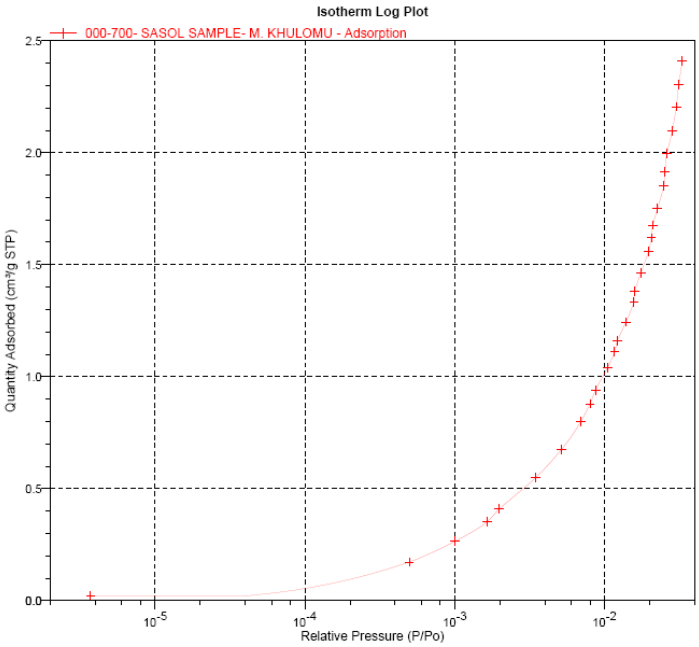


**Figure A1.2:** The G ash isotherm log plot

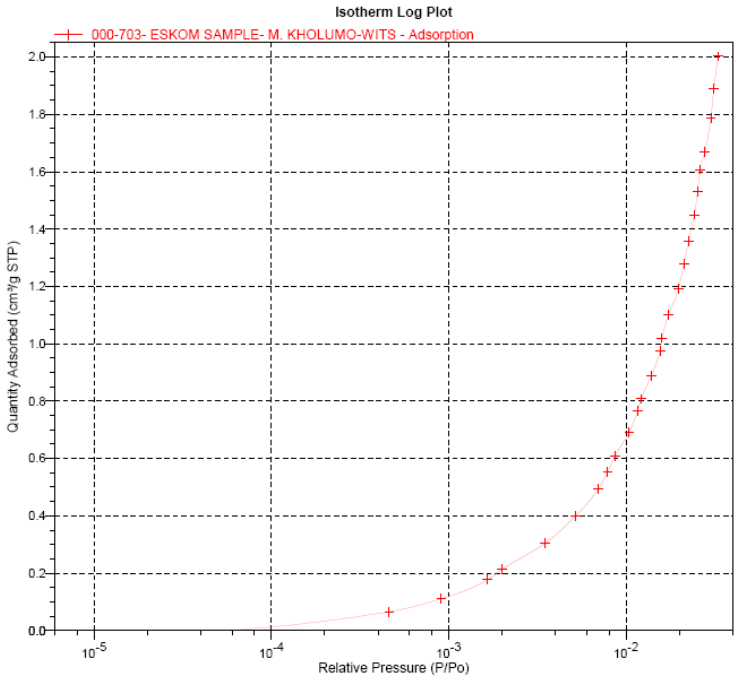


**Figure A1.3:** The PF ash Isotherm log plot

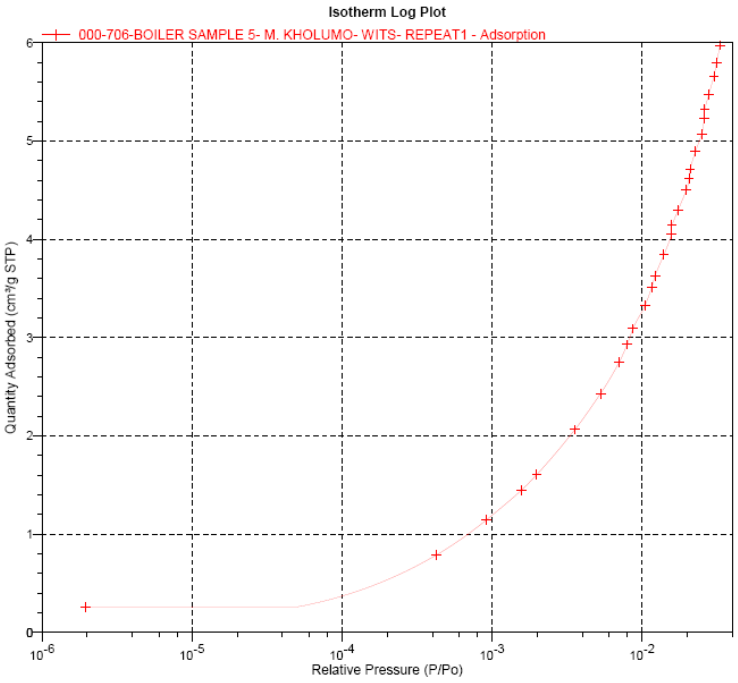


**Figure A1.4:** The SS ash isotherm log plot

## **A2:** Pre-Adsorption BET Full Report Sets

micromeritics®

**Full Report Set**

ASAP 2020 V3.01 H | Unit 1 | Serial #: 715 | Page 1

Sample: 000-698- BOILER 4 SAMPLE- M. kHOLUMO- WITS-1
Operator: GREGORY
Submitter: GREGORY
File: C:\2020\DATA\COAL1\000-698.SMP

Started: 01/05/2011 20:57:19PM
Completed: 02/05/2011 1:40:24PM
Report Time: 07/05/2011 4:38:38PM
Sample Mass: 0.2210 g
Cold Free Space: 32.7981 cm³
Low Pressure Dose: None

Analysis Adsorptive: CO2
Analysis Bath Temp.: 0.000 ℃
Thermal Correction: No
Warm Free Space: 31.1905 cm³ Measured
Equilibration Interval: 15 s
Automatic Degas: Yes

**Summary Report**

**Surface Area**

Single point surface area at P/Po = 0.033676912: 27.3950 m²/g

BET Surface Area: 32.6001 m²/g

Langmuir Surface Area: 35.9897 m²/g

**Pore Volume**

Single point adsorption total pore volume of pores less than 5.264 Å diameter at P/Po = 0.000005140: 0.000006 cm³/g

**Pore Size**

Adsorption average pore width (4V/A by BET): 0.0076 Å

**Horvath-Kawazoe**

Maximum pore volume at P/Po = 0.033676912: 0.011361 cm³/g

Median pore width: 0.000 Å

**Dubinin-Astakhov**

Micropore surface area: 45.600088 m²/g

Limiting micropore volume: 0.018073 cm³/g

**Figure A2.1**: Pre-adsorption full report of the CG ash sample

micromeritics®

**Full Report Set**

ASAP 2020 V3.01 H | Unit 1 | Serial #: 715 | Page 1

Sample: 000-700- SASOL SAMPLE- M. KHULOMU
Operator: GREGORY
Submitter: GREGORY
File: C:\2020\DATA\COAL1\000-700.SMP

Started: 04/05/2011 11:04:37PM
Completed: 04/05/2011 16:17:08PM
Report Time: 07/05/2011 4:57:55PM
Sample Mass: 0.2225 g
Cold Free Space: 30.8206 cm³
Low Pressure Dose: None

Analysis Adsorptive: CO2
Analysis Bath Temp.: 0.000 ℃
Thermal Correction: No
Warm Free Space: 29.2242 cm³ Measured
Equilibration Interval: 15 s
Automatic Degas: Yes

## Summary Report

### Surface Area

Single point surface area at P/Po = 0.033034462: 10.6476 m²/g

BET Surface Area: 12.9971 m²/g

Langmuir Surface Area: 14.2445 m²/g

### Pore Volume

Single point adsorption total pore volume of pores less than 5.218 Å diameter at P/Po = 0.000003713: 0.000039 cm³/g

### Pore Size

Adsorption average pore width (4V/A by BET): 0.1192 Å

**Figure A2.2**: Pre-adsorption full report of the G ash sample

micromeritics®

**Full Report Set**

ASAP 2020 V3.01 H | Unit 1 | Serial #: 715 | Page 1

Sample: 000-703- ESKOM SAMPLE- M. KHOLUMO-WITS
Operator: GREGORY
Submitter: GREGORY
File: C:\2020\DATA\COAL1\000-703.SMP

| | | | |
|---|---|---|---|
| Started: | 07/05/2011 4:00:57PM | Analysis Adsorptive: | CO2 |
| Completed: | 07/05/2011 8:12:21PM | Analysis Bath Temp.: | 0.000 ℃ |
| Report Time: | 07/05/2011 23:28:00PM | Thermal Correction: | No |
| Sample Mass: | 0.2018 g | Warm Free Space: | 29.3656 cm³ Measured |
| Cold Free Space: | 30.8566 cm³ | Equilibration Interval: | 15 s |
| Low Pressure Dose: | None | Automatic Degas: | Yes |

## Summary Report

### Surface Area

Single point surface area at P/Po = 0.033073672: 8.8446 m²/g

BET Surface Area: 17.1148 m²/g

Langmuir Surface Area: 22.7289 m²/g

**Figure A2.3**: Pre-adsorption full report of the PF ash sample

micromeritics®

**Full Report Set**

ASAP 2020 V3.01 H | Unit 1 | Serial #: 715 | Page 1

Sample: 000-702-BOILER SAMPLE 5- M. KHOLUMO- WITS- REPEAT
Operator: GREGORY
Submitter: GREGORY
File: C:\2020\DATA\COAL1\000-702.SMP

| | | | |
|---|---|---|---|
| Started: | 06/05/2011 19:12:43PM | Analysis Adsorptive: | CO2 |
| Completed: | 07/05/2011 0:42:40PM | Analysis Bath Temp.: | 0.000 ℃ |
| Report Time: | 07/05/2011 5:13:23PM | Thermal Correction: | No |
| Sample Mass: | 0.2064 g | Warm Free Space: | 32.5057 $cm^3$ Measured |
| Cold Free Space: | 34.3032 $cm^3$ | Equilibration Interval: | 15 s |
| Low Pressure Dose: | None | Automatic Degas: | Yes |

**Summary Report**

**Surface Area**

Single point surface area at P/Po = 0.033110788: 27.6301 $m^2/g$

BET Surface Area: 30.6974 $m^2/g$

Langmuir Surface Area: 32.8730 $m^2/g$

**Pore Volume**

Single point adsorption total pore volume of pores less than 5.129 Å diameter at P/Po = 0.000001924: 0.000333 $cm^3/g$

**Pore Size**

Adsorption average pore width (4V/A by BET): 0.4335 Å

**Figure A2.4**: Pre-adsorption full report set of the SS ash sample

## **A3:** Post-adsorption BET full report sets

micromeritics®

**Full Report Set**

ASAP 2020 V3.01 H | Unit 1 | Serial #: 715 | Page 1

Sample: 000-756- Mookho- Boiler 4 Sample after ads
Operator: Gregory
Submitter: Gregory
File: C:\2020\DATA\COAL1\000-756.SMP

Started: 15/08/2011 0:38:43PM
Completed: 15/08/2011 5:17:12PM
Report Time: 03/09/2011 23:17:15PM
Sample Mass: 0.1601 g
Cold Free Space: 32.7449 cm³
Low Pressure Dose: None

Analysis Adsorptive: CO2
Analysis Bath Temp.: 0.000 ℃
Thermal Correction: No
Warm Free Space: 31.2978 cm³ Measured
Equilibration Interval: 15 s
Automatic Degas: Yes

**Summary Report**

**Surface Area**

Single point surface area at P/Po = 0.032998988: 37.6632 m²/g

BET Surface Area: 42.9004 m²/g

Langmuir Surface Area: 46.1136 m²/g

**Pore Volume**

Single point adsorption total pore volume of pores less than 5.248 Å diameter at P/Po = 0.000004604: 0.000025 cm³/g

**Pore Size**

Adsorption average pore width (4V/A by BET): 0.0235 Å

**Horvath-Kawazoe**

Maximum pore volume at P/Po = 0.032998988: 0.015608 cm³/g

Median pore width: 0.000 Å

**Dubinin-Astakhov**

Micropore surface area: 73.207958 m²/g

Limiting micropore volume: 0.030365 cm³/g

**Figure A3.1**: Post-adsorption full report of the CG ash sample

micromeritics®

**Full Report Set**

ASAP 2020 V3.01 H | Unit 1 | Serial #: 715 | Page 1

Sample: 000-753- Mookho- Sasol sample after ads
Operator: Gregory
Submitter: Gregory
File: C:\2020\DATA\COAL1\000-753.SMP

| | | | |
|---|---|---|---|
| Started: | 11/08/2011 23:52:04PM | Analysis Adsorptive: | CO2 |
| Completed: | 12/08/2011 4:03:57PM | Analysis Bath Temp.: | 0.000 ℃ |
| Report Time: | 13/08/2011 14:55:36PM | Thermal Correction: | No |
| Sample Mass: | 0.2040 g | Warm Free Space: | 32.7876 cm³ Measured |
| Cold Free Space: | 34.4070 cm³ | Equilibration Interval: | 15 s |
| Low Pressure Dose: | None | Automatic Degas: | Yes |

**Summary Report**

**Surface Area**

Single point surface area at P/Po = 0.033013193: 11.9588 m²/g

BET Surface Area: 17.4158 m²/g

Langmuir Surface Area: 20.6008 m²/g

**Pore Volume**

Single point adsorption total pore volume of pores less than 5.267 Å diameter at P/Po = 0.000005271: 0.000001 cm³/g

**Pore Size**

Adsorption average pore width (4V/A by BET): 0.0027 Å

**Horvath-Kawazoe**

Maximum pore volume at P/Po = 0.033013193: 0.004956 cm³/g

Median pore width: 3.894 Å

**Dubinin-Astakhov**

Micropore surface area: 21.974655 m²/g

Limiting micropore volume: 0.009241 cm³/g

**Figure A3.2**: Post-adsorption full report of the G ash sample

micromeritics®

**Full Report Set**

ASAP 2020 V3.01 H | Unit 1 | Serial #: 715 | Page 1

Sample: 000-754- Mookho- Eskom sample after ads
Operator: Gregory
Submitter: Gregory
File: C:\2020\DATA\COAL1\000-754.SMP

| | | | |
|---|---|---|---|
| Started: | 12/08/2011 16:41:56PM | Analysis Adsorptive: | CO2 |
| Completed: | 12/08/2011 20:59:23PM | Analysis Bath Temp.: | 0.000 ℃ |
| Report Time: | 03/09/2011 23:33:50PM | Thermal Correction: | No |
| Sample Mass: | 0.1759 g | Warm Free Space: | 30.3138 cm³ Measured |
| Cold Free Space: | 31.8752 cm³ | Equilibration Interval: | 15 s |
| Low Pressure Dose: | None | Automatic Degas: | Yes |

**Summary Report**

**Surface Area**

Single point surface area at P/Po = 0.033071450: 10.4811 m²/g

BET Surface Area: 19.1842 m²/g

Langmuir Surface Area: 25.2598 m²/g

**Horvath-Kawazoe**

Maximum pore volume at P/Po = 0.033071450: 0.004344 cm³/g

Median pore width: 4.055 Å

**Dubinin-Astakhov**

Micropore surface area: 88.771295 m²/g

Limiting micropore volume: 0.055955 cm³/g

**Figure A3.3**: Post-adsorption full report of the PF ash sample

micromeritics®

**Full Report Set**

ASAP 2020 V3.01 H | Unit 1 | Serial #: 715 | Page 1

Sample: 000-757- Mookho- Boiler Sample 5 after adsorption
Operator: Gregory
Submitter: Gregory
File: C:\2020\DATA\COAL1\000-757.SMP

| | | | |
|---|---|---|---|
| Started: | 17/08/2011 22:12:20PM | Analysis Adsorptive: | CO2 |
| Completed: | 18/08/2011 7:52:59PM | Analysis Bath Temp.: | 0.000 ℃ |
| Report Time: | 03/09/2011 23:24:48PM | Thermal Correction: | No |
| Sample Mass: | 0.1630 g | Warm Free Space: | 30.4196 cm³ Measured |
| Cold Free Space: | 31.8966 cm³ | Equilibration Interval: | 15 s |
| Low Pressure Dose: | None | Automatic Degas: | Yes |

**Summary Report**

**Surface Area**

Single point surface area at P/Po = 0.032982033: 33.1065 m²/g

BET Surface Area: 37.0051 m²/g

Langmuir Surface Area: 39.5431 m²/g

**Pore Volume**

Single point adsorption total pore volume of pores less than 5.184 Å diameter at P/Po = 0.000002902: 0.000720 cm³/g

**Pore Size**

Adsorption average pore width (4V/A by BET): 0.7779 Å

**Horvath-Kawazoe**

Maximum pore volume at P/Po = 0.032982033: 0.013719 cm³/g

Median pore width: 3.524 Å

**Dubinin-Astakhov**

Micropore surface area: 74.232604 m²/g

Limiting micropore volume: 0.035133 cm³/g

**Figure A3.4**: Post-adsorption full report of the SS ash sample

# APPENDIX B: TGA ANALYSIS GRAPHS

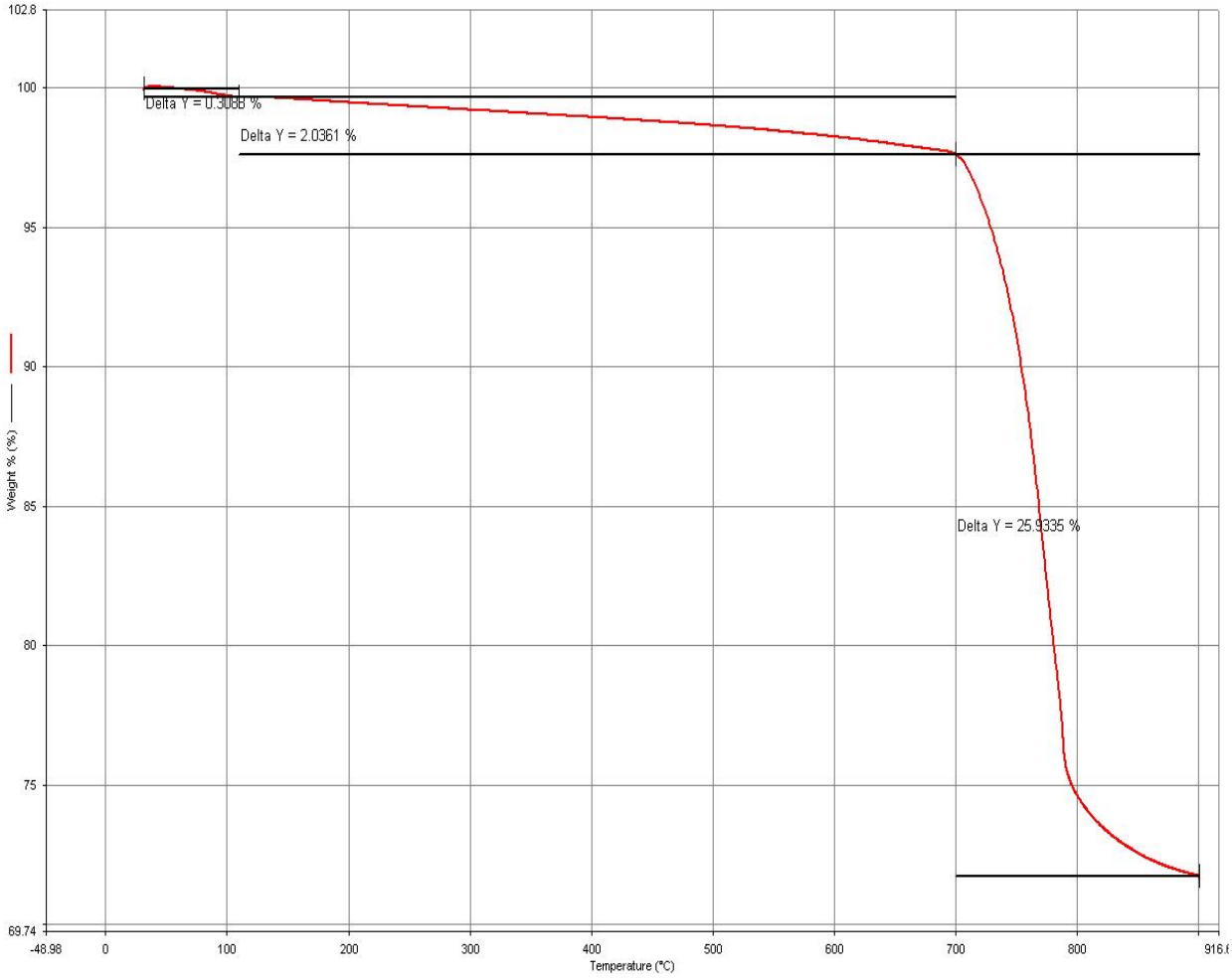


**Figure B.1**: CG ash sample TGA graph

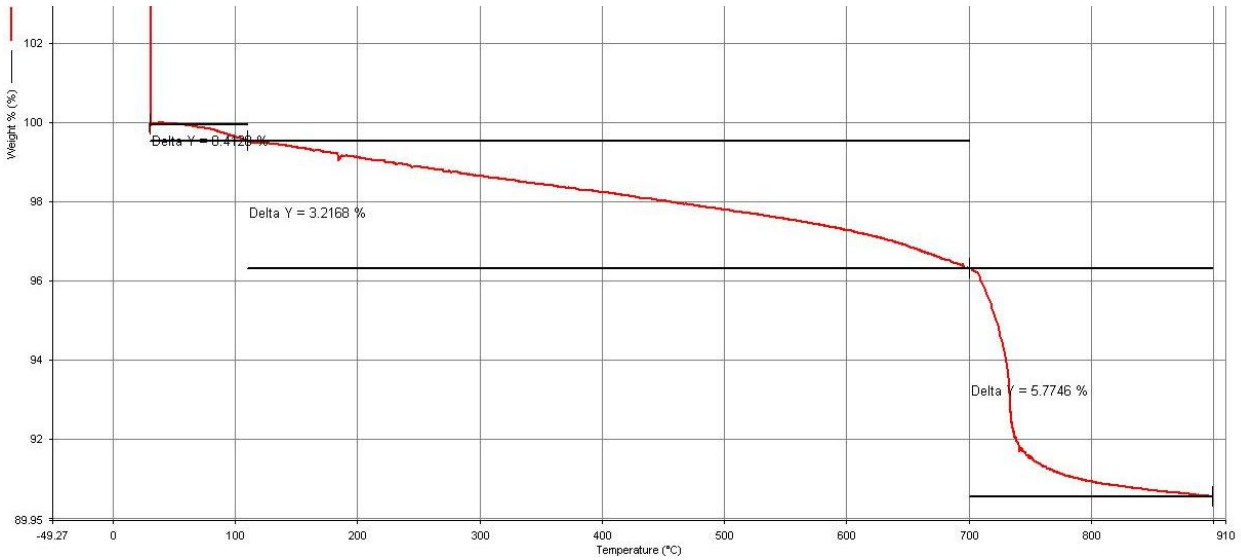


**Figure B.2**: G ash sample TGA graph

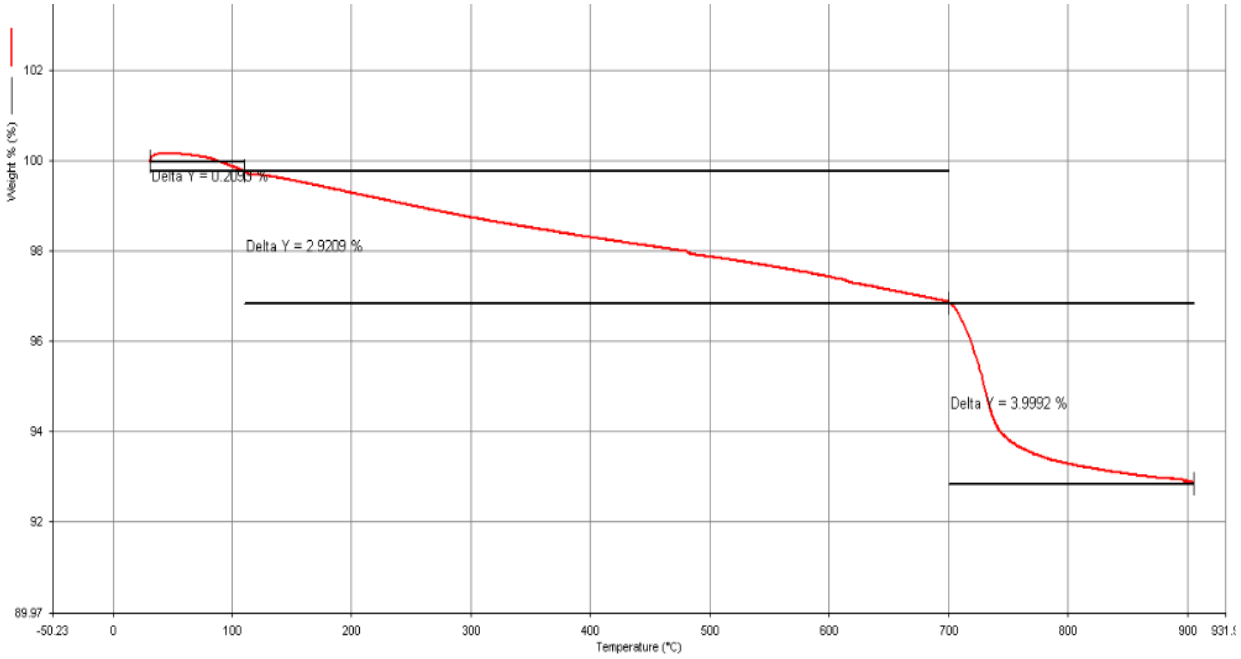


**Figure B.3**: PF ash sample TGA graph

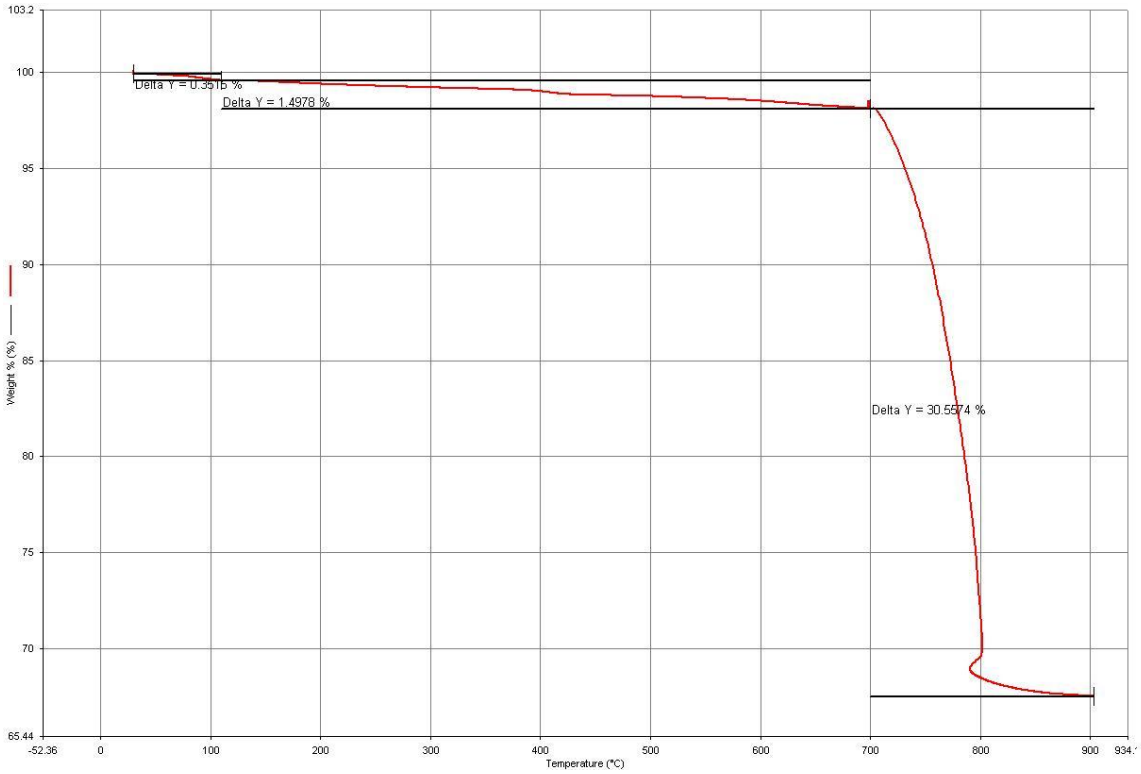


**Figure B.4**: SS ash sample TGA graph

# APPENDIX C: DETAILED XRD ANALYSIS RESULT

It is worth noting that at the time of the analysis of the samples, the CG ash was named Boiler 4, SS ash named Boiler 5, PF ash named Eskom and G ash called Sasol. Three repetitive analyses were conducted per sample.

| | Boiler 4 (1) | | | Boiler 4 (2) | | | Boiler 4 (3) | |
|---|---|---|---|---|---|---|---|---|
| Akermanite | 0.17 | 0.21 | Akermanite | 0.07 | 0.21 | Akermanite | 0.11 | 0.22 |
| Amorphous | 70.91 | 1.98 | Amorphous | 71.56 | 1.92 | Amorphous | 70.79 | 2.01 |
| Anhydrite | 1.3 | 0.39 | Anhydrite | 1.52 | 0.36 | Anhydrite | 1.49 | 0.36 |
| CaO Lime | 0 | 0 | CaO Lime | 0.12 | 0.08 | CaO Lime | 0.11 | 0.11 |
| Corundum | 1.5 | 0.63 | Corundum | 1.68 | 0.45 | Corundum | 1.48 | 0.42 |
| Hematite | 2.07 | 0.33 | Hematite | 2.04 | 0.33 | Hematite | 2.29 | 0.33 |
| Magnetite | 2.4 | 0.36 | Magnetite | 2.68 | 0.33 | Magnetite | 2.69 | 0.33 |
| Mullite | 13.4 | 1.5 | Mullite | 13.28 | 1.44 | Mullite | 14.24 | 1.5 |
| Periclase | 0.9 | 0.25 | Periclase | 0.6 | 0.22 | Periclase | 0.66 | 0.22 |
| Plagioclase | 4.81 | 1.2 | Plagioclase | 3.69 | 1.17 | Plagioclase | 3.94 | 1.2 |
| Pyrite | 0.06 | 0.17 | Pyrite | 0.17 | 0.17 | Pyrite | 0 | 0 |
| Quartz | 2.47 | 0.39 | Quartz | 2.59 | 0.39 | Quartz | 2.19 | 0.36 |

| | Boiler 5 (1) | | | Boiler 5 (2) | | | Boiler 5 (3) | |
|---|---|---|---|---|---|---|---|---|
| Akermanite | 0 | 0 | Akermanite | 0 | 0 | Akermanite | 0 | 0 |
| Amorphous | 68.3 | 1.8 | Amorphous | 68.75 | 1.89 | Amorphous | 68.88 | 1.77 |
| Anhydrite | 1.02 | 0.33 | Anhydrite | 1.11 | 0.33 | Anhydrite | 1.18 | 0.33 |
| CaO Lime | 0.59 | 0.15 | CaO Lime | 0.54 | 0.15 | CaO Lime | 0.55 | 0.16 |
| Corundum | 1.1 | 0.39 | Corundum | 1.2 | 0.39 | Corundum | 1.36 | 0.39 |
| Hematite | 1.41 | 0.3 | Hematite | 1.8 | 0.3 | Hematite | 1.38 | 0.29 |
| Magnetite | 2.44 | 0.27 | Magnetite | 2.55 | 0.29 | Magnetite | 2.6 | 0.26 |
| Mullite | 18.46 | 1.38 | Mullite | 17.89 | 1.35 | Mullite | 17.66 | 1.32 |
| Periclase | 0.87 | 0.22 | Periclase | 0.81 | 0.21 | Periclase | 0.79 | 0.21 |
| Plagioclase | 3.38 | 1.08 | Plagioclase | 3.02 | 1.14 | Plagioclase | 3.41 | 1.11 |
| Pyrite | 0 | 0 | Pyrite | 0.18 | 0.19 | Pyrite | 0 | 0 |
| Quartz | 2.43 | 0.36 | Quartz | 2.15 | 0.33 | Quartz | 2.18 | 0.33 |

| | Eskom A (1) | | | Eskom A (2) | | | Eskom A (3) | |
|---|---|---|---|---|---|---|---|---|
| Akermanite | 0 | 0 | Akermanite | 0 | 0 | Akermanite | 0.16 | 0.22 |
| Amorphous | 48.98 | 2.1 | Amorphous | 46.86 | 2.22 | Amorphous | 46.97 | 2.25 |
| Anhydrite | 1.71 | 0.33 | Anhydrite | 1.56 | 0.3 | Anhydrite | 1.63 | 0.33 |
| CaO Lime | 0.35 | 0.18 | CaO Lime | 0.36 | 0.17 | CaO Lime | 0.28 | 0.15 |
| Corundum | 1.32 | 0.42 | Corundum | 1.43 | 0.42 | Corundum | 2.2 | 0.42 |
| Hematite | 2.09 | 0.33 | Hematite | 2.28 | 0.33 | Hematite | 2.24 | 0.33 |
| Magnetite | 1.23 | 0.29 | Magnetite | 1.13 | 0.28 | Magnetite | 0.98 | 0.29 |
| Mullite | 30.54 | 1.65 | Mullite | 32.3 | 1.74 | Mullite | 31.78 | 1.8 |
| Periclase | 0.68 | 0.2 | Periclase | 0.74 | 0.21 | Periclase | 0.69 | 0.21 |
| Plagioclase | 1.16 | 0.72 | Plagioclase | 1.06 | 0.75 | Plagioclase | 1.32 | 0.75 |
| Pyrite | 0.43 | 0.27 | Pyrite | 0.2 | 0.28 | Pyrite | 0.16 | 0.2 |
| Quartz | 11.51 | 0.78 | Quartz | 12.06 | 0.81 | Quartz | 11.59 | 0.84 |

| | Sasol (1) | | | Sasol (2) | | | Sasol (3) | |
|---|---|---|---|---|---|---|---|---|
| Akermanite | 1.29 | 0.51 | Akermanite | 1.93 | 0.63 | Akermanite | 1.65 | 0.42 |
| Amorphous | 46.83 | 2.4 | Amorphous | 43.5 | 2.58 | Amorphous | 43.12 | 2.52 |
| Anhydrite | 0.66 | 0.3 | Anhydrite | 0.33 | 0.21 | Anhydrite | 0.55 | 0.42 |
| CaO Lime | 0 | 0 | CaO Lime | 0 | 0 | CaO Lime | 0.05 | 0.08 |
| Calcite | 1.96 | 0.54 | Calcite | 2.36 | 0.57 | Calcite | 2.23 | 0.39 |
| Corundum | 1.5 | 0.39 | Corundum | 1.63 | 0.42 | Corundum | 1.79 | 0.39 |
| Cristobalite | 1.81 | 0.72 | Cristobalite | 1.49 | 0.72 | Cristobalite | 1.83 | 0.57 |
| Hematite | 0.12 | 0.16 | Hematite | 0.11 | 0.16 | Hematite | 0.52 | 0.3 |
| Iron alpha | 0.62 | 0.1 | Iron alpha | 0.62 | 0.1 | Iron alpha | 0.71 | 0.11 |
| Magnetite | 0.91 | 0.26 | Magnetite | 0.76 | 0.27 | Magnetite | 0.57 | 0.28 |
| Mullite | 18.63 | 1.53 | Mullite | 21.47 | 1.74 | Mullite | 20.31 | 1.65 |
| Periclase | 0.5 | 0.22 | Periclase | 0.68 | 0.22 | Periclase | 0.7 | 0.22 |
| Plagioclase | 12.22 | 1.26 | Plagioclase | 11.99 | 1.26 | Plagioclase | 12.66 | 1.26 |
| Pyrite | 0.13 | 0.28 | Pyrite | 0.25 | 0.28 | Pyrite | 0.11 | 0.16 |
| Quartz | 12.82 | 0.81 | Quartz | 12.86 | 0.87 | Quartz | 13.2 | 0.84 |

**Figure C.1**: XRD analyses results for all samples